Reverse genetics for Human Coronavirus NL63

Dissertation

zur

Erlangung des Doktorgrades (Dr. rer. nat.)

der

Mathematisch-Naturwissenschaftlichen Fakultät

der

Rheinischen Friedrich-Wilhelms-Universität Bonn

vorgelegt von

Petra Herzog

aus

Mailand

Bonn Dezember 2013

Angefertigt mit Genehmigung der Mathematisch-Naturwissenschaftlichen Fakultät der
Rheinischen Friedrich-Wilhelms-Universität Bonn

1. Gutachter: Herr Professor Christian Drosten
2. Gutachter: Herr Professor Bernhard Misof

Tag der Promotion: 19.09.2014
Erscheinungsjahr: 2015

Index

1 Introduction 1
1.1 Coronaviridae 1
1.1.1 Taxonomy 1
1.1.1.1 Alphacoronavirus 2
1.1.1.2 Betacoronavirus 3
1.1.1.3 Gammacoronavirus 4
1.1.1.4 Deltacoronavirus 5
1.1.2 HCoV-NL63 epidemiology and pathogenesis 5
1.1.3 Coronavirus replication and life cycle 6
1.1.4 Coronavirus genome organization 9
1.2 Reverse genetics 10
1.3 Aim of the thesis 12
2 Material and Methods 13
2.1 Material 13
2.1.1 Equipment 13
2.1.2 Chemicals 14
2.1.3 Consumables 16
2.1.4 Buffer/Solutions 17
2.1.5 *E. coli* culture 18
2.1.5.1 Media 18
2.1.5.2 Antibiotic Stock solutions 18
2.1.5.3 Bacteria 18
2.1.6 Cell culture 19
2.1.6.1 Media and overlays 19
2.1.6.2 Cells 20
2.1.6.3 Virus 20
2.1.7 Kits 20
2.1.8 Enzymes 21
2.1.9 Restriction Enzymes 21
2.1.10 Antibodies 22
2.1.10.1 Primary antibodies 22
2.1.10.2 Secondary antibodies 22
2.1.11 Molecular Weight Markers 22
2.1.12 Plasmids and BACs 23
2.1.13 Primer 25
2.1.13.1 NL63 forward primers 25
2.1.13.2 NL63 reverse primers 26
2.1.13.3 Vector primers 26
2.1.13.4 Construction primers 27
2.1.13.5 RT Real-Time PCR primers 28
2.1.13.6 Mutagenesis primers 28
2.2 Methods 29
2.2.1 Molecular biology methods 29
2.2.1.1 RNA extraction 29
2.2.1.2 Isolation of plasmid DNA 29
2.2.1.3 Purification of PCR products 29
2.2.1.4 DNA extraction from agarose gels 30
2.2.1.5 Phenol/chloroform extraction and alcohol precipitation of nucleic acids (NAs) 30
2.2.1.6 Agarose gel electrophoresis of nucleic acids (NAs) 30
2.2.1.7 Photometric analysis of nucleic acid concentration 31
2.2.1.8 Sequencing of DNA 31
2.2.1.9 *In vitro* synthesis of capped RNA 32
2.2.1.10 cDNA synthesis 33
2.2.1.11 PCR using Phusion Enzyme 34
2.2.1.12 PCR using Platinum Taq 35
2.2.1.13 PCR using Herculase enzyme 36

2.2.1.14 One-step RT-PCR 36
2.2.1.15 Real-time RT PCR 37
2.2.1.16 Phusion mutagenesis PCR 38
2.2.1.17 Quick Change mutagenesis PCR 40
2.2.1.18 Sequencing and genome size verification using Phusion polymerase 40
2.2.1.19 RNA ligase-mediated rapid amplification of cDNA ends (RLM-RACE) 40
2.2.1.20 Restriction and dephosphorylation 40
2.2.1.21 Ligation 41
2.2.1.22 Cloning 41
2.2.1.23 Preparation of media for bacteria culture 42
2.2.1.24 Production of competent *E. coli* cells and transformation 42
2.2.1.25 High-copy plasmid culture 43
2.2.1.26 BAC culture 43
2.2.2 Cell culture Methods 43
2.2.2.1 Preparation of media and solutions 43
2.2.2.2 Cell culture conditions 44
2.2.2.3 Cultivation of cell lines 44
2.2.2.4 Cryopreservation of cell lines 44
2.2.2.5 Transfection of mammalian cells by electroporation 45
2.2.3 Virus culture methods 45
2.2.3.1 HCoV-NL63 virus stock 45
2.2.3.2 Infection of cells 46
2.2.3.3 Overlays 46
2.2.3.4 Plaque assays 46
2.2.3.5 Limiting dilution infection series and plaque purification 46
2.2.4 Immunodetection assays 47
2.2.4.1 Spotting of HCoV-NL63 slides 47
2.2.4.2 Immunofluorescence 47
2.2.4.3 Detection of HCoV-NL63 strain Amsterdam1 and recombinant HCoV-NL63 by immunofluorescence assay (IFA) 47

3 Results 49

3.1 Sequencing of the parental HCoV-NL63 Amsterdam 1 49
3.2 Susceptibility of different cell lines to HCoV-NL63 and cytopathogenic effects 51
3.3 Comparison of different plaque assay overlays 53
3.4 Optimization of incubation times 54
3.5 Plaque preparation 55
3.6 Adaptation of HCoV-NL63 to CaCo-2 cells and full genome sequencing 57
3.7 Cloning strategy 58
3.7.1 Construction of the HCoV-NL63-modified vector backbone 60
3.7.2 Construction of the subclones A- E 63
3.7.2.1 Construction of subclone A 64
3.7.2.2 Construction of subclone B1 65
3.7.2.3 Construction of subclone B2 65
3.7.2.4 Construction of subclone C 65
3.7.2.5 Construction of subclone D 66
3.7.2.6 Construction of subclone E 67
3.7.2.7 Correction of the subclones 67
3.7.3 Assembly of the subclones 68
3.7.3.1 Assembly of subclone AF 70
3.7.3.2 Assembly of subclone AB1 72
3.7.3.3 Assembly of subclone B2C 73
3.7.3.4 Assembly of subclone DE 73
3.7.3.5 Assembly of subclone BC 73
3.7.3.6 Assembly of subclone ADEF 73
3.7.3.7 Assembly of subclone ABC 74
3.7.3.8 Assembly of the NL full-length cDNA clone 74
3.8 *In vitro* transcription (IVT) of full-length rNL63 and N gene 75
3.9 Transfection into mammalian cells 77

3.10 Rescue of rNL63 wt 77
3.10.1 Proof of marker mutations 78
3.10.2 Immunofluorescence Assay (IFA) of rNL63 wt 80
3.10.3 Plaque purification 81
4 Discussion 84
4.1 Susceptibility studies with HCoV-NL63 and development of a plaque assay 84
4.2 Establishment of a reverse genetics system for HCoV-NL63 86
5 Summary 90
6 Zusammenfassung (Summary in German) 91
7 References 92
8 Appendix 100
8.1 Abbreviations 100
8.1.1 Viruses 100
8.1.2 Others 100
8.2 Publications 104

1 Introduction

1.1 Coronaviridae

Coronaviruses contain the largest single-stranded positive-sense RNA genome of any known virus family to date. The genome size varies from 27-32 kilobase pairs (kb). The spherical enveloped virions measure 120 to 160 nm in diameter. Prominent spike proteins on the surface of the virions lead to a morphology resembling a crown (lat: corona) when examined by electron microscopy. Therefore the first viruses discovered in this family were named “Coronavirus”. Every coronavirus genome contains five major open reading frames (ORFs). These encode the replicase polyprotein, the spike (S), envelope (E), and membrane (M) glycoproteins; and the nucleocapsid protein (N) (see Figure 1).

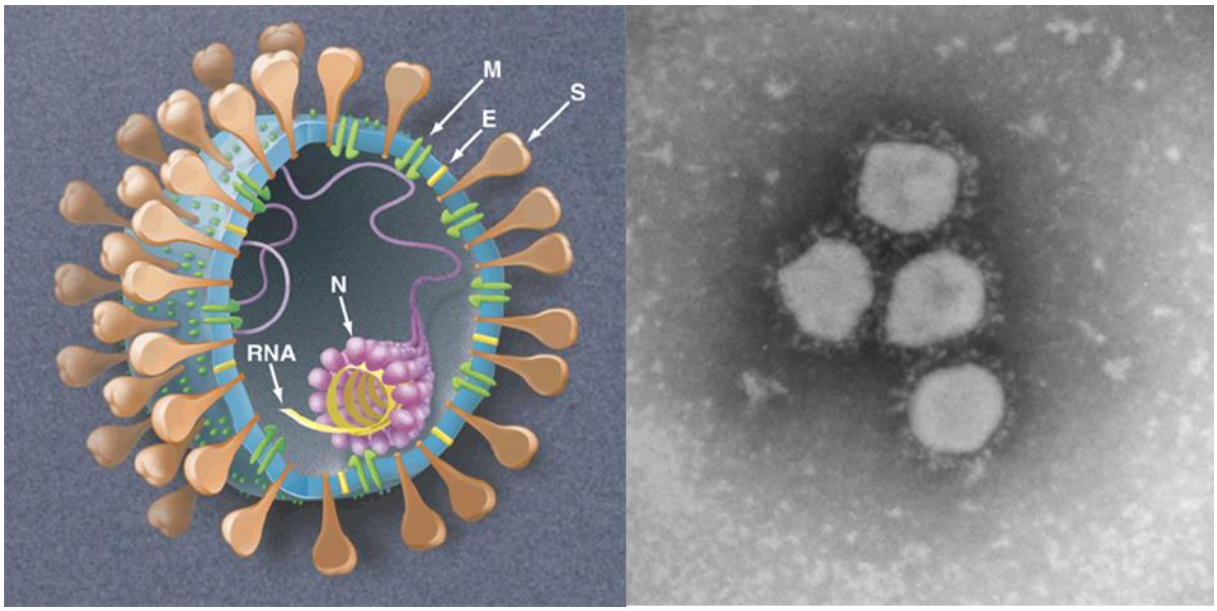

Figure 1: Coronavirus model (left) and electron micrograph of human coronavirus NL63 (HCoV-NL63, right). Left: a coronavirus model showing the organization of the spike (S), membrane (M) and envelope (E) glycoproteins, as well as the RNA and helical nucleocapsid (N) arrangement. Model from (Holmes et al. 2003). Right: an electron micrograph of HCoV-NL63 with prominent spike proteins giving the particles a crown-like appearance (van der Hoek et al. 2006).

1.1.1 Taxonomy

The human coronavirus NL63 (HCoV-NL63) belongs to the family of *Coronaviridae* which comprises two subfamilies, the *Coronavirinae* and the *Torovirinae*. Together with the *Roniviridae* and the *Arteriviridae* the *Coronaviridae* belong to the order *Nidovirales*. With the 2011 release of the International Committee on Taxonomy of Viruses (ICTV) the

Coronavirinae are subdivided in four genera, the *Alpha-*, *Beta-*, *Gamma-, and Deltacoronaviruses* (see Figure 2).

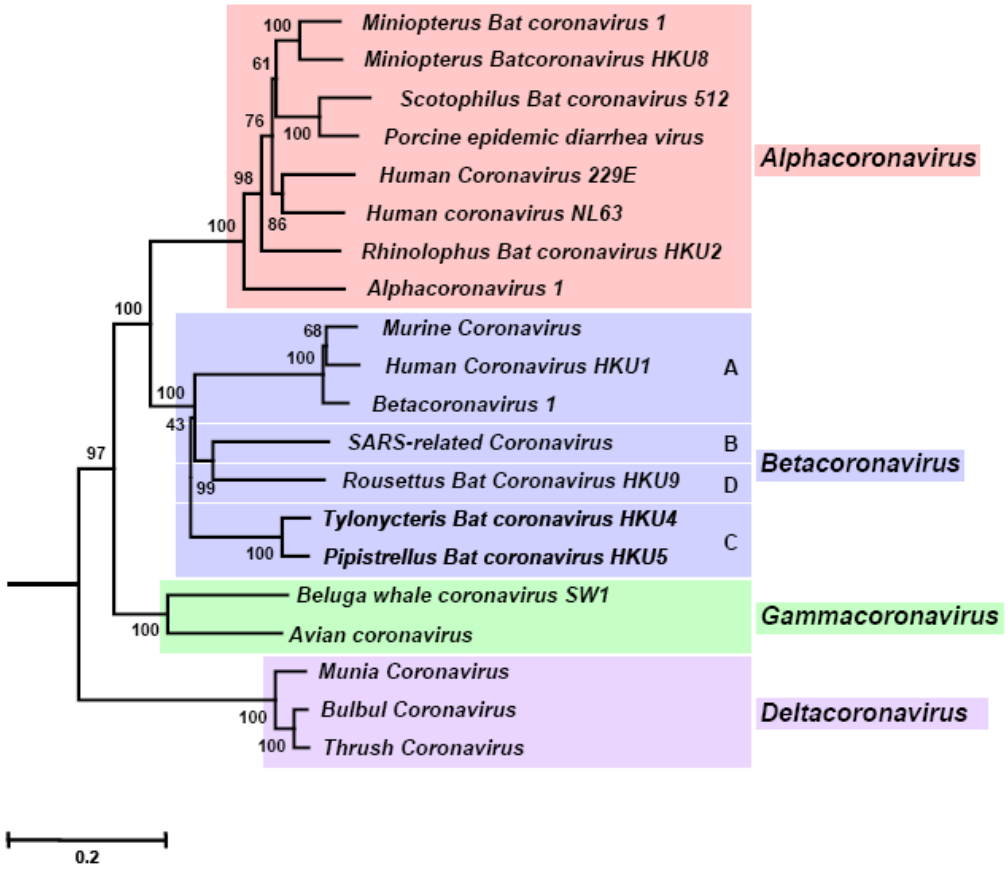

Figure 2: Phylogenetic relationships among the members of the subfamily Coronavirinae. A rooted Neighbour-Joining tree was generated from amino acid sequence alignments of RdRp and helicase domains with equine torovirus Berne as outgroup. The tree reveals four main monophyletic clusters corresponding to genera Alpha-, Beta- and Gammacoronavirus and an envisaged new genus Deltacoronavirus (color-coded). From the proposal "A new genus and three new species in the subfamily Coronavirinae"(2010.023a-dV) to the ICTV by Raoul J. de Groot and Alexander E. Gorbalenya.

1.1.1.1 Alphacoronavirus

The genus *Alphacoronavirus* contains two human coronavirus species, the long known HCoV-229E (Hamre et al. 1966) and the recently discovered HCoV-NL63 (van der Hoek et al. 2004). With the porcine epidemic diarrhea virus (PEDV) (Wood 1977; Chasey et al. 1978; Pensaert et al. 1978; Hofmann et al. 1988; Kusanagi et al. 1992) and the transmissible gastroenteritis virus (TGEV) (Bohl et al. 1972; Bohl et al. 1972; Saif et al. 1972; Garwes 1988; Enjuanes et al. 1995; Kim et al. 2000) it further contains coronaviruses that had an economic impact on agriculture due to high mortality rates in piglets. Vaccination against

TGEV reduced the losses in pig farms by TGEV, but suddenly uprising PEDV (Shibata et al. 2000) epidemics in north America showed similar symptoms and economic impact.
Other viruses closely related to TGEV and also affecting domestic animals are the feline and canine coronaviruses (FCoV, CCoV). Due to their high sequence identity (>96% sequence identity within the replicase polyprotein pp1ab) TGEV, FCoV and CCoV are grouped into the type species alphacoronavirus 1, formerly known as subgroup 1a (Gonzalez et al. 2003) (see Figure 2). They cause mainly mild gastroenteritis but in case of FCoV a spontaneous mutation in vivo can cause the highly lethal feline infectious peritonitis (FIP) in domestic cats (Vennema et al. 1998). A highly virulent variant of CCoV is known since 2005 (Buonavoglia et al. 2006). FCoV, CCoV and TGEV have an evolutionary history of common ancestors as well as several recombination events (Le Poder 2011), proving the ability of coronaviruses to cross species barriers repeatedly.
Human and porcine alphacoronaviruses could be associated with common colds and infections of the respiratory tract. For HCoV-229E, TGEV and PEDV a correlation with gastroenteritis could be shown (Tyrrell et al. 1965; Bradburne et al. 1967; Garwes 1988; Hofmann et al. 1988).
A rapidly increasing number of bat coronaviruses (Poon et al. 2005; Chu et al. 2006; Tang et al. 2006; Dominguez et al. 2007; Lau et al. 2007; Chu et al. 2008; Gloza-Rausch et al. 2008; Pfefferle et al. 2009; Drexler et al. 2010) is also allocated to this genus as unclassified alphacoronaviruses. These findings support the thesis that bats serve as genetic reservoir for alpha- and betacoronaviruses (Woo et al. 2012).

1.1.1.2 Betacoronavirus

The genus *Betacoronavirus* contains three human coronavirus species, human coronavirus OC43 (HCoV-OC43), severe acute respiratory syndrome (SARS) coronavirus (SARS-CoV), human coronavirus HKU1 (HCoV-HKU1) and the novel human coronavirus EMC (HCoV-EMC). HCoV-OC43 (McIntosh et al. 1967) was isolated in 1967 from throat swabs of patients with common cold. Until the SARS outbreak in 2003 (Drosten et al. 2003; Peiris et al. 2003; Rota et al. 2003) it was the only known human coronavirus in this group. With the discovery of SARS-CoV as the causative agent for the SARS epidemic the focus on coronaviruses led to the discovery of many new viruses including the HCoV-HKU1 (Woo et al. 2005), several novel bat (Tang et al. 2006; Woo et al. 2006; Woo et al. 2007; Drexler et al. 2010), bat SARS-like (Lau et al. 2005; Li et al. 2005; Yuan et al. 2010) and civet SARS-like coronavirus species (Guan et al. 2003; Wang et al. 2005). The betacoronaviruses HCoV-OC43 and HCoV-HKU1 together with the alphacoronaviruses HCoV-229E and HCoV-NL63 belong to the group of coronaviruses associated with respiratory tract infections (RTI) and common

colds in humans. HCoV-HKU1 was also associated with pneumonia (Lau et al. 2006) and in some cases with gastrointestinal disease (Vabret et al. 2006).
The type species is represented by murine coronavirus (MHV) (Nelson 1957), the species betacoronavirus 1 contains bovine coronavirus (BCoV) (Stair et al. 1972), canine respiratory coronavirus (CRCoV) (Erles et al. 2003), equine coronavirus (ECoV) (Huang et al. 1983), HCoV-OC43 (McIntosh et al. 1967) and the porcine hemagglutinating encephalomyelitis virus (PHE-CoV) (Mengeling et al. 1972). HCoV-HKU1 (Woo et al. 2005), and SARS-related CoV represent single species, additionally several species containing exclusively bat coronaviruses were defined, namely the former coronavirus groups 2b (Drexler et al. 2010), and 2c (Tang et al. 2006), the Pipistrellus bat coronavirus HKU5 (Woo et al. 2006), the Rousettus bat coronavirus HKU9 (Woo et al. 2007) and the Tylonycteris bat coronavirus HKU4 (Woo et al. 2006) (see Figure 2). Several other bat, bovine and one human coronavirus species (Reusken et al. 2010; Watanabe et al. 2010) are subsumed as unclassified betacoronaviruses.
The most prominent and best studied members of the betacoronaviruses are MHV and SARS-CoV. MHV causes bronchiolitis, infects the liver and brain of mice and is used as a model organism to study the pathogenesis of coronaviruses (Perlman et al. 1987). Infection of mice with MHV poses a challenge for unbiased research in specific pathogen free (SPF) facilities (Torrecilhas et al. 1999; Na et al. 2010). SARS-CoV is studied intensely since its sudden, rapid outbreak in early 2003 and due to the comparatively high mortality caused by SARS (Drosten et al. 2003; Guan et al. 2003; Rota et al. 2003).
The novel human coronavirus MERS-CoV (Zaki et al. 2012) was discovered in 2012, its zoonotic potential and suspected potential of person-to-person transmission are currently under investigation (Kindler et al. 2013).

1.1.1.3 Gammacoronavirus

The genus *Gammacoronavirus* comprises mainly avian born coronaviruses, pooled in a species designated avian coronavirus. The infectious bronchitis virus (IBV) was the first avian coronavirus discovered, causing impaired egg production in adult and respiratory symptoms in young chickens (Cunningham 1970) and being the sole representative of *Gammacoronavirus* for several decades. The number of coronaviruses discovered in different bird species belonging to different orders increased rapidly over the past years. To date bulbul, duck, goose, munia, pheasant, pigeon, thrush and turkey coronaviruses are known (Gough et al. 1996; Jonassen et al. 2005; Liu et al. 2005; Gomaa et al. 2008; Woo et al. 2009). In view of the genetic diversity of alpha- and betacoronaviruses, the narrower

genetic range of gammacoronaviruses suggests that many undiscovered members of the genus may exist (Woo et al. 2009) (see Figure 2).
The only mammalian-associated species in this genus is represented by the beluga whale coronavirus SW1 (Mihindukulasuriya et al. 2008).

1.1.1.4 Deltacoronavirus

In 2010 a new genus was proposed to and accepted by ICTV, named *Deltacoronavirus.* The genus comprises several new avian born coronaviruses, represented by bulbul coronavirus HKU11, thrush coronavirus HKU12 and munia coronavirus HKU13 (Woo et al. 2012). Interestingly also mammalian coronaviruses like the porcine coronavirus HKU15 are closely related to the avian coronaviruses within the genus *Deltacoronavirus*. These novel coronaviruses support the thesis of bat coronaviruses being the reservoir and ancestral lineage of alpha- and betacoronaviruses in contrast to avian coronaviruses being the gene source of gamma- and deltacoronaviruses (see Figure 3).

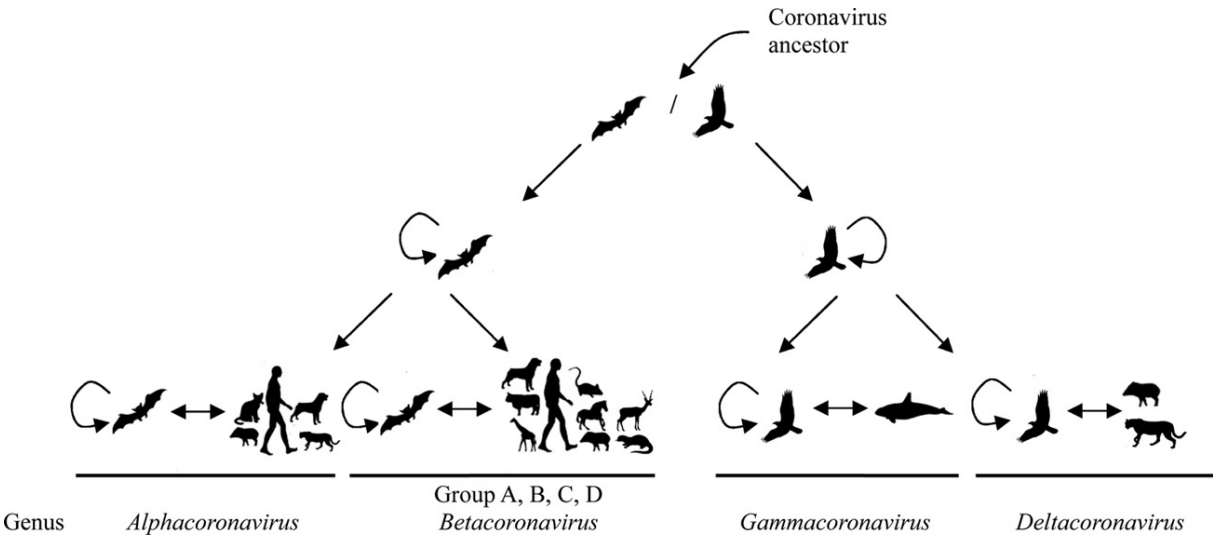

Figure 3: A model of coronavirus evolution. CoVs in bats are the gene source of Alphacoronavirus and Betacoronavirus, and CoVs in birds are the gene source of Gammacoronavirus and Deltacoronavirus (Woo et al. 2012).

1.1.2 HCoV-NL63 epidemiology and pathogenesis

The human coronavirus NL63 was isolated independently by two work groups in the Netherlands in 2004. Both isolates were obtained from young children, aged seven and eight months, suffering from respiratory tract infections (Fouchier et al. 2004; van der Hoek et al. 2004). Although HCoV-NL63 was discovered recently, it has presumably been circulating in the human population worldwide for many decades. The oldest sample known to date was detected in a nasal wash specimen from 1981 (Talbot et al. 2009).

Several studies were carried out to determine the prevalence of HCoV-NL63 infections in respiratory samples of inpatients and outpatients of different ages. In the age cohort of children under five years the incidence of HCoV-NL63 ranged from 1.1 to 9.3%, depending on the type of study, location, period and population screened (Abdul-Rasool et al. 2010; Principi et al. 2010). As shown in a birth cohort study on 13 newborns, seroconversion against HCoV-NL63 occurs in young children, foremostly at an age below 3.5 years (Dijkman et al. 2008). HCoV-NL63 infection is also observed frequently in elderly and immunocompromised patients and in patients with underlying pulmonary conditions (Fouchier et al. 2004; Arden et al. 2005; Bastien et al. 2005; Bastien et al. 2005; Moes et al. 2005).

A variety of respiratory symptoms is connected to HCoV-NL63 infections. Mild symptoms in otherwise healthy children include common colds and upper respiratory tract infections (URTI) with fever, cough, rinorrhea and pharyngitis (Vabret et al. 2005). More severe symptoms like bronchiolitis (Arden et al. 2005; Bastien et al. 2005; Ebihara et al. 2005) and croup (Arden et al. 2005; Chiu et al. 2005; van der Hoek et al. 2005; Wu et al. 2008; van der Hoek et al. 2010) occur during lower respiratory tract infections (LTRI). In temperate climates HCoV-NL63 circulates mainly during the winter season along with influenza A virus, respiratory syncytial virus, parainfluenza virus, human metapneumovirus and other human coronaviruses. Double infections with other respiratory viruses are often present in HCoV-NL63 positive patients (Chiu et al. 2005; Kaiser et al. 2005; van der Hoek et al. 2005; Lambert et al. 2007; Wu et al. 2008), making it sometimes difficult to correlate symptoms with one causative virus (Pyrc et al. 2006).

1.1.3 Coronavirus replication and life cycle

Coronavirus infections are initiated by binding of viral spikes to cellular receptors. Interestingly, even though HCoV-NL63 and SARS-CoV are only 46% identical on nucleotide level and 21% similar on amino acid level (van der Hoek et al. 2006), these viruses use the same receptor for cell entry, the membrane-bound angiotensin-converting enzyme 2 (ACE2) (Hofmann et al. 2005). However, the spike proteins of both viruses seem to bind to different domains of the receptor (Wu et al. 2009). The use of ACE2 by HCoV-NL63 is exceptional as almost all known alphacoronaviruses use the aminopeptidase N (CD13).

Coronavirus´ cellular entry is mediated by the spike subunits and can facilitate entry in two ways. Most coronaviruses apply a receptor-mediated endocytosis followed by fusion of virus and host cell membranes in the acidic environment of an endosome to enter cells (Huang et al. 2006; Heald-Sargent et al. 2012). Alternatively coronaviruses facilitate a direct fusion of the virus envelope with the cellular plasma membrane mediated by proteases (Heald-

Sargent et al. 2012). This way of entry was proven for SARS-CoV using transmembrane protease serine 2 (TMPRSS2) or human airway trypsin-like protease (Matsuyama et al. 2010; Glowacka et al. 2011).

The nucleocapsid is released into the cytoplasm and the genomic positive strand RNA serves as mRNA for the synthesis of the first viral proteins, namely the product of ORF 1a/b, the replicase polyprotein. Autocatalytic proteases cleave the nascent polyprotein and release up to 16 non-structural proteins (nsp, see Figure 4) (Ziebuhr et al. 2000; Snijder et al. 2003).

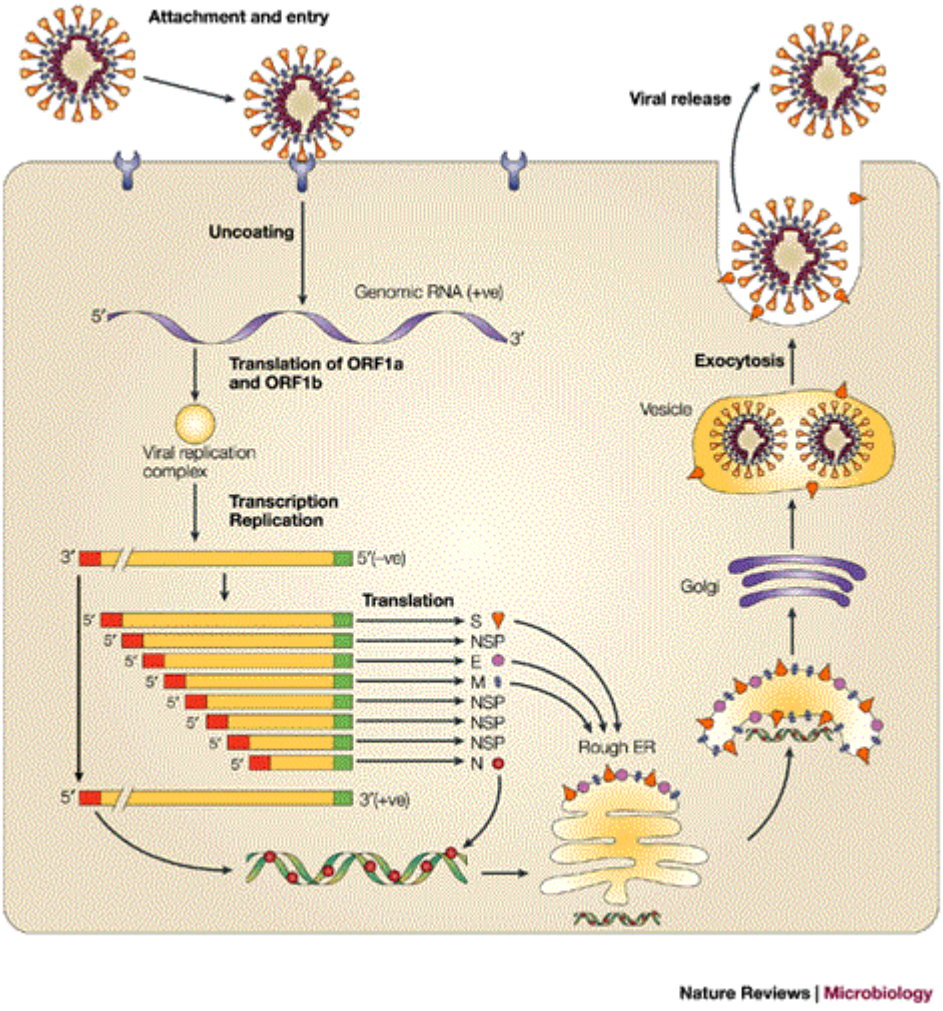

Figure 4: The Coronavirus life cycle. The coronaviruses enter their target cells through membrane fusion or an endosomal pathway. The viral genome is released and translated into viral replicase polyproteins (pp) 1a and 1ab, which are then autocatalytically cleaved into smaller products by viral proteases. Products of the ORF 1a/b form the replication complex, which synthesizes the full-length negative strand genome and also the subgenomic negative strand templates by discontinuous transcription. These negative strand RNAs serve as templates for the plus strand genome and plus strand mRNA synthesis. Viral nucleocapsids are assembled from genomic RNA and N protein in the cytoplasm, followed by budding into the lumen of the ERGIC (endoplasmic reticulum (ER)–Golgi intermediate compartment). Virions are then released from the cell via exocytosis (Stadler et al. 2003).

Recent data suggest that most, if not all of the encoded proteins, play a role in *in vivo* replication of the coronaviruses (Perlman et al. 2009). The RNA modifying enzymes form a replication complex that is associated with cytoplasmic membranes (Hagemeijer et al. 2010). In this replication complex a full-length negative strand copy of the genome is synthesized, which serves as template for the positive strand genomic RNA. Additionally the subset of shorter, subgenomic mRNAs is derived from discontinuous minus-strand synthesis. Their formation is facilitated by the leader and body transcription regulatory sequence (TRS) (Sawicki et al. 2007). All subgenomic mRNAs have a common 5' end corresponding to the 60-100 most proximal nucleotides at the 5' end of the genome. During minus-strand synthesis, base pairing complementarity of leader and body TRS enable redirection of the nascent minus strand RNA and by this means the addition of the 5' untranslated sequence to every subgenomic minus-strand RNA and the subgenomic mRNAs transcribed thereof ((Pasternak et al. 2006) see Figure 5).

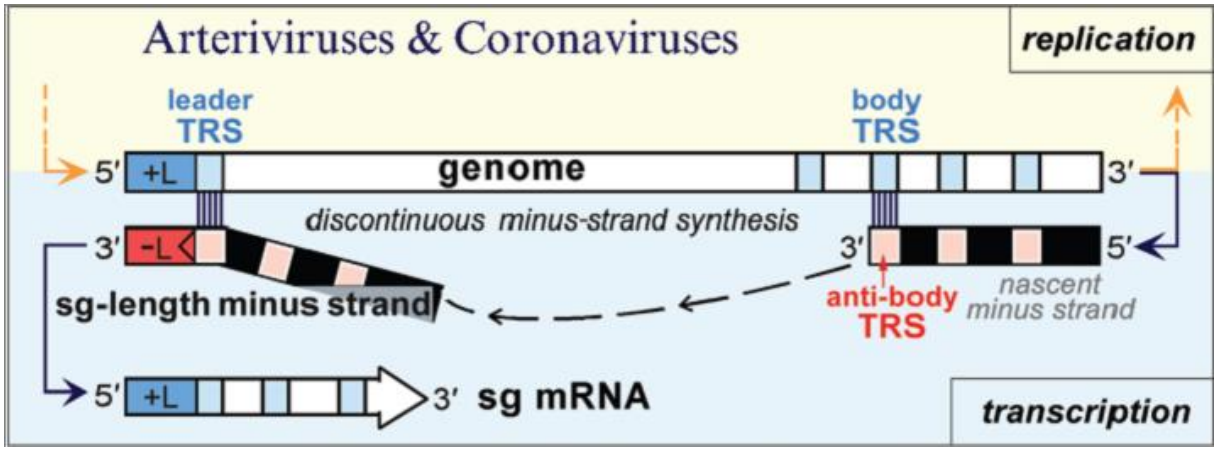

Figure 5: Model-based on discontinuous extension of minus-strand RNA synthesis. Minus-strand RNA can be either continuous (producing the anti-genome) or discontinuous (yielding sg-length minus strands). The body TRSs in the genome act as attenuation signals for minus-strand RNA synthesis, after which the nascent minus strand, having an anti-body TRS at its 3' end, are redirected to the 5'-proximal region of the template, guided by a base-pairing interaction with the leader TRS. Following the addition of the anti-leader (''L) to the nascent minus strands, the sg-length minus strands serve as templates for transcription. Modified from (Pasternak et al. 2006)

Nucleocapsid and genomic RNA are assembled and transported to the membrane system where membrane, envelope and spike proteins are located. Viral particles are assembled and bud into the lumen of the ERGIC. The virions mature during their passage through the Golgi system and are released by endocytosis (see Figure 4) (Masters 2006; Acheson 2007). New publications prove coronavirus-induced membrane alterations, namely the formation of a reticulovesicular network (RVN), derived from endoplasmatic reticulum (ER) membranes. Viral RNA synthesis was detected in double-membrane vesicles (DMVs) which are part of

the RVN (Knoops et al. 2008; Perlman et al. 2009). Nevertheless an involvement of the ERGIC remains possible and the interaction of the viral replication/transcription complex (RTC) with cellular pathways needs further investigation (Knoops et al. 2010).

1.1.4 Coronavirus genome organization

The coronavirus genome consists of positive-sense single-stranded RNA, carrying a 5' terminal cap and a 3' polyadenylated poly(A) tail (Perlman et al. 2009). Depending on the virus species it codes for six to ten genes.

All coronaviruses show a highly conserved order of genes, starting with the ORF 1a/b that covers two third of the whole genome and encodes the replicase complex, followed by the spike (S), the small envelope protein (E), the membrane protein (M) and the nucleocapsid protein (N) (see Figure 6).

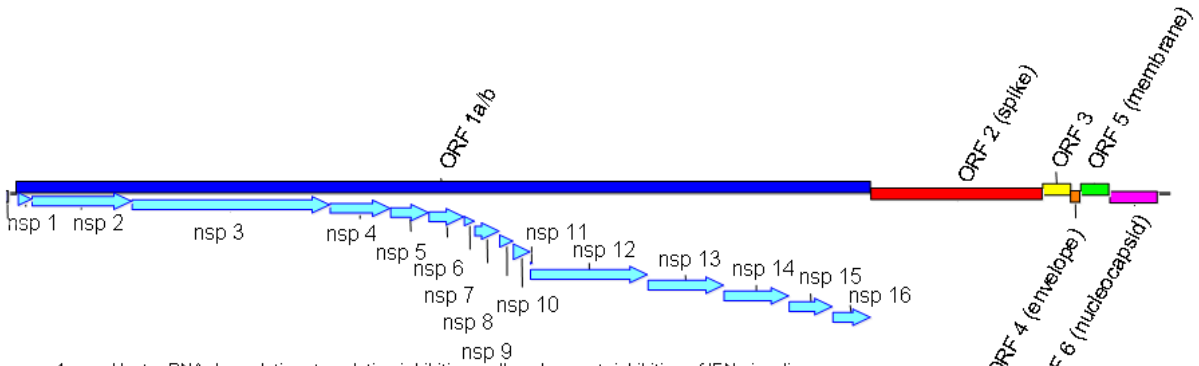

nsp 1	Host mRNA degradation; translation inhibition; cell cycle arrest; inhibition of IFN signaling
nsp 2	Unknown
nsp 3	Papain-like proteases (PL1pro, PL2pro) (polyprotein processing); poly(ADP-ribose) binding; DMV formation (?); IFN antagonist; nucleic acid binding; deubiquitinating activity
nsp 4	DMV formation (?)
nsp 5	Main protease (Mpro, 3CLpro); polyprotein processing
nsp 6	DMV formation (?)
nsp 7	Single-stranded RNA binding
nsp 8	Primase
nsp 9	Part of replicase complex
nsp 10	Part of replicase complex
nsp 11	Unknown
nsp 12	RNA-dependent RNA polymerase
nsp 13	Helicase; nucleoside triphosphatase activity; RNA 5'-triphosphatase activity
nsp 14	3'→5' exoribonuclease; RNA cap formation (guanine-N7)-methyltransferase
nsp 15	Endonuclease
nsp 16	RNA cap formation (2'O-methytransferase)

Figure 6: Genome organization of HCoV-NL63. Open reading frames (ORF) 1-6 and non-structural proteins (nsp) 1-16 with their putative functions. Function of nsps from SARS-CoV, see (Perlman et al. 2009).

Some of the coronavirus species carry additional genes like the hemagglutinin esterase (HE) acquired by some *Betacoronavirus* species (Lissenberg et al. 2005; Zeng et al. 2008). In particular SARS-CoV has a multitude of accessory open reading frames encoding proteins

3a, 3b, 6, 7a, 7b, 8a, 8b, and 9b. Most of those genes are groups-specific and dispensable for virus replication *in vitro* (McBride et al. 2012). A common accessory gene for most coronaviruses is ORF 3 (Tang et al. 2006). In case of HCoV-NL63 protein 3 is a glycosylated membrane protein that is incorporated into viral particles with yet unknown *in vivo* function (Muller et al. 2010). The role of some of the nsps (see Figure 6) and accessory proteins in coronavirus replication and life cycle is yet unknown.

1.2 Reverse genetics

A viral reverse genetics system is a tool to examine the role of specific genes and proteins in a whole virus context during the viral life cycle. The basic approach in reverse genetics is to alter the sequence of the gene of interest, create a genetically modified recombinant organism and compare the phenotype of the modified virus with that of the wild type (Almazan et al. 2000; Yount et al. 2000; Thiel et al. 2001; Gonzalez et al. 2002; Yount et al. 2002; Yount et al. 2003; Coley et al. 2005; Thiel et al. 2005; Almazan et al. 2006; Pasternak et al. 2006; Zust et al. 2007; Donaldson et al. 2008; Pfefferle et al. 2009; Cervantes-Barragan et al. 2010; Ribes et al. 2010; Tischer et al. 2012).

Using reverse genetics for plus strand RNA viruses requires the assembly of clones carrying the genome as complementary DNA (cDNA). Modifications are introduced *in vitro* on cDNA clone level. After transcription of RNA from the cDNA, the RNA is transfected into cells. The transfected cells produce modified virus particles, which can be further investigated (Semler et al. 1984; van der Werf et al. 1986; Rice et al. 1987).

Reverse genetics systems generally have a high potential not only to examine gene functions, but also to clone chimeric viruses. By that virus-host interactions as well as recombination and host-switching events can be investigated. This can contribute greatly to a better understanding of sudden shifts in pathogenesis and host range as occurred prior to the SARS-CoV outbreak in 2002/2003. Further promising applications lie in the development of vaccines using recombinant coronaviruses as vehicles for antigen delivery. Similar approaches were already successfully realized with TGEV and MHV (Zust et al. 2007; Cervantes-Barragan et al. 2010; Ribes et al. 2010).

As coronaviruses carry the largest single-strand RNA genome known to date, various pitfalls complicate the assembly of 27-32 kb in one cDNA clone (Almazan et al. 2000; Yount et al. 2000; Thiel et al. 2001). Genome size is the major challenge; additionally parts of the coronavirus genome appear to have toxic effects on *E. coli* leading to cloning and stability difficulties on cDNA clone level (Almazan et al. 2000; Yount et al. 2000; Thiel et al. 2001; Tischer et al. 2012).

A BAC-based cloning strategy was previously established to generate an infectious full-length SARS-CoV cDNA clone (Pfefferle et al. 2009). The full-length SARS-CoV cDNA genome was cloned into a BAC backbone, including a T7 polymerase promoter at the 5' end of the genome and a poly (A) tail at the 3' end. Linearized cDNA served as template for T7 driven *in vitro* transcription (IVT). The capped, polyadenylated infectious RNA was electroporated into mammalian cells and recombinant virus could be rescued. This approach combines the advantage of mutagenesis-friendly plasmid-based handling of the virus cDNA genome as well as the transfection of capped infectious RNA into the cytosol of the host cell, mimicking a natural virus infection (see Figure 7).

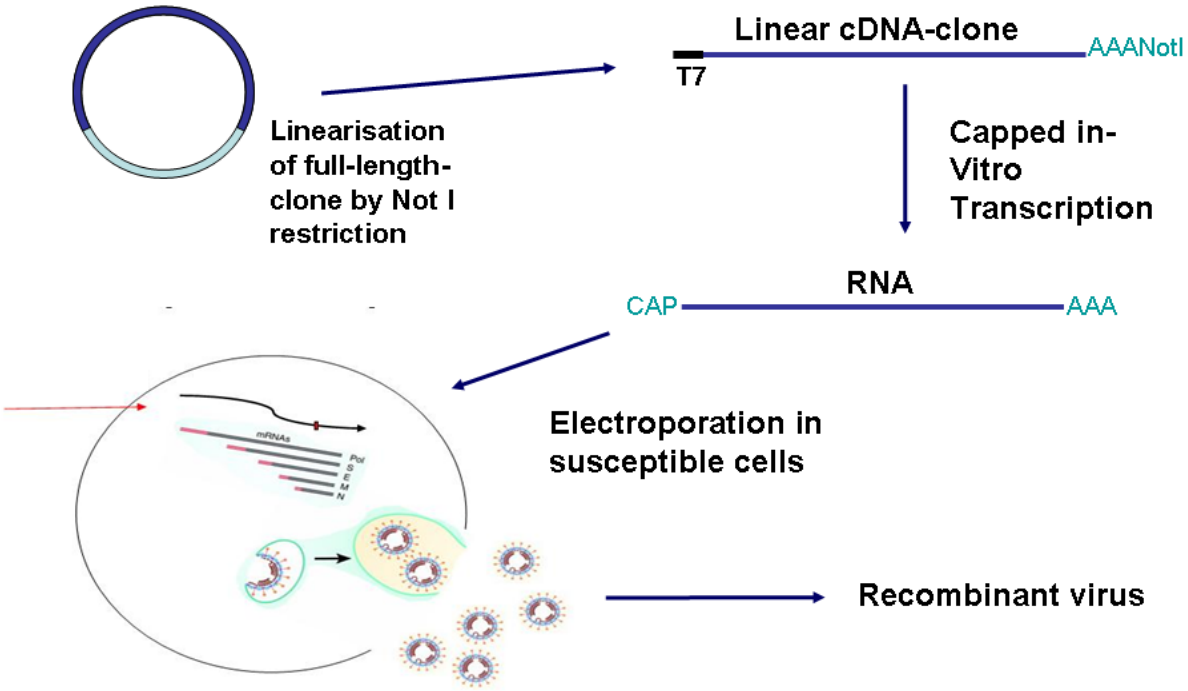

Figure 7: BAC-based reverse genetics system of SARS-CoV. Schematic illustration of SARS-CoV infectious cDNA clone. The virus full-length cDNA genome is integrated into a pBelo BAC backbone, a T7 promoter and a poly (A) tail are added at the 5' and 3' end, respectively. Linearized pBelo BAC serves as template for capped T7 driven *in vitro* transcription. RNA is electroporated into susceptible mammalian cells and recombinant virus is rescued.

1.3 Aim of the thesis

The aim of the thesis was the characterization and construction of a novel reverse genetics system for HCoV-NL63 strain Amsterdam 1 that is based on a BAC backbone, that uses phage promoter-driven *in vitro* RNA synthesis from a cDNA full-length clone, and that involves efficient transfection of infectious RNA into the cytosol of susceptible mammalian cells.

For this purpose sequence correctness of the parental HCoV-NL63 strain Amsterdam 1 had to be verified. Additionally, it was desirable to identify susceptible cell lines that support replication of HCoV-NL63 to higher titers and to develop a novel HCoV-NL63 plaque assay, serving as useful tool in the establishment of a reverse genetics system.

2 Material and Methods

2.1 Material

2.1.1 Equipment

Equipment	Type	Source
Autoclave	V 120	Systec, Wettenberg
Balance	SPO 61	Scaltec, Göttingen
	SBA 32	Scaltec, Göttingen
blue-light transilluminator	Flu-O-Blu	Biozym, Hess. Oldendorf
Centrifuges	Biofuge Pico	Heraeus, Hanau
	5804R	Eppendorf, Hamburg
	Sorvall Evolution RC	Thermo Fischer Scientific, Waltham, USA
Electroporation System	Gene Pulser Xcell	Bio-Rad Laboratories, Munich
Freezer	-20°C Liebherr premium	Liebherr, Biberach a. d. Riß
	-70°C	
	Liquid nitrogen LS 750	Taylor-Wharton, Mildstedt
Gel documentation	CCTV camera	Monacor international, Bremen
	Video graphic printer UP-895 CE	Sony, Berlin
	Monitor	Sony, Berlin
Gel electrophoresis	Mini-Sub Cell GT	Bio-Rad Laboratories, Munich
	PerfectBlue Gelsystem Mini M	PEQLAB, Erlangen
	Horizon 11.14	(Gibco BRL Life Technologies), Invitrogen, Karsruhe
Heating block	Thermomixer comfort	Eppendorf, Hamburg
Laminar flow	Gelaire BSB-4A	ICN Biochemicals, Eschwege
Incubators	INB 500	Memmert, Schwabach
	CB 150	Binder, Tuttlingen
Magnetic plate	Agencourt SPRIPlate Super Magnet Plate	Beckman Coulter, Krefeld
Magnetic stirrer	REO basic IKAMAG	IKA-Labortechnik, Staufen

Microscopes	Leitz Diavert	Leitz, Wetzlar
	Leica DM IL + DFC 320	Leica Microsystems, Wetzlar
Column loader for MultiScreen plates	Multiscreen Column Loader,45 µl	Millipore, Munich
Cell counting chamber	Neubauer	Roth, Karlsruhe
Photometer	BioPhotometer	Eppendorf, Hamburg
Pipette assistance	Accu-jet® pro	Brand, Wertheim
Pipettes	0,5-10 µl, 2-20 µl, 20-200 µl, 100-1000 µl	Eppendorf, Hamburg
Power supplies	E865 E425 E132	Consort, Turnhout, Belgium
Real-Time Cycler	LightCycler 1.5	Roche Diagnostics, Mannheim
	LightCycler 480	Roche Diagnostics, Mannheim
	ABI Prism 7000	Applied Biosystems, Carlsbad, USA
Refrigerator	Liebherr Premium	Liebherr, Biberach a. d. Riß
Rotating incubator	GFL-3033	GFL, Burgwedel
Sequencer	ABI PRISM® 3100 Genetic Analyzer	Applied Biosystems, Carlsbad, USA
Thermocycler	Mastercycler ep	Eppendorf, Hamburg
	Primus 25 advanced	PEQLAB, Erlangen
UV transilluminator	Bioview UXDT-40SL-15E	Biostep, Jahnsdorf
Vertical shaker	Mini Rocker MR-1	PEQLAB, Erlangen
Vortexer	Vortex VF2	IKA-Labortechnik, Staufen
Water bath	1002	GFL, Burgwedel

2.1.2 Chemicals

Item	**Source**
5-bromo-4-chloro-3-indolyl-beta-D-galactopyranoside (X-Gal)	Roth, Karlsruhe
Acetone	Roth, Karlsruhe
Agarose Broad Range	Roth, Karlsruhe
Agarose GTQ	Roth, Karlsruhe
Albumin from bovine serum	Roche Diagnostics, Mannheim
Ampicillin	Sigma-Aldrich, Munich

Ampuwa® (sterile water)	Fresenius Kabi, Bad Homburg
Bovine Serum Albumin (BSA)	New England Biolabs, Frankfurt am Main
Bromophenol blue (Tetrabromophenol sulfonephthalein)	Sigma-Aldrich, Munich
Calcium chloride (CaCl2)	Roth, Karlsruhe
Carbenicillin	Roth, Karlsruhe
Chloramphenicol	Sigma-Aldrich, Munich
Hydrochloric acid (HCl)	Roth, Karlsruhe
Chloroform	Roth, Karlsruhe
Crystal violet	Sigma-Aldrich, Munich
DakoCytomation	DakoCytomation, Glostrup, Denmark
Deionized water (Milli-Q)	Millipore, BNI
Diethylpyrocarbonate (DEPC)	Roth, Karlsruhe
Dimethyl sulfoxide (DMSO)	Roth, Karlsruhe
Disodium hydrogen phosphate	Merck, Darmstadt
dNTP set (dATP, dTTP, dGTP, dCTP)	Qiagen, Hilden
Ethanol (> 96%)	Roth, Karlsruhe
Ethidium bromide (10 mg/ml)	Roth, Karlsruhe
Ethylenediaminetetraacetic acid (EDTA)	Serva, Heidelberg
Formaldehyde (37%)	Roth, Karlsruhe
FuGENE ® HD transfection reagent	Roche Diagnostics, Mannheim
GelStar® Nucleic Acid Gel Stain	Lonza, Rockland, USA
Glycerol	Roth, Karlsruhe
Hi-Di™ Formamide	Applied Biosystems, Carlsbad, USA
Isopropyl alcohol	Roth, Karlsruhe
Isopropyl β-D-1- thiogalactopyranoside (IPTG)	Roth, Karlsruhe
Kanamycin	Sigma-Aldrich, Munich
LiChrosolv® (HPLC water)	Merck, Darmstadt
Magnesium chloride	Sigma-Aldrich, Munich
Opti-MEM®	Invitrogen, Karlsruhe
Phenol (Rotiphenol®)	Roth, Karlsruhe
POP-6™ Polymer for the 310 Genetic Analyzer	Applied Biosystems. Carlsbad, USA
Potassium chloride (KCl)	Roth, Karlsruhe
Potassium dihydrogen phosphate (KH_2PO_4)	Merck, Darmstadt

RNAlater	Qiagen, Hilden
Roti® Block	Roth, Karlsruhe
Saccharose	Roth, Karlsruhe
Sephadex G-50 Superfine	GE Healthcare, Munich
Sodium carbonate anhydrous	Roth, Karlsruhe
Sodium chloride (NaCl)	Roth, Karlsruhe
Sodium dodecyl sulfate (SDS)	Serva, Heidelberg
Sodium hydrogen phosphate (Na_2HPO_4)	Merck, Darmstadt
Sodium hydroxide (NaOH)	Roth, Karlsruhe
Sucrose	Sigma-Aldrich, Munich
Tris hydroxymethyl aminomethane (Tris)	Roth, Karlsruhe
Triton X-100	Sigma-Aldrich, Munich
Trizol®	Invitrogen, Karlsruhe
Trypsin	PAA, Cölbe
Tween® 20	Sigma-Aldrich, Munich
Xylene cyanol FF	Sigma-Aldrich, Munich

2.1.3 Consumables

Item	**Source**
96 well septa	Applied Biosystems, Carlsbad, USA
Cell culture flasks with filter cap (25 cm², 75 cm², 175 cm²)	Sarstedt, Nümbrecht
Cell culture plates (6-well, 24-well)	Sarstedt, Nümbrecht
Cell scraper	TPP, Trasadingen, Switzerland
Cover glass slides (12 mm, round)	Roth, Karlsruhe
Cryotubes	Sarstedt, Nümbrecht
Cuvettes (Eppendorf UVette®)	Eppendorf, Hamburg
Electroporation cuvettes (1 mm, 2 mm gap)	Biozym, Hess. Oldendorf
LightCycler® Capillaries, 20 µl	Roche Diagnostics, Mannheim
MultiScreen$_{HTS}$-HV Plates	Millipore, Schwalbach
Parafilm	Alcan Packaging, Neenah, USA
PCR reaction tubes 0,2 ml	Sarstedt, Nümbrecht
Petri dishes	Sarstedt, Nümbrecht
Pipette Tips (10 µl, 20 µl, 200 µl, 1000 µl)	Sarstedt, Nümbrecht
Reaction tubes (1.5 ml, 2 ml)	Sarstedt, Nümbrecht
Reaction tubes, safe lock (1.5 ml, 2 ml)	Eppendorf, Hamburg

Reaction tubes (15 ml, 50 ml)	Sarstedt, Nümbrecht
Scalpel	B. Braun Aesculap, Tuttlingen
Seropipettes (5 ml, 10 ml, 25 ml)	Sarstedt, Nümbrecht
Sterile filtration unit (Stericup and Steritop)	Millipore, Schwalbach
Sterile filter (0.22 µm)	Sarstedt, Nümbrecht

2.1.4 Buffer/Solutions

Name	Composition	Source
6x Loading Dye	40% Sucrose 0.15% Bromophenol blue 0.15% Xylene cyanol FF In deionized water	-
Crystal violet stock solution	20 g/l crystal violet 100 ml/l Formaldehyde (37%) 200 ml/l Ethanol (>96%) In deionized water	-
Crystal violet working solution	100 ml/l Crystal violet stock solution 100 ml/l Formaldehyde (37%) In deionized water	-
Diethylpyrocarbonate (DEPC) water	0.1% DEPC (v/v) In deionized water	-
Phosphate buffered saline (PBS) 10x buffer	1.37 M NaCl 27 mM KCl 100 mM Na_2HPO_4 20 mM KH_2PO_4 pH 7.4 In deionized water	AccuGene; BioWhittaker, Rockland, USA
PBS 1x buffer	100 ml/l 10x PBS In deionized water	-
Tris-acetate-EDTA (TAE) 50x buffer	2 M Tris-acetate 0.05 M EDTA 1 M glacial acetic acid In deionized water pH 7.8	-
TAE 1x buffer	20 ml/l 50x TAE	-

	In deionized water
PBST	0.05% Tween 20 (v/v)
	In 1x PBS
0,1% Triton X-100	0.1% Triton X-100 (v/v)
	In 1x PBS
0,5% Triton X-100	0.5% Triton X-100 (v/v)
	In 1x PBS
Blocking solution	10% FCS (v/v)
	In 1x PBS
4% Formaldehyde	4% Formaldehyde (v/v)
	In 1x PBS

2.1.5 *E. coli* culture

2.1.5.1 Media

LB (lysogenic broth)	20 g/l in deionized water	Roth, Karlsruhe
LB Agar	35 g/l in deionized water	Roth, Karlsruhe
S.O.C. Medium		Invitrogen, Karlsruhe
Recovery Medium		Lucigen, Middleton, USA

2.1.5.2 Antibiotic Stock solutions

Carbenicillin	50 mg/ml in 50% Ethanol	Roth, Karlsruhe
Chloramphenicol	34 mg/ml in > 96% Ethanol	Sigma-Aldrich, Munich
Kanamycin	50 mg/ml in 0.9% sodium chloride	Sigma-Aldrich, Munich

2.1.5.3 Bacteria

Name	Genotype	Source
E. cloni 10G (supreme, elite) Electrocompetent cells	F- *mcrA* Δ(*mrr-hsd*RMS-*mcr*BC) *end*A1 *rec*A1 Φ80*dlac*ZΔM15 Δ*lac*X74 *ara*D139 Δ(*ara,leu*)7697 *gal*U *gal*K *rps*L *nup*G λ- *ton*A	Lucigen, Middleton, USA
One Shot® Stbl3™ chemically competent cells	F– *mcr*B *mrr hsd*S20(r_B–, m_B–) *rec*A13 *sup*E44 *ara*-14 *gal*K2 *lac*Y1 *pro*A2 *rps*L20(Str^R) *xyl*-5 λ– *leu mtl*-1	Invitrogen, Karlsruhe

One Shot® TOP10 chemically competent cells	F– *mcr*A Δ(*mrr-hsd*RMS-*mcr*BC) Φ80*lac*ZΔM15 Δ*lac*X74 *rec*A1 *ara*D139 Δ(*ara leu*) 7697 *gal*U *gal*K *rps*L (StrR) *end*A1 *nup*G	Invitrogen, Karlsruhe

2.1.6 Cell culture

2.1.6.1 Media and overlays

Name	Composition	Source
DMEM (Dulbecco's Modified Eagles Medium) high glucose (4,5 g/L)	100 ml/l Fetal Calf Serum (FCS) 10 ml/l 100x Penicillin/Streptomycin (Pen/Strep) 10 ml/l 100x MEM nonessential amino acids (MEM NEAA) 10 ml/l 100x L-glutamine 10 ml/l 100x Sodium pyruvate In DMEM	all PAA, Cölbe
OptiPro™ SFM (serum-free medium)	10 ml/l 100x L-glutamine	PAA, Cölbe
	10 ml/l 100x Pen/Strep	PAA, Cölbe
	in OptiPro™ SFM	Invitrogen, Karlsruhe
2x DMEM	13.54 g/l INSTAMED DMEM dry powder	Biochrom, Berlin
	200 ml/l FCS	PAA, Cölbe
	20 ml/l 100x Pen/Strep	PAA, Cölbe
	20 ml/l 100x MEM NEAA	PAA, Cölbe
	20 ml/l 100x L-glutamine	PAA, Cölbe
	20 ml/l 100x Sodium pyruvate	PAA, Cölbe
	In DMEM	PAA, Cölbe
Avicel® RC581	2.4% Avicel® RC581 (w/v) In deionized water	FCM BioPolymer, Brussels, Belgium
Biozym Plaque Agarose	2% Plaque Agarose (w/v) In deionized water	Biozym, Hess. Oldendorf
Carboxymethyl-cellulose sodium salt (CMC)	1.6% CMC (w/v) In DMEM	BDH, Poole, UK PAA, Cölbe

Cryopreservation medium	10% DMSO (v/v)	Roth; Karlsruhe
	40% DMEM (v/v)	PAA, Cölbe
	50% FCS (v/v)	PAA, Cölbe

2.1.6.2 Cells

293lp	human embryonic kidney (ATCC CRL-1573),
BHK-J	Baby hamster kidney (cell culture collection of the BNI)
BSR-T7	BHK cell line constitutively expressing a T7 RNA polymerase, (BNI, originating from K.-K. Conzelmann, Ludwig-Maximilians-University Munich)
CaCo-2	human colon carcinoma (ATCC HTB-37)
Calu1	human lung carcinoma (ICLC HTL95002)
Calu6	human lung carcinoma (ICLC HTL97003)
FeA	feline embryonic fibroblast (kindly provided by Dr. Marcel Asper, NewLab Inc., Cologne)
LLC-MK2	rhesus monkey kidney (ATTC CCL-7, kindly provided by Lia van der Hoek, Academic Medical Center Amsterdam, The Netherlands).
PK 13	porcine kidney (cell culture collection of the Bernhard-Nocht-Institute (BNI)
POEK	porcine fetal kidney (cell culture collection of the Robert Koch-Institute (RKI), Berlin, Germany)
PS	porcine kidney cells (RKI)
RD	human rhabdomyosarcoma cells (RKI)
Vero E6	rhesus monkey kidney (ATCC CRL-1586)
Vero FM	rhesus monkey kidney (ATCC CCL-81)

2.1.6.3 Virus

Name	**Strain (Accession No.)**	**Source**
HCoV-NL63	Amsterdam 1, 8th passage (NC_00581)	Dr. Lia van der Hoek, Academic Medical Center (AMC) Amsterdam, The Netherlands

2.1.7 Kits

Name	**Source**
310 Running Buffer 10x	Applied Biosystems, Carlsbad, USA
Agencourt® AMPure®	Beckman Coulter, Krefeld
BigDye® Terminator v3.1 Cycle Sequencing Kit	Applied Biosystems, Carlsbad, USA
CloneSmart® Blunt LC Cloning Kit	Lucigen, Middleton, USA

GeneJET™ Plasmid Miniprep Kit	Thermo Fisher Scientific (Fermentas), St. Leon Roth
GeneRacer™ Kit	Invitrogen, Karlsruhe
mMessage mMachine® Kit T7 and SP6	Ambion (Applied Biosystems), Darmstadt
NucleoBond Xtra Midi	Macherey & Nagel, Düren
Opti-4CN™ Substrate Kit	Bio-Rad Laboratories, Munich
Phusion™ Site-Directed Mutagenesis Kit	NEB (Finnzymes), Frankfurt am Main
QIAamp Viral RNA Mini Kit	Qiagen, Hilden
QIAEX II Gel Extraction Kit	Qiagen, Hilden
QIAGEN OneStep RT-PCR Kit	Qiagen, Hilden
QuickChange® II XL Site-Directed Mutagenesis Kit	Agilent Technologies (Stratagene), Böblingen
SuperScript® III One-Step RT-PCR System with Platinum® Taq DNA Polymerase	Invitrogen, Karlsruhe
SuperScript™ One-Step RT-PCR with Platinum® Taq	Invitrogen, Karlsruhe
TOPO TA Cloning® Kit for Sequencing	Invitrogen, Karlsruhe

2.1.8 Enzymes

Name	**Source**
Herculase® II Fusion DNA Polymerase	Agilent Technologies (Stratagene), Böblingen
Phusion® High-Fidelity DNA Polymerase	NEB (Finnzymes), Frankfurt am Main
Platinum® Taq DNA Polymerase	Invitrogen, Karlsruhe
RNase H	Invitrogen, Karlsruhe
RNaseOUT™ Recombinant Ribonuclease Inhibitor	Invitrogen, Karlsruhe
SuperScript III® Reverse Transcriptase	Invitrogen, Karlsruhe
T4 DNA Ligase (5 U/µl)	Roche Diagnostics, Mannheim

2.1.9 Restriction Enzymes

Name	**Source**
AatII	NEB, Frankfurt am Main
AatII	Roche Diagnostics, Mannheim
AatII Fast Digest	Thermo Fisher Scientific (Fermentas), St. Leon Roth
BamHI	NEB, Frankfurt am Main
BamHI Fast Digest	Thermo Fisher Scientific (Fermentas), St. Leon Roth

BsaHI	NEB, Frankfurt am Main
BsrGI	NEB, Frankfurt am Main
EcoRI	NEB, Frankfurt am Main
EcoRI Fast Digest	Thermo Fisher Scientific (Fermentas), St. Leon Roth
FauI	NEB, Frankfurt am Main
KasI	NEB, Frankfurt am Main
MluI	NEB, Frankfurt am Main
NheI	NEB, Frankfurt am Main
NheI Fast Digest	Thermo Fisher Scientific (Fermentas), St. Leon Roth
NotI	NEB, Frankfurt am Main
NotI Fast Digest	Thermo Fisher Scientific (Fermentas), St. Leon Roth
PacI	NEB, Frankfurt am Main
PspOMI	NEB, Frankfurt am Main
SphI	NEB, Frankfurt am Main

2.1.10 Antibodies

2.1.10.1 Primary antibodies

Name	**Source**
Human Anti HCoV-NL63	Serum, BNI
Rabbit Anti M (HCoV-NL63)	(Muller 2007)
Rabbit Anti N (HCoV-NL63)	(Muller 2007)

2.1.10.2 Secondary antibodies

Name	**Source**
Donkey Anti-Rabbit IgG H & L Chain Specific Cy3 Conjugate	Dianova, Hamburg
Goat Anti-Human IgG H & L Chain Specific Peroxidase Conjugate	Merck (Calbiochem), Darmstadt
Goat Anti-Human IgG, H & L Chain Specific Fluorescein Conjugate	Merck (Calbiochem), Darmstadt

2.1.11 Molecular Weight Markers

Name	**Source**
GeneRuler™ 100bp Plus DNA Ladder (fragment sizes [bp]: 100, 200, 300, 400, **500**, 600, 700, 800, 900, **1000**, 1200, 1500,	Thermo Fisher Scientific (Fermentas), St. Leon Roth

2000, 3000)	
GeneRuler™ 1kb DNA Ladder (fragment sizes [bp]: 250, 500, 750, **1000**, 1500, 2000, 2500, **3000**, 3500, 4000, 5000, **6000**, 8000, 10000)	Thermo Fisher Scientific (Fermentas), St. Leon Roth
High Molecular Weight DNA Markers (fragment sizes [bp]: 8271, 8612, 10086, 12220, 15004, 17057, 19399, 22621, 24776, 29942, 33498, 38416, 48502)	Invitrogen, Karlsruhe
Supercoiled DNA Ladder, 2-10kb (band sizes [kb]: 2, 3, 4, **5**, 6, 7, 8, 9, 10)	Promega, Mannheim
Supercoiled DNA Marker Set (band sizes [kb]: 8, 13, 18, 23, 28)	Epicentre, Madison, USA

2.1.12 Plasmids and BACs

Name	Map	Source
pCR®2.1	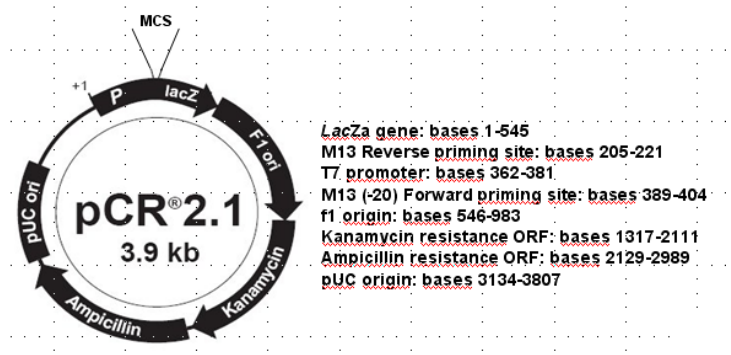 www.invitrogen.com	Invitrogen, Karlsruhe

pUC19

Invitrogen, Karlsruhe

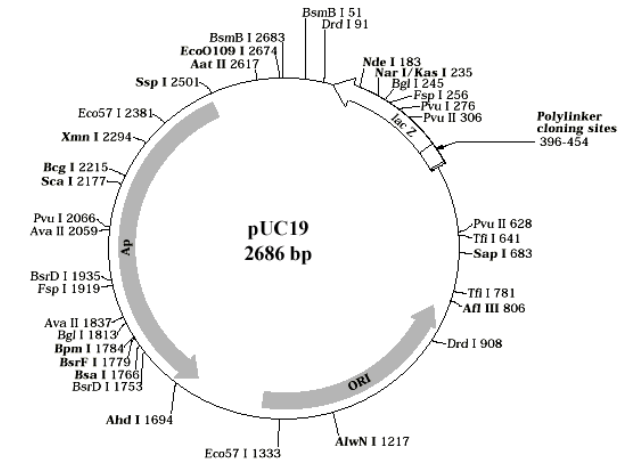

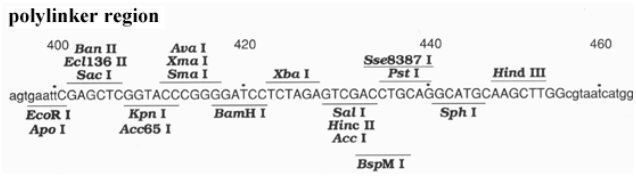

www.invitrogen.com

pBeloBAC11

NEB (Finnzymes), Frankfurt am Main

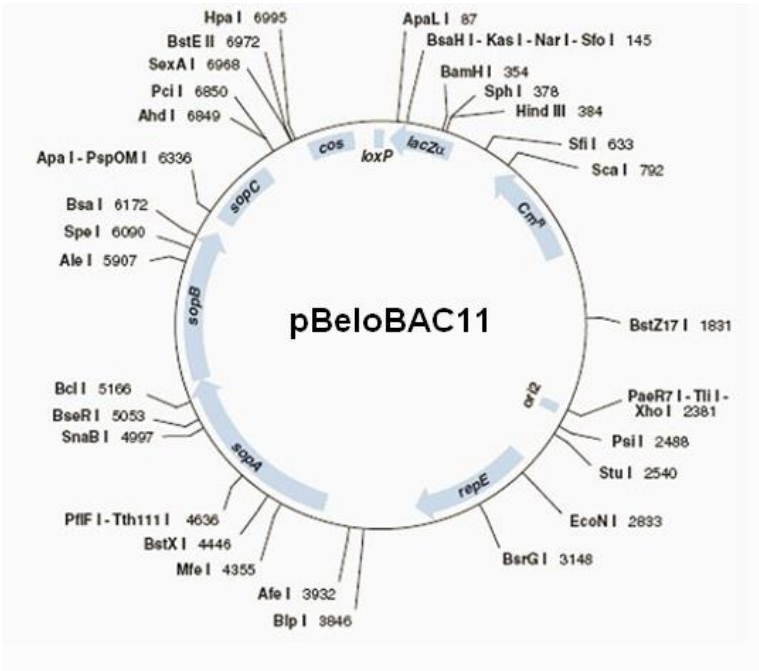

www.neb.com

pSMART® LCKan	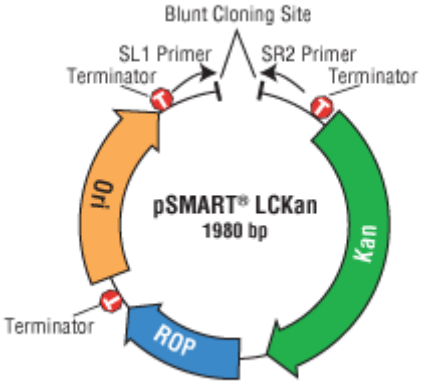 www.lucigen.com	Lucigen, Middleton, USA

2.1.13 Primer

2.1.13.1 NL63 forward primers

Names of primers correspond approximately to the 5’ nucleotide position of HCoV-NL63 GenBank Accession number NC_005831.

Name	Sequence
398F	GTAGCCGTTCGCGCTTATAG
1154F	CTGGTAATGTCGTTCCTGGTG
1928F	CTGTTATTGAACTTGCCACTG
2670F	CACTGCTGGTGTTTGCATCA
3100F	GAAGATGATGTTGTTACCAGTCT
3370F	GGTGAGTGTTGTATTTGTCA
4500F	GCTTTGTTTAGTTGTGACAT
B fw	TCTGTAGCTCCAGAAGTTGACTG
5730F	GACGTGTTGTTATTACCAATGT
6660F	TAGCTACATTTATTGTCTGCA
7010F	TCGTCTTTATAGTGGTGACACT
7430F	TGTCCGTTTATGACATTGCT
8290F	CTAGAGGTTTTGGCTTACGTACT
9091F	GACATGTTATATTCTCCACCTAC
10004F	CACTAGCTGAAGTTGTGAAGC
10458F	GTGTTCTCTTATAGCAGTTGC
10840F	CTTGGTATTGGTGGTGACCG
11566F	GGTTCTGTTCATTATGCTGGAG
12300F	GTATGGATGGTTACTGTAAGT
13105F	GCTTACCTAATATGGGTGTTCC
14040F	CTCCCTACTATGACACAGCTG
14467F	GTGGTACGACTTCTGGTGAC

15264F	ACTGTACTTCGTTGTGGTGA
15977F	AACCAAGAGAAGTATTCTAGC
16510F	CTCAACGTATGTGTGCTATAGG
17102F	GTCGTTGTCAGATCAGTTTAAGAC
18832F	GGGATTATGAAGCTGAAAGACC
E fw	ATGGATTTGTTGTTGGACGACT
20185F	GCACGTCTGTTAATACATCCTC
20836F	TGCTTCTAGTTCTTTTGACTG
21637F	TGTTGCTAGAACTGGCCAGT
22246F	GCTTGAAGCCACCTGGCATTAC
23001F	TGCTAACTTTCGATAGCAATGCT
23751F	GTTCGTGGTTCAAGACGCTTAGCAC
24465F	CTACAGGTTGTTGTGGTTGTTGC
24498F	CTTCATCAATGCGAGGCTGTTG
25873F	GTGATGGCTGCACCTACAGG
26519F	CGTAATCAGAAACCTTTGGAACC
26999F	GCTGAATTGATTCCTAATCAG

2.1.13.2 NL63 reverse primers

Names of primers correspond approximately to the 5’ nucleotide position of HCoV-NL63 GenBank Accession number NC_005831.

Name	Sequence
490R	ATCATCATCATTAATACCGGTTACAC
7520R	AGTATTAAAGTCCTTGACAC
11531R	CTCCAGCATAATGAACAGAACC
C rev	CTATAACAATTATCATACAGACGTC
14629R	CATCAATGAATGACTCTTCAACAC
18086R	ACAGTACCATTTGGCATCAG
18964R	TACGAACCCTGAATACTATTG
S22016R	ACCATTAAGAGATATATTAACCTG
22304R	CTCACGAATACCAGAGACAGG
25644R	AGACAAAGCTAGAACAAGTGGC
26096R	CTCCTGAGAGGCAACACCAG

2.1.13.3 Vector primers

Name	Sequence
pBelo	
pBelo790F	CATTAAGCATTCTGCCGACATG
pBelo 1050R	GCAAGATGTGGCGTGTTACGGTGA
pBelo1290R	CCTATAACCAGACCGTTCAGCTGGA
pBeSCfwd	GCCCTTAAACGCCTGGTTGCTAC
pBeSCrev	CGACAGGTGCTGAAAGCGAGC
pBeSCrev_1	CTTTCCGGTGATCCGACAGG

pBeSCrev_2	GAATGAACAATGGAAGTCCGAGC
pBELO Seq1	CCAGGGCTTCCCGGTATC
pBELO Seq2	GAACAACCTAATGAACACAGAACC
pBELO Seq3	GGAAGCCAGTAAGGATATACG
pBELO Seq4	GCAGTTTGTCACAGTTGATTTCC
pBELO Seq5	ATTGCGACGTGCTGAAGACG
pBELO Seq6	GAAGTTGGTAAAGGTCAGATCC
pBELO Seq7	GTATCAACACCGCCAAATTGC
pBELO Seq8	CCCACTGTTCCACTTGTATCG
pBELO Seq9	CCCGTATTCAGTGTCGCTG
pSMART	
SL1	CAGTCCAGTTACGCTGGAGTC
SR2	GGTCAGGTATGATTTAAATGGTCAGT
pCR 2.1	
M13 reverse	CAGGAAACAGCTATGAC
M13 forward	GTAAAACGACGGCCAG
GeneRacer Kit	
GeneRacer™ 5′ Primer	CGACTGGAGCACGAGGACACTGA
GeneRacer™ 5′ Nested Primer	GGACACTGACATGGACTGAAGGAGTA

2.1.13.4 Construction primers

Names of primers correspond approximately to the 5’ nucleotide position of HCoV-NL63 GenBank Accession number NC_005831.

Fragment A0	
NL63T7fwd +pspom Mlu	atgct**GGGCCCACGCGT**taatacgactcactatagcttaaagaatttttctatct
490R_lang_AatII	cagatgctg**GACGTC**atcatcatcattaataccggttacac
Fragment A	
NL 350 F*	gccattccttctgtagccgt
NL4000R_AatII*	tcatgc**GACGTC**tcaccagcttctatttctacactatg
Fragment B1	
NL3716F*	gttggttgtttgttttggattatg
NL3716FplusMluI	atgct**ACGCGT**gttggttgtttgttttggattatg
NL7520R_2+AatII*	ttatgc**GACGTC**aagagtattaaagtccttgacaccc
Fragment B2	
NL7430FplusMluI	atgct**ACGCGT**tgtccgtttatgacattgct
NL 12460 R +Aat	tgatgc**GACGTC**ggttctagtcgagctgcact
Fragment C	
S12300plusMluI	atgct**ACGCGT**gtatggatggttactgtaagt
NL 14629 R	catcaatgaatgactcttcaacac
Fragment D	
NL 14507 F	ACATTAACAGGTTGCTTAGTGTCC
NL 21824 R plusNotI	tcatgc**GCGGCCGC**ctgcaagtgctcacactgc

Fragment E	
S 21637+Aat	agaatgctg**GACGTC**TGTTGCTAGAACTGGCCAGT
NL 25873 RplusNotI	tcatgc**GCGGCCGC**CCTGTAGGTGCAGCCATCAC
Fragment F	
NL 25644 F +Aat	agaatgctg**GACGTC**GCCACTTGTTCTAGCTTTGTCT
NL27553R+20t+NotI	atgctga**GCGGCCGC**ttttttttttttttttttttgtgtatccatatcaaaaacaatatcattaac
SP6 forward	
NL_SP6_F_Mlu	ggcc**ACGCGT**atttaggtgacactataggcttaaagaatttttctatctatag

* = 5'end phosphate; bold: restriction sites.

2.1.13.5 RT Real-Time PCR primers

63RF2	CTTCTGGTGACGCTAGTACAGCTTAT
63RP	FAM – CAGGTTGCTTAGTGTCCCATCAGATTCAT - TAMRA
63RR2	AGACGTCGTTGTAGATCCCTAACAT

2.1.13.6 Mutagenesis primers

Subclone AF	
ORF1_delAar_fw2	GTTCCTGGTAATGTCGTTCCTGGTG
ORF1_delAar_rev2	AACACAAAGTTTCTTAGCAGG**C**GTGC
ORF1a1b_delNhe_fw	TTTGCTGC**C**AGCACTGGTGTTATTG
ORF1a1b_delNhe_rev	TTTAACATCTTCTGTAACAGAAGCACC
ORF6delNhe_fw	CTAATAACTCATCTCGTGC**C**AGCAGTC
ORF6delNhe_rev	AGCGATCCTCAAACTCAACAACAGAG
NL63-pB-NLA3-mut494F	GTTGCAAGTGATT**C**GGAAATTTCAGG
NL63-pB-NLA3-mut494R2	AGCAAGTGTCACTTGATTGTAAAACATGG
Subclone C	
NL63-pB-C-mut2002F	GACAATACCATCAAAAACATCTTAAATCCATTGC
NL63-pB-C-mut2002R2	GCAATGGATTTAAGATGTTTTTGATGGTATTGTC
Subclone D	
D2936corFw	GCTTGCAATGTAAA**C**CGTTTTAATGTTG
D2936corRev	ATGTGCAGTGTCAGAAGTTTGTGCATAG
Subclone E	
pB_E_mut1562F_2	CAGACCAAGTAG**C**TGTTTATCAACAAAGC
pB_E_mut1562R_2	GTTGGTTACATGGTGTCACAATAAAAATGTTAC
pB_E_mut2503F_2	TACATACTGTTACTATTGCACTTAATAAGATTCAG
pB_E_mut2503R_2	TAGCCTCTGCAGTTT**G**TGTAATAGCATC
Deletion KasI subclone ADEF	
KasI_del_lang	tgacccgcTTGGCG**G**CGTGTTAAAACTTTTTGG
ADRP mutant subclone NLA3	
nsp3_NmutA_F	GAGGCGGTGTTGCACGTGCTATTGATATTTTG
nsp3_NmutA_R	CATGCAAGAGATTTTCA**GC**AGCAGCATTGACAAC

Bold: introduced mutations.

2.2 Methods

2.2.1 Molecular biology methods

Working with nucleic acids in general and with RNA in particular requires some precaution. To keep the risk of potential contamination with other nucleic acids as well as unspecific enzyme activities (RNase, DNase) low, plastic material was autoclaved (120°C and 1 bar pressure) and equipment like pipettes were decontaminated frequently. Additionally, only commercially available molecular grade water and guaranteed sterile and nuclease-free filter pipette tips were used for handling of RNA. If possible, commercially available kits and reagents were used to guarantee working with low contamination risk. In-house produced buffers and solutions for RNA handling were prepared with DEPC treated water.

2.2.1.1 RNA extraction

Viral RNA was extracted using the QIAamp Viral RNA Mini Kit (Qiagen) according to the manufacturers' instructions. Elution was carried out with 60 µl of pre-warmed (80°C) elution buffer. Total RNA from cells was extracted using Trizol Reagent (Invitrogen) according to the manufacturers' instructions. Additionally the RNA was routinely diluted 1:10 in sterile deionized water for downstream applications. Extracted RNA and dilutions thereof were stored at -20°C for short term and -80°C for long term.

2.2.1.2 Isolation of plasmid DNA

Bacteria were cultured in LB-broth (High copy plasmids only) or on LB-agarose plates (High copy plasmids and BAC) containing the appropriate antibiotic and harvested by centrifugation or scraping. Small scale isolation of high copy plasmids and BACs was done using the GeneJET™ Plasmid Miniprep Kit (Fermentas) according to the manufacturers' instructions. Mid-scale isolation of high copy plasmids and BACs was done using the NucleoBond Xtra Midi Kit (Macherey & Nagel) according to the manufacturers' instructions. Plasmid DNA was stored at -20°C or at -70°C for long term.

2.2.1.3 Purification of PCR products

Purification of PCR products was routinely done using Agencourt Ampure (Beckman Coulter). Prior to use the Ampure solution was mixed vigorously for 30 seconds using a Vortex. The 1.8 volumes of Ampure were added to one volume of a PCR reaction. Solutions were mixed well by pipetting up and down and incubated at room temperature. This step facilitates the binding of DNA to the Ampure beads. After 10 minutes the tube was transferred to a magnetic plate and incubated further 10 minutes to separate the beads from the supernatant. The supernatant was removed by pipetting and the beads were washed

twice with 200 µl of 70% ethanol. After air drying for 5 minutes, the beads and the DNA were resuspended in an appropriate volume of sterile deionized water. During this step the DNA elutes from the beads. The beads were separated from the DNA containing supernatant by incubation on the magnetic plate. The supernatant was carefully pipetted in a new tube and used immediately or stored at 4°C for short or -20°C for long term.

2.2.1.4 DNA extraction from agarose gels

After excision of DNA fragments from Broad Range agarose (Roth) gels with a scalpel the DNA was extracted using the QIAEX II Gel Extraction Kit (Qiagen) according to the manufacturers' instructions. The supernatant containing the DNA was generally used immediately for downstream applications.

2.2.1.5 Phenol/chloroform extraction and alcohol precipitation of nucleic acids (NAs)

For the generation of transcription- and transfection-quality DNA and RNA templates the elimination of any possible enzyme contamination is crucial. Therefore the linearized plasmids and the *in vitro* transcribed RNAs were extracted using phenol/chloroform as described in (Sambrook et al. 2001) with following modifications: Mixing was always carried out by inverting the tubes in order to prevent shearing of the long (> 35 kb) NA fragments. DNA was precipitated preferably over night at -20°C or pelleted immediately. RNA was always stored at -20°C for at least 15 minutes, preferably overnight.
RNA was always resuspended in Ambion water. For linearized plasmids the concentration was usually adjusted to 0.2 µg/µl. Concentration and purity of the samples was analyzed by agarose gel electrophoresis (2.2.1.6) and photometric analysis (2.2.1.7).
The DNA was used immediately or stored at -20°C. RNA was stored at -70°C.

2.2.1.6 Agarose gel electrophoresis of nucleic acids (NAs)

NAs have a negatively charged phosphate backbone. Therefore they can be separated by agarose gel electrophoresis. According to their size and conformation the NA fragments migrate through the gel matrix differently. The smaller the fragments and the more supercoiled the conformation, the faster is the mobility towards the anode.
The detection is performed with ethidium bromide which intercalates with nucleic acids and can be visualized by UV light. Samples were mixed with Loading Dye, the high content of sucrose keeps the aqueous NA solutions in the pocket of the gel and the dyes help visualizing the velocity of NA migration.
For standard gels GTQ agarose (Roth) was weighed and dissolved in TAE buffer by heating. Preparative gels were prepared with Broad Range agarose (Roth) and sterile TAE buffer. Dissolved agarose was cooled down and supplied with 0.5 µg/ml ethidium bromide. Samples

and appropriate molecular weight markers (2.1.11) were loaded onto the gel. Generally 0.8-2% agarose gels were used and run at 60-140 Volts. For some applications gels were stained with ethidium bromide or GelStar® Nucleic Acid Gel Stain (1:1000) post run.

2.2.1.7 Photometric analysis of nucleic acid concentration

Nucleic acids absorb monochromatic light and concentrations can thus be measured by photometry. Disposable plastic cuvettes (Eppendorf UVette®) with a thickness of 1 cm were used in a Biophotometer (Eppendorf). The blank was measured with a minimum of 50 µl water or the corresponding buffer. Samples were measured at a wavelength of 260 nm (maximum absorption of nucleic acids), 280 nm (maximum absorption of proteins and phenol) and 320 nm (maximum absorption of carbohydrates) to assess impurities.
For DNA a result of one compared to the reference means a concentration of 50 µg/ml and for RNA 40 µg/ml, respectively.
Formula for calculation: $C = (E_{260} – E_{320}) \times d \times f$ [µg/ml]
C = concentration
E = extinction
d = dilution factor
f = factor for DNA (50 µg/ml) and RNA (40 µg/ml) when using a 1 cm cuvette

2.2.1.8 Sequencing of DNA

Sequencing was done using the ABI PRISM® Big Dye® Terminator Cycle Sequencing Ready Reaction kit (Applied Biosystems) which is based on Sanger's method (Sanger et al. 1977). The 5x Sequencing Buffer was diluted to 2,5x with HPLC H_2O and stored at 4°C until usage. Big Dye Terminator Sequencing Ready Reaction Mix Version 3 was always stored at -20°C in small aliquots and thawed immediately before use to prevent repeated freeze/thaw cycles.
Templates for sequencing were obtained by generating PCR products (2.2.1.11) of the region of interest. Size, purity and quantity of the PCR products were analyzed using agarose gel electrophoresis (2.2.1.6) and purified using Ampure (see 2.2.1.3).
Big Dye Mix was prepared freshly prior to sequencing PCR as listed in Table 1 for one reaction (1 rxn).

Table 1: Big Dye Mix

1 rxn	
1 µl	Big Dye Ready Reaction Mix (2.5x)
3 µl	Sequencing Buffer (2.5x)

Sequencing PCR reaction (see Table 2) was supplied with 4 µl of the Big Dye Mix.

Table 2: Big Dye sequencing PCR reaction

1 rxn		
1-5 µl	PCR-Product	up to 100 ng
0-4 µl	H_2O	-
1 µl	Primer (10 µM)	1 µM
4 µl	Big Dye Mix (2,5x)	1x

The reaction was cycled as specified in Table 3.

Table 3: Big Dye sequencing PCR program

96°C	3 min	1x
96°C	30 sec	
50°C	15 sec	25x
60°C	4 min	

The protocol was done as described in (Etchevers 2007) with minor modifications.
PCR Products were purified with a quick clean up method using Sephadex G-50 superfine (GE Healthcare) and MultiScreen Filter plates (Millipore).
Dry Sephadex was added to a column loader (Millipore) and applied to a MultiScreen plate (Millipore). 300 µl HPLC-H_2O were added and the plate was incubated two hours at room temperature. After swelling, the excess water was removed by centrifugation (3000 rpm, 5 minutes); the sequencing PCR products were added and eluted into a clean plate by centrifugation (3000 rpm, 5 minutes). HiDi™ Formamide (12 µl) and 4.5 µl of purified PCR reaction were added to each well of a PCR multiwell plate. The plate was covered with a 96 well septum, centrifuged briefly and loaded in the 3100 Genetic Analyzer (Applied Biosystems). Processing was done according to the manufacturers' instructions using a 50 cm 16 capillary array with Performance Optimized Polymer POP-6. Settings for Dye Set Z and the default 50 cm POP-6 Run Module were chosen.

2.2.1.9 *In vitro* synthesis of capped RNA

For the *in vitro* synthesis or *in vitro* transcription (IVT) of capped full-length virus RNA the Ambion mMESSAGE mMACHINE® kit was used. The manufacturers' protocol was adapted to long templates and high yield by supplying additional GTP, increasing the reaction volume and the incubation time:
The 10x buffer, 2x NTP/Cap and GTP were thawed, mixed and centrifuged briefly prior to use. The 2x NTP/Cap, GTP and the enzyme mix were then placed on wet ice. Short term storage of the 10x buffer and the assembly of the reaction were done at room temperature

(Table 4).

Table 4: mMessage mMachine IVT reaction setup

1 rxn T7/SP6 (30 µl)	Reagent	2 rxn SP6 (N)
15 µl	2x NTP/Cap	20 µl
3 µl	10x Buffer	4 µl
4 µl	GTP	2 µl
3 µl	Enzyme Mix	4 µl
25 µl	Sum	2x 15 µl
5 µl	Template (1 µg)	2x 5 µl

Purified PCR products (2.2.1.3) or linearized plasmids (2.2.1.20) served as template DNA. The reactions were mixed by pipetting or flicking and spinning down. Reaction tubes were incubated at 37°C in an incubator or a heating block (Thermomixer, Eppendorf). After approximately 2 hours of incubation 1 µl Turbo-DNase was added and the reaction was mixed by tapping and spinning or pipetting. The enzymatic reaction was stopped after 15 minutes by adding ammonium acetate stop solution and water (Table 5):

Table 5: Stopping of *in vitro* synthesis

1 rxn T7/SP6	Reagent	SP6 (N, pool 2 rxn)
30 µl	Sum IVT reaction	40 µl
15 µl	AmAc Stop Solution	15 µl
105 µl	Ambion H_2O	95 µl
150 µl	Total	150 µl

Reactions were mixed by pipetting and purified by phenol/chloroform extraction and isopropyl alcohol precipitation according to 2.2.1.5.

2.2.1.10 cDNA synthesis

RNA dependant DNA polymerases like MMLV RT (Moloney Murine Leukemia Virus Reverse Transcriptase) synthesize cDNA from an RNA template. This process is called reverse transcription (RT). The SuperScript III® Reverse Transcriptase Kit was used in combination with RNaseOUT™ Recombinant Ribonuclease Inhibitor and RNase H (all Invitrogen). The protocol was based on the manufacturers' instruction and adapted to long cDNA products. For the assembly of the reaction two master mixes were prepared (Table 6):

Table 6: Assembly of cDNA synthesis master mix 1 and 2

Mix 1	1 rxn	Mix 2	1 rxn
dNTPs (10 mM)	1 µl (0.5 mM)	5x First Strand Buffer	4 µl
Reverse Primer (10 µM)	1 µl (0.5 µM)	0.1 M DTT	1 µl (5 mM)
H2O	4 µl (4-8 µl)	Superscript III (200 U/µl)	2 µl (400 U)
BSA (1 mg/ml)	1 µl (1 µg)	RNase out (40 U/µl)	1 µl (40 U)
RNA	5 µl (1-5 µl)		
Total	12 µl	Total	8µl
Total Mix 1 + 2	20 µl		

After assembly Mix 1 was mixed well by pipetting and heated to 65°C for five minutes using a thermocycler. This step allows denaturation of the RNA and annealing of the reverse primer. After cooling of Mix 1 to 4°C Mix 2 was added, the reaction was mixed by pipetting and heated to 55°C for 60 minutes to allow cDNA synthesis. The enzymes were inactivated at 75°C for 5 minutes. After inactivation the reaction mix was cooled to 4°C. RNase H was added (1 µl, 2 U) to degrade the remaining RNA. The reaction was mixed by pipetting and incubated at 37°C for 15 minutes. cDNA was used immediately or stored at -20°C.

2.2.1.11 PCR using Phusion Enzyme

Generally PCRs were done using Phusion® High-Fidelity DNA Polymerase (Finnzymes). This enzyme is a *Pyrococcus*-like DNA-polymerase, combining a proofreading activity with enhanced processivity. PCR products have blunt ends and are therefore unsuitable for TA-Cloning. The PCR was setup as listed in Table 7.

Table 7: PCR setup using Phusion enzyme

Reagent	1 rnx
H_2O	to 25 µl
5x Phusion HF Buffer	5 µl
dNTPs (10 mM)	0.5 µl (0.2 mM)
Forward primer (10 µM)	0.5 µl (0.2 µM)
Reverse primer (10 µM)	0.5 µl (0.2 µM)
Phusion (2 U/µl)	0.25 µl (0.5 U)
Template	1-5 µl (1 pg-50 ng)

Cycling was done as specified in Table 8.

Table 8: PCR program using Phusion enzyme

Step	Temperature	Time
Initial denaturation	98°C	20 sec
	30 cycles	
Denaturation	98°C	10 sec
Annealing	58°C	20 sec
Elongation	72°C	15 sec/ 1 kb
Final elongation	72°C	30 sec/ 1 kb
Cooling	4°C	Forever

2.2.1.12 PCR using Platinum Taq

PCR products with A overhangs for TA cloning were generated with Platinum® *Taq* (*Thermus aquaticus*) Polymerase (Invitrogen). It has a non-template-dependent terminal transferase activity that adds a single deoxyadenosine (A) to the 3' ends of PCR products. Like standard *Taq*, it has both 5' to 3' polymerase and 5' to 3' exonuclease activity. PCR was setup as listed in Table 9 and the cycling program was done as specified in Table 10.

Table 9: PCR setup using Platinum *Taq*

Reagent	1 rnx
H_2O	to 50 µl
10x PCR Buffer	5 µl
dNTPs (10 mM)	1 µl (0.2 mM)
$MgSO_4$ (50 mM)	2 µl
Forward primer (10 µM)	1 µl (0.2 µM)
Reverse primer (10 µM)	1 µl (0.2 µM)
Platinum Taq (5 U/µl)	0.2- 0.5 µl (1- 2.5 U)
Template	1-5 µl (1 pg-50 ng)

Table 10: PRC program using Platinum *Taq*

Step	Temperature	Time
Initial denaturation	94°C	2 min
	35 cycles	
Denaturation	94°C	25 sec
Annealing	55°C	25 sec
Elongation	72°C	1 min/ 1 kb

2.2.1.13 PCR using Herculase enzyme

Herculase II Fusion DNA polymerase was used to generate long PCR fragments from cDNA templates. The enzyme is *Pfu*-based (*Pyrococcus furiosus*) and has a proofreading activity (3' to 5' exonuclease activity). PCR was setup as listed in Table 11 and cycled according to Table 12.

Table 11: PCR setup using Herculase enzyme

Reagent	1 rnx
H_2O	to 50 µl
5x Herculase II Buffer	10 µl
dNTPs (25 mM)	0.8 µl (0.4 mM)
Forward primer (10 µM)	2 µl (0.4 µM)
Reverse primer (10 µM)	2 µl (0.4 µM)
Herculase II Fusion Polymerase	1 µl
Template	1-10 µl cDNA

Table 12: PCR program using Herculase enzyme

Step	Temperature	Time
Initial denaturation	94°C	2 min
	35 cycles	
Denaturation	94°C	15 sec
Elongation	68°C	30 sec/ 1 kb

2.2.1.14 One-step RT-PCR

For the generation of PCR products directly from RNA, a one-step reverse transcription PCR (one-step RT-PCR) was used. One-step RT PCR Kits contain buffers, dNTPs and a mixture of two (or more) polymerases. The RNA-dependent DNA polymerase (reverse transcriptase) synthesizes the cDNA and a hot-start DNA-dependent DNA polymerase (*Taq* polymerase) exponentially amplifies the cDNA template. Hot-start *Taq* polymerases are inactivated by either antibodies or chemical modifications. Heating of the reaction mix to 95°C activates the enzyme, thus enabling an unbiased reverse transcription beforehand.
One-step RT-PCRs using the QIAGEN OneStep RT-PCR Kit were setup as listed in Table 13 and cycled according to Table 14.

Table 13: QIAGEN One-Step RT-PCR setup

Reagent	1 rnx
H_2O	to 25 µl
5x OneStep RT-PCR Buffer	5 µl
dNTPs (10 mM)	0.5 µl (0.2 mM)
Forward primer (10 µM)	0.5 µl (0.2 µM)
Reverse primer (10 µM)	0.5 µl (0.2 µM)
OneStep RT PCR Enzyme Mix	1 µl
Template	1-5 µl (1 pg-2 µg)

Table 14: QIAGEN One-Step RT PCR program

Step	Temperature	Time
Reverse transcription (RT)	50°C	15-30 min
Initial denaturation	95°C	15 min
	30-45 cycles	
Denaturation	95°C	15 sec
Annealing	55°C	15 sec
Elongation	72°C	1 min/ 1 kb
Cooling	4°C	Forever

2.2.1.15 Real-time RT PCR

The real-time RT PCR is a one-step RT PCR that allows the detection of amplification products in real-time during the amplification process. Special oligonucleotides linked with fluorescent dyes (probes) are added to the reaction mixture. The probes hybridize with the nascent PCR strands and fluorescent dyes are released by the 5' to 3' exonuclease activity of the *Taq* polymerase. These dyes can be detected during the cycle process using special real-time cyclers and the gain in fluorescence is diagrammed by special software. The cycle number, at which the fluorescence rises above the background or threshold level, is referred to as crossing point (Cp) or crossing threshold (Ct). By adding standard samples with known RNA concentration, the unknown samples can be quantified. In a logarithmic dilution series and under optimal PCR conditions the Cp between two ten-fold dilutions is 3.3.
For the analysis of RNA in real-time the SuperScript™ One-Step RT-PCR with Platinum® *Taq* and the SuperScript® III One-Step RT-PCR System with Platinum® Taq DNA Polymerase Kits (both Invitrogen) were used. Table 15 shows the real-time RT PCR setup.

Table 15: Real-Time RT PCR setup

Reagent	1 rnx
H_2O	to 25 µl
2x Reaction mix	12.5 µl
$MgSO_4$ (50 mM)	2 µl (4 mM)
BSA (1 mg/ml)	1 µl (1 µg)
Forward primer (10 µM)	0.5 µl (0.2 µM)
Reverse primer (10 µM)	1 µl (0.4 µM)
Probe (10 µM)	1 µl (0.4 µM)
Superscript RT/Platinum *Taq* Mix	0.5 µl
Template	5 µl

The cycling conditions are listed in Table 16.

Table 16: Real-Time RT PCR program

Step	Temperature	Time
Reverse transcription (RT)	45°C	20 min
Initial denaturation	95°C	2 min
45 cycles		
Denaturation	95°C	15 sec
Annealing & Elongation	60°C	30 sec (acquisition)
Cooling	40°C	30°C

Samples were only stored for troubleshooting in case of doubtful results.

2.2.1.16 Phusion mutagenesis PCR

Positive clones up to a size of 15 kb were corrected or mutated using the Phusion™ Site-Directed Mutagenesis Kit (Finnzymes). Primers were designed according to the manufacturers' recommendations. The mutagenesis PCR was adapted to long products (see Table 17) and cycled as listed in Table 18.

Table 17: Phusion mutagenesis PCR setup

Reagent	1 rnx
H_2O	to 50 µl
5x Phusion HF Buffer	10 µl
dNTPs (10 mM each)	2 µl (0.4 mM)
Forward primer (10 µM)	1 µl (0.2 µM)
Reverse primer (10 µM)	1 µl (0.2 µM)
Phusion Hot Start DNA Polymerase (2 U/µl)	1 µl (2 U)
Template	1 µl (10-20 ng)

Table 18: Phusion mutagenesis PCR program

Step	Temperature	Time
Initial denaturation	98°C	30 sec
25 cycles		
Denaturation	98°C	10 sec
Annealing	58-62°C	20 sec
Elongation	72°C	30 sec/ 1 kb
Final elongation	72°C	45 sec/ 1 kb
Cooling	4°C	Forever

Mutagenesis PCR Products were analyzed using agarose gel electrophoresis and ligated according to Table 19.

Table 19: Phusion mutagenesis ligation setup

Reagent	1 rnx
H_2O	to 10 µl
PCR Product	1 µl (25 ng)
2x Quick Ligation Buffer	5 µl
Quick T4 DNA Ligase	0.5 µl

The ligation reaction was incubated for not longer than 2 hours at room temperature, then chilled on wet ice and either used immediately for transformation of *E. coli* cells or stored at -20°C. Transformation and downstream applications were done as depicted in chapter 2.2.1.22 and 2.2.1.24.

2.2.1.17 Quick Change mutagenesis PCR

Positive clones up to a size of 10 kb were corrected or mutated using the QuickChange® II XL Site-Directed Mutagenesis Kit (Stratagene) following the instruction manual. Primers were designed according to the manufacturers' recommendations.

2.2.1.18 Sequencing and genome size verification using Phusion polymerase

For verification of full-length pBelo BACs and generation of PCR products for sequencing, eight PCRs were performed per full-length BAC. The PCR setup was done as described in 2.2.1.11, primers were used as listed in Table 20. The calculated product sizes were compared with the PCR product sizes using agarose gel electrophoresis (2.2.1.6).

Table 20: Phusion polymerase PCR primers and products for sequencing and genome size verification

No	Primer fw	Primer rev	Product size (bp)
1	pBSCrev	4000R	4219
2	3370F	7520R	3780
3	7010F	11531R	4583
4	10458F	14629R	4207
5	14040F	18086R	4026
6	17903F	S22016R	4157
7	21637F	25644R	4029
8	24465F	pBSCfw	3257

2.2.1.19 RNA ligase-mediated rapid amplification of cDNA ends (RLM-RACE)

The RLM-RACE is a method for sequencing and cloning of unknown 5' and 3' ends from viral RNA or mRNA. The GeneRacer™ Kit (Invitrogen) was used and primers were designed according to the manufacturers' instructions.
The 5' and 3' end PCR products they were either sequenced directly or first cloned and subsequently sequenced.

2.2.1.20 Restriction and dephosphorylation

Restriction enzymes cut DNA at or in the vicinity of a specific recognition site. Using enzymes that leave non-compatible 3' or 5' overhangs in vector and insert DNA allows unidirectional cloning. Screening for orientation is obsolete.
Dephosphorylation means the hydrolysis of the 5' phosphate of DNA. Vector DNA was dephosphorylated in order to prevent religation. As the 5' phosphate is necessary for a successful ligation only plasmids with inserts should be formed.

Restriction was done according to the manufacturers' instruction. If possible and proved functional, double digestion was performed. Fast Digest (Fermentas) enzymes were applied with a ratio of one Unit per microgram DNA. All other enzymes were applied in excess paying tribute to the supercoiled nature of the template plasmid DNA. Restriction success was monitored by agarose gel electrophoresis (2.2.1.6).
After restriction the fragments were dephosphorylated if necessary, purified and concentrated by alcohol precipitation and separated by agarose gel electrophoresis (2.2.1.6), excised and extracted (2.2.1.4). Subsequent downstream applications, usually ligations, were initiated immediately. For short term storage the restriction reaction was frozen as a mixture with salt and alcohol (see 2.2.1.5) at -20°C.

2.2.1.21 Ligation

Ligation of DNA fragments was either done according to the Kit manufacturers' instructions or with T4 DNA Ligase (high concentrated, 5 U/µl) (Roche) as listed in Table 21.

Table 21: Ligation setup with Roche T4 DNA ligase

Reagent	1 rxn
10x Ligase buffer	1 µl
DNA fragments	0.5 - 7.50 µl
H_2O	0 - 7 µl
DNA ligase 1:10 (0.5 U/µl)	1.5 µl (0.75 U)

The ligation reactions included up to three different DNA fragments. They were incubated for >16 hours (overnight) at 14°C and used for the transformation of *E. coli* cells without further modification or inactivation (see 2.2.1.22, 2.2.1.24).

2.2.1.22 Cloning

The TOPO TA Cloning® Kit for Sequencing (Invitrogen) was used for TA cloning according to the manufacturers' instructions. The CloneSmart® Blunt LC Cloning Kit (Lucigen) was used for blunt end cloning according to the manufacturers' instructions.
Cloning with the pBelo BAC (2.1.12) comprised different modifications of the vector for the adaptation to the HCoV-NL63 cloning strategy. For this approach modified pBelo BAC11 vectors pBelodNco3 and pBeloAd4 were used.
Vector pBelodNco3 was created by excision of 613 bp, containing the multiple cloning site (MCS), from pBelo BAC11 using a digestion with *NotI*. A new MCS was introduced by an oligonucleotide adapter containing *NsiI*, *BsaHI*, *SphI* and *NotI* restriction sites in sequence, resulting in pBeloAd4.The excision of *cos*, *loxP* and *lacZ* containing the MCS as well as the addition of a new multiple cloning site was done as described previously (Pfefferle et al.

2009).

2.2.1.23 Preparation of media for bacteria culture

Media for the cultivation of bacteria were prepared according to the manufacturers' instructions. The pre-mixed dry medium was weighed, dissolved in an appropriate volume of deionized water and autoclaved (120°C and 1 bar pressure). LB agar was cooled to 50°C, supplemented with the appropriate antibiotics and poured into Petri dishes. After cooling for several hours the plates were stored at 4°C. LB broth was only used intermittently and therefore stored at 4°C without antibiotics. These were added from stock solutions immediately before use to guarantee full effectiveness. Antibiotics from stock solutions were added to a concentration of 50 µg/ml (carbenicillin, kanamycin) and 12.5 µg/ml (chloramphenicol) in working solution.

2.2.1.24 Production of competent *E. coli* cells and transformation

For transformation of *E. cloni* 10G electrocompetent cells and One Shot® TOP10 chemically competent cells original stocks were used.
One Shot® Stbl3™ chemically competent cells were initially purchased and then generally produced in-house:
Conical flasks containing LB medium were inoculated with 1/1000 (v/v) of an overnight *E. coli* culture. The culture was grown at 37°C with 160 rpm (GFL-3033) until an OD_{600} of 0.5-0.7 was reached (after approximately 2 hours). Cells were cooled down shaking on wet ice and incubated at 4°C for 15 minutes. They were harvested by centrifugation at 4°C and 3000 rpm in a pre-cooled centrifuge (Sorvall Evolution RC) for 15 minutes. The supernatant was discarded; cells were resuspended in 50 ml of 80 mM $CaCl_2$ on wet ice and incubated at 4°C for 40 minutes. Cells were pelleted again as described above. The supernatant was removed carefully and the cells were resuspended in 5 ml 80 mM $CaCl_2$ supplemented with 20% glycerol. Aliquots of 100 µl were dispensed in pre-chilled 1.5 ml reaction tubes and deep-frozen immediately using either liquid nitrogen or dry ice. Aliquots were stored at -70°C until usage. Test transformations were done with a pUC19 plasmid originally provided by the manufacturer (Invitrogen). Electrocompetent *E. cloni* cells were transformed according to the manufacturers' instructions using the Gene Pulser Xcell (Bio-Rad).
Chemically competent cells were thawed completely on wet ice, in-house produced Stbl3 were split in two 50 µl aliquots and commercially supplied cells were treated as indicated in the manual. Up to 5 µl (or 100 ng) of plasmid DNA or a ligation reaction were added to the cells and mixed by gentle stirring with the pipette tip. Cells were incubated on ice for 30 minutes and heat-shocked for 30 or 45 seconds in a heating block (Thermomixer comfort, Eppendorf). Immediately after the heat shock cells were incubated on ice for two minutes.

275 µl of pre-warmed S.O.C. medium was added to the cells and they were further incubated at 37°C for one hour in a heating block at 350 rpm (Thermomixer comfort, Eppendorf). Cells were spread on selective agar plates using different volumes and incubated over night at 37°C. Single colonies were transferred to fresh plates with appropriate antibiotics and incubated until plasmid DNA preparation (2.2.1.2) or additionally directly screened by PCR.

2.2.1.25 High-copy plasmid culture

E. coli (TOP10) containing high-copy plasmids like pCR 2.1 were either cultivated on one eighth of a selective agar plate or in 2 ml of LB broth supplemented with the appropriate antibiotics. The cells were incubates over night at 37°C and harvested as described in 2.2.1.2.

2.2.1.26 BAC culture

Cultivation of *E. coli* (Stbl3, *E. cloni*) containing BACs was always done using agar plates. For small scale plasmid DNA preparation one quarter of a selective agar plate was inoculated with bacteria from a single colony. For medium scale plasmid DNA preparations five to ten agar plates were plated. The bacteria were incubated over night at 37°C and harvested as described in 2.2.1.2.

2.2.2 Cell culture Methods

2.2.2.1 Preparation of media and solutions

Cell culture media and solutions were always prepared under sterile conditions. If possible commercially available, sterile and endotoxin free products were used.
Fetal calf serum (FCS) was inactivated for 30 minutes at 56°C, sterilized by filtration (Stericup, Millipore) and stored in 50 ml aliquots at -20°C until usage.
Dulbecco´s Modified Eagles Medium (DMEM) was supplemented with 100 ml/l FCS, MEM NEAA (L-alanine 890 mg/l, L-asparagine 1320 mg/l, L-aspartic acid 1330 mg/l, L-glutamic acid 1470 mg/l, L-glycine 750 mg/l, L-proline 1150 mg/l, L-serine 1050 mg/l), L-glutamine (2 mM), sodium pyruvate (1 mM) and penicillin/streptavidin (100 Units/ml and 0.1 mg/ml) under sterile conditions (2.1.6.1).
OptiPro SFM was supplemented with, L-glutamine (2 mM) and penicillin/streptavidin (100 Units/ml and 0.1 mg/ml) under sterile conditions.
Double concentrated DMEM (2x DMEM) was produced by adding 13.54 g/l powdered DMEM (Biochrom) to a bottle of liquid DMEM. Supplements were added in double concentration, 200 ml/l FCS, MEM NEAA (L-Alanine 1780 mg/l, L-Asparagine 2640 mg/l, L-Aspartic Acid 2660 mg/l, L-Glutamic Acid 2940 mg/l, L-Glycine 1500 mg/l, L-Proline 2300 mg/l, L-Serine 2100 mg/l), L-glutamine (4 mM), sodium pyruvate (2 mM) and penicillin/streptavidin (200

Units/ml and 0.2 mg/ml) (2.1.6.1). This double concentrated DMEM was sterilized by filtration (Stericup, Millipore).
1x PBS was obtained by diluting 100 ml/l 10x PBS (Accugene) with deionized water. The solution was sterilized by filtration (Stericup, Millipore).
Avicel and plaque agarose overlays were prepared as follows (2.1.6.1): 2.4% Avicel® RC581 (w/v) was dissolved in deionized water and autoclaved (120°C and 1 bar pressure). 2% Plaque Agarose (w/v) was added to deionized water and autoclaved (120°C and 1 bar pressure). The sterile solutions were stored at room temperature.
CMC granules were weighed according to the desired volume of overlay medium to a concentration of 1.6% (w/v) and autoclaved (120°C and 1 bar pressure). Prior to use the sterile CMC was dissolved by stirring in sterile DMEM over night (2.1.6.1).
Unless otherwise noted all media and solutions were stored at 4°C until usage; supplements were stored as indicated by the manufacturer.

2.2.2.2 Cell culture conditions

All cell lines were grown at 37°C and 5% CO_2 in DMEM. Either cell culture flasks with filter caps or cell culture plates were used for the propagation of cells lines.

2.2.2.3 Cultivation of cell lines

All cell lines were split one to two times a week at a ratio of 1:2 up to 1:10 according to the experimental needs. Cells were washed with PBS, trypsin was added and cells were incubated at 37°C and 5% CO_2 until detachment. The enzymatic process was stopped by adding DMEM containing 10% FCS. Cells were counted and subsequently diluted or first concentrated by centrifugation and then diluted according to the cell numbers to be seeded. In order to avoid prolonged trypsinization, CaCo-2 cell lines were alternatively detached by scraping.

2.2.2.4 Cryopreservation of cell lines

For long-term storage in liquid nitrogen cells were cryopreserved in medium containing 10% DMSO (v/v), 40% DMEM (v/v), 50% FCS (v/v). Before adding the cryopreservation medium cells were trypsinized, washed and counted. 1-5 x 10^6 cells were added to each cryovial. Thawing of cell lines was done quickly at 37°C and 5% CO_2. Cells were resuspended in fresh medium, transferred to a sterile 15 ml reaction tube and pelleted at 1000 rpm (5804R, Eppendorf). The cell pellet was resuspended in fresh medium and transferred to a cell culture flask with filter cap. Medium was changed the next day or after cells became adherent.

2.2.2.5 Transfection of mammalian cells by electroporation

For the transfection of mammalian cells 175 cm² flasks were seeded and grown to 70-80% confluency. Cells were washed with PBS and trypsinized. Trypsin was inactivated by addition of DMEM with 10% FCS. Cells were counted and washed twice with ice cold PBS. Washing was done by resuspension of the cells and centrifugation for 5 minutes at 4°C and 1200 rpm (5804R, Eppendorf). After the last centrifugation step the supernatant was removed completely by aspiration. The cell number was adjusted to 2x 10^7 cells/ml with ice cold PBS or Opti-MEM and stored on ice until usage. For each transformation 100-400 µl of the cell suspension were mixed with *in vitro* transcribed (IVT) RNA (see 2.2.1.9) and transferred to an electroporation cuvette with 2 mm gap. Pulse was applied as listed in Table 22.

Table 22: Electroporation protocols for mammalian cells

Program	Cell line	Volts	µF	msec	Ohms	nP	Method
BHK21	BHK21	140	-	25	-	1	Square wave
CaCo2	CaCo-2	300	950	-	∞	1	Exponential decay
CaCo2b	CaCo-2	1500	25	-	∞	2	Exponential decay
CV1	LLC-MK2	100	-	25	-	1	Square wave
LLC-MK2	LLC-MK2	200	950	-	∞	1	Exponential decay

After electroporation, cells were incubated for 10 minutes at room temperature and then transferred to 25, 75 or 175 cm² flasks containing 6-30 ml DMEM. Samples were taken after seeding into the flasks and every 2-3 days during incubation.

2.2.3 Virus culture methods

2.2.3.1 HCoV-NL63 virus stock

An eighth passage virus stock of HCoV-NL63 was kindly provided by Lia van der Hoek, AMC Amsterdam. It was grown in LLC-MK2 cells in limiting dilution series, recovering it three times from the last well of a dilution series still showing diffuse CPE. Subconfluent LLC-MK2 monolayers were infected in 75 cm² flasks with virus supernatant from the last round of limiting dilution culture at a ratio of 1:100 (200 µl virus supernatant in 20 ml fresh medium) as described in 2.2.3.2. The flasks were incubated at 37°C, 5% CO_2, and harvested on day four. For harvesting, flasks were frozen at -70°C and thawed. Cells and supernatant were centrifuged for 10 min at 5000 rpm. Cleared supernatant was aliquoted and stored at -70°C. This virus stock is hereafter referred to as LLC-MK2 NP (for non-purified).
This virus stock was the parental stock for all non-recombinant viruses like the CaCo-2-adapted virus and served as template for the recombinant BACs and viruses. All stocks from

modified or adapted viruses were prepared as depicted above.

2.2.3.2 Infection of cells

Cells were seeded (2.2.2.3) in six-well plates at approximately 4 x 10^5 cells per well (24-well plates: approximately 10^5 cells per well) and incubated (2.2.2.2) until the monolayer was 70-80% confluent. CaCo-2 cells were grown to 100% confluence. Prior to infection cells were washed with 1x PBS. Virus dilution was prepared in OptiPro serum free medium (Invitrogen), six-well plates were infected with a volume of 1 ml, 24-well plates with 500 µl, respectively. Inoculum was removed after one hour of incubation. Cells were washed twice with 1x PBS and supplemented with an appropriate volume of DMEM or overlay medium per well. Cells in cell culture flasks were treated and infected correspondingly.

2.2.3.3 Overlays

For CMC overlays using six-well plates, 1 ml DMEM was added to each well. Subsequently 1 ml of 1.6% CMC solution was slowly added per well (2.2.2.1). Using 24-well plates 500 µl were used instead of 1 ml. Agarose overlays (1% final concentration) were prepared by melting 2% agarose at 70°C, cooling it in a water bath to 42°C and mixing it immediately before application with an equal volume of 2x DMEM stored at room temperature (2.2.2.1). Two ml of the mixture were carefully applied to each well using six-well plates; 1 ml was added per well using 24-well plates. Avicel overlays were made by mixing 2.4% Avicel solution with an equal volume of 2x DMEM (2.2.2.1). 2 ml of the mixture were immediately added to each well using six-well plates, 1 ml was used for 24-wells, respectively.

2.2.3.4 Plaque assays

Plaque assays were incubated without disturbing at 37°C and 5% CO_2. (2.2.2.2) Overlays were commonly removed on day five and cells were fixed with a solution of 4% formaldehyde in PBS. After 30 minutes the formaldehyde solution was removed, cells were washed twice with PBS, and stained with a 0.2% crystal violet solution (2.1.4).

2.2.3.5 Limiting dilution infection series and plaque purification

Limiting dilution infections were done on six-well plates. For plaque purification the cells were overlaid with plaque agarose. After 5 days, cytopathic foci were identified by microscopy at low magnification, lighting through the clear agarose overlay. The positions of CPE foci were marked. The agarose overlay was penetrated with a pipette and 10 to 20 µl of fluid were aspirated underneath the overlay. This fluid was resuspended in 100 µl of OptiPro, which served as the starting solution for a new limiting dilution infection in the next six-well plate. After the last round, aspirated fluid was used to inoculate 5 ml of OptiPro, which was then overlaid on confluent cells in a 25 cm² flask for infection. After infection for one hour and

washing, 5 ml DMEM were added and flasks were incubated at 37°C, 5% CO_2 for four days. Virus stocks were prepared as described in 2.2.3.1.
For limiting dilution series without an overlay, 100 µl supernatant of the last well with visible CPE after 5 days were used for the next limiting dilution infection series. This was repeated for 3-10 times, after the last round virus stock was produced as described above.

2.2.4 Immunodetection assays

2.2.4.1 Spotting of HCoV-NL63 slides

LLC-MK2 cells were infected as described above (2.2.3.1 and 2.2.3.2) and harvested after four days: Supernatant was removed, aliquoted and stored at -70°C. Infected and uninfected cells were washed with PBS and trypsinized. Trypsin was inactivated and cells were mixed at a ratio of 2:1 (infected: uninfected). This mixture was pelleted and washed three times with PBS. The cell pellet was resuspended in PBS and spotted on slides by pipetting and immediate re-aspiration. The slides were dried overnight and placed in aluminum pouches. Vacuum was applied to the pouches; they were sealed and stored at -20°C until usage.

2.2.4.2 Immunofluorescence

For the detection and proof of virus replication an indirect immunofluorescence assay (IFA) can be used. Monolayers of cells are grown and after infection fixed to glass slides by using different fixatives. Whereas PFA maintains cell structures and protein epitopes by building protein networks, fixation with methanol and acetone results in relatively strong defragmentation of membrane systems. After fixation the cells are incubated with primary and secondary antibodies. The secondary antibodies are labeled with fluorophores and can therefore be detected by fluorescence microscopy.

2.2.4.3 Detection of HCoV-NL63 strain Amsterdam1 and recombinant HCoV-NL63 by immunofluorescence assay (IFA)

LLC-MK2 or CaCo-2 cells were seeded on glass slides in a 24-well plate (8x 10^4 cells/well) and infected with HCoV-NL63 (2.2.3.2). Three to four days after the infection the cells were fixed with PFA (4%) for 15 minutes, permeabilized with 0.1% Triton X-100 for 10 minutes. Subsequently the cells were washed twice with phosphate buffered saline Tween 20 (PBST), blocked with PBST containing 3% FCS for 30 minutes at room temperature and washed again twice with PBST. Primary antibody, diluted 1:100 in PBS was added and incubated at 37°C for 1 hour. For the detection of different viral proteins (M, N) peptide generated rabbit antisera (2.1.10.1) and patients' sera were applied. Cells were washed twice with PBST and the secondary antibody (2.1.10.2) was added and incubated at 37°C in a wet chamber for 30 minutes. Slides were mounted with DakoCytomation Fluorescent Mounting Medium and

analyzed by inverted fluorescence microscopy (Leica DM IL).

3 Results

This work aimed at the construction of a full-length HCoV-NL63 cDNA clone. A prerequisite was a high degree of sequence stability and correctness of the cDNA clone. The subsequent transfection of genome-like full-length RNA into the cytosol of the host cell should mimic a natural infectious cycle. Therefore the advantage of a continuous full-length viral genome sequence embedded into a BAC was combined with a T7-driven *in vitro* transcription of infectious, capped full-length RNA, and a subsequent electroporation in mammalian cells.
In our laboratory an approach for the construction of a full-length cDNA clone of SARS-CoV using a pBelo BAC vector backbone was already established (Pfefferle et al. 2009). For HCoV-NL63 a similar approach was chosen. The cloning strategy included a parallel subcloning into a pSMART as well as a pBelo BAC vector backbone with identification of and focusing on the more efficient method. The final full-length clone ought to be reconstructed gradually from the subclones, using a pBelo BAC backbone.

3.1 Sequencing of the parental HCoV-NL63 Amsterdam 1

The construction of a cDNA clone-based on reverse transcribed virus RNA is error-prone. When using M-MLV reverse transcriptase, for example, errors occur every 30,000 bases (Roberts et al. 1989). To assure the construction of a full-length clone with a sequence corresponding to the sequence of the viable HCoV-NL63 strain Amsterdam 1 kindly provided by Lia van der Hoek (van der Hoek et al. 2004), sequencing of the parental HCoV-NL63 strain was done in parallel to the construction of subclones.
An initial virus stock was produced from the HCoV-NL63 strain Amsterdam 1 using LLC-MK2 cells (2.2.3.1). Slides were spotted with a mixture of infected and uninfected cells (2.2.4.1). A productive infection was proven by real-time RT PCR (2.2.1.15, data not shown) and an immunofluorescence assay (IFA, 2.2.4.2) of the cells using patients' serum as primary antibody (see Figure 8).
This virus stock, designated HCoV-NL63 LLC-MK2 NP (for non-purified), served as the origin of all virus stocks generated in this work using infectious cDNA clones or conventional cell culture methods. The virus RNA extracted from this stock served as template for all subsequent sequencing and the assembly of the full-length clone. Sequencing primers were designed based on the sequence of HCoV-NL63 Amsterdam 1 (GenBank accession number NC_005831).

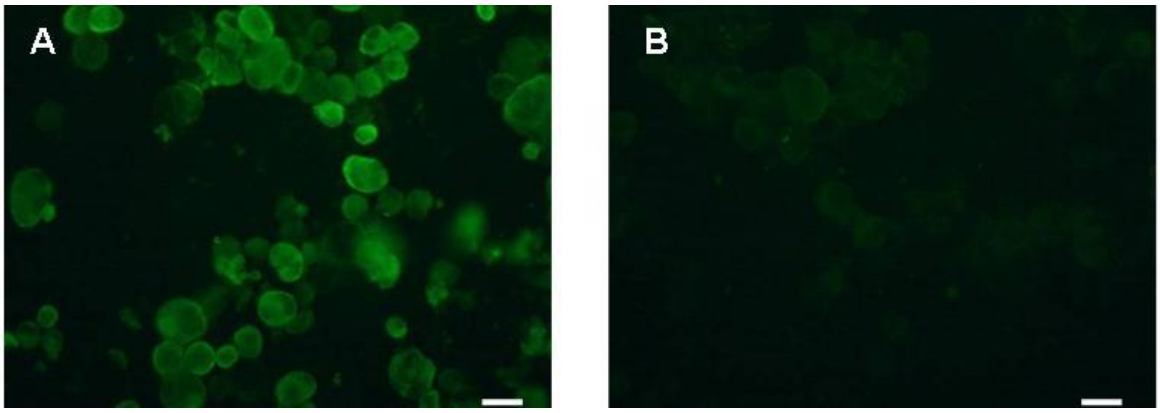

Figure 8: Indirect immunofluorescence of HCoV-NL63 infected LLC-MK2 cells

A: HCoV-NL63 infected LLC-MK2 cells incubated with HCoV-NL63 positive serum. Secondary antibody (Goat Anti-Human IgG, H & L Chain Specific Fluorescein Conjugate) was added and fluorescence was detected and documented using a fluorescence microscope with camera. **B:** Negative control on the same slide as A. HCoV-NL63 infected LLC-MK2 cells incubated with HCoV-NL63 negative serum. Secondary antibody, detection and documentation were done as described for A. The white bar corresponds to 50 µm

The subclones were constructed as described below; positive clones were sequenced (2.2.1.8). The sequencing data was compared to the NCBI GenBank entry NC_005831 from HCoV-NL63 Amsterdam 1. In case of discrepancy the questionable part of the genome sequence was reamplified freshly from viral RNA by one-step RT PC (2.2.1.14) and sequenced. Overall, the RNA showed seven point mutations compared to the HCoV-NL63 Amsterdam 1 sequence deposited in GenBank (Table 23).

Table 23: Sequence comparison between HCoV-NL63 LLC-MK2 NP and GenBank accession number NC_005831 (Version NC_005831.2). Nucleotide position is based on the GenBank accession number NC_005831. * double peaks with underlying C-peak.

Position NC_005831	Base NC_005831	Base LLC-MK2 NP	Amino acid NC_005831	Amino acid LLC-MK2 NP
327	C	T*	Serine	Leucine
2956	T	A	Proline	Proline
2977	T	A	Alanine	Alanine
12477	C	T	Cysteine	Cysteine
16875	C	T*	Threonine	Isoleucine
22525	C	T	Alanine	Valine
23466	C	A*	Glutamine	Lysine

All four mutations leading to a change in the amino acid code at nucleotide position 327, 16875, 22525 and 23466 were corrected on the subclone level (see below). Silent mutations

at positions 2956, 2977 and 12477 remained unchanged and served as marker mutations for the identification of recombinant DNA and RNA.

3.2 Susceptibility of different cell lines to HCoV-NL63 and cytopathogenic effects

LLC-MK2 and Vero cells did not cause a clear cytopathogenic effect (CPE) after infection with HCoV-NL63. Because this virus uses the same receptor as the SARS-CoV, 12 different cell lines susceptible to SARS-CoV infection were tested for susceptibility to HCoV-NL63 (Weingartl et al. 2004; Hattermann et al. 2005; Yamashita et al. 2005) (Table 24). Cells in six-well plates were infected with 10^4 plaque-forming units of HCoV-NL63 virus stock LLC-MK2 NP. RNA concentrations in supernatants were measured shortly after virus adsorption (2.2.3.2), and 7 days later (Table 24).

Table 24: Comparison of HCoV-NL63 replication by real time RT-PCR using different cell cultures.

Designation (see 2.1.6.2)	Day 0 [copies/µl]	Day 7 [copies/µl]	Amplification factor	Cytopathogenic effect (CPE)
Vero E6	6.94e3	3.05e7	4.39e3	None
Vero FM	1.78e4	4.51e9	2.54e5	None
CaCo-2	3.55e3	1.25e10	3.54e6	round and detached, dead cells with cell debris in supernatant, strong effect
Calu1	2.61e4	5.33e6	2.04e2	None
Calu6	7.95e3	5.00e5	6.29e1	None
POEK	8.11e4	3.03e5	3.74e0	None
PK13	2.66e2	7.78e5	2.93e3	None
293lp	3.67e3	3.09e7	8.42e3	None
FeA	1.45e4	5.83e5	4.03e1	None
RD	3.14e5	1.57e4	4.99e-2	None
PS	1.20e4	1.44e6	1.19e2	None
LLC-MK2	4.00e3	2.65e6	6.62e2	round and detached, weak effect

Increase of virus RNA was less than 1000-fold in 7 of 12 cultures. Interestingly, this included LLC-MK2, the prototype cell culture for NL63. In spite of a low amplification factor these cells showed the usual weak CPE that is typically observed upon HCoV-NL63 infection.
Vero cells supported virus growth efficiently but did not result in CPEs. Interestingly, there

was a remarkable difference between Vero E6 and Vero FM cells (Table 24). In our hands these cells also showed differences upon SARS-CoV infection (data not shown). Vero FM consistently showed a more pronounced CPE than Vero E6 but there were no significant differences in RNA amplification (not shown).
CaCo-2 cells amplified virus RNA most efficiently, and showed a clearly visible CPE starting from day 4 after infection. Cells became rounded, detached from the surface, and showed morphological signs of cell death (Figure 9).

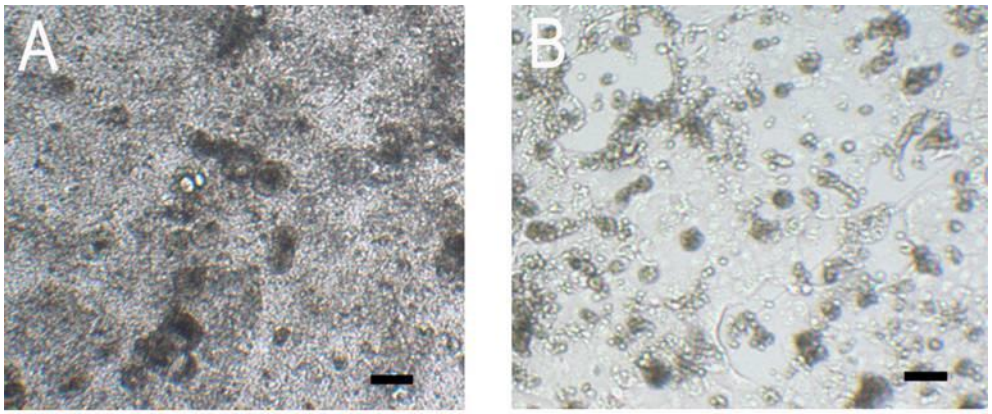

Figure 9: Cytopathogenic effect of HCoV-NL63 on human colon carcinoma cells (CaCo-2).
CaCo-2 cells 5 days after infection with HCoV-NL63 at a multiplicity of infection of 0.1 (agarose overlay technique). A: mock infection, B: infection. Photographs were taken at 40-fold magnification; bars represent 20 µm.

For confirmation of differential replication efficiencies, CaCo-2 and LLC-MK2 cells were infected in parallel. Both cell lines were seeded in 25 cm^2 flasks, and infected at multiplicities of infection (MOI) of 0.005. Samples of supernatants were taken daily from day 0 to 7 and analyzed by real time RT-PCR. As shown in Figure 10, CaCo-2 cells replicated virus more efficiently than LLC-MK2.

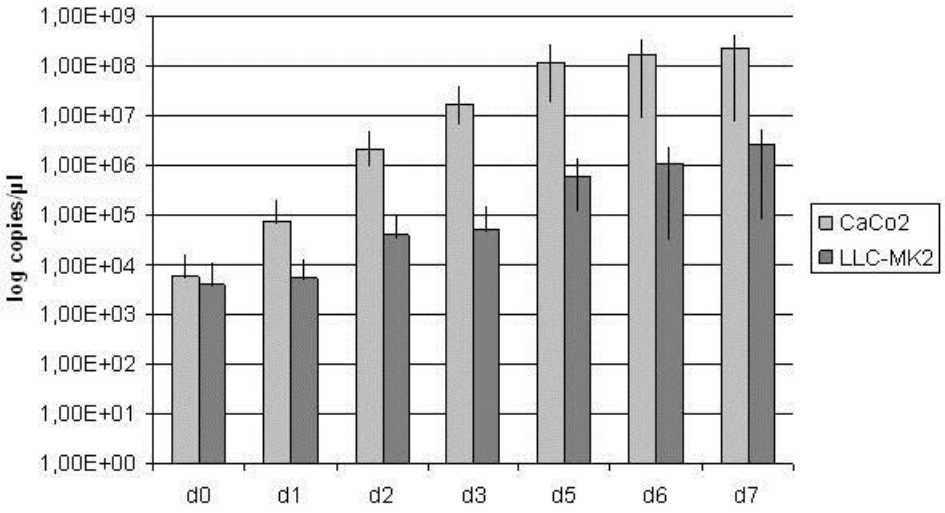

Figure 10: Growth kinetics of HCoV-NL63 on LLC-MK2 and CaCo-2 cells.

25 cm^2 flasks of LLC-MK2 or CaCo-2 cells were infected at multiplicities of infection of 0.005 for 1 h, washed twice with PBS, and subsequently supplied with 10 ml DMEM. Samples were taken daily from day 0 to 7 (except day 4) and analyzed by real time RT-PCR. Error bars indicate ranges of three independent experiments.

From day 3 onward, RNA concentrations were more than 100-fold higher in CaCo-2 cells. Because of the clear CPE observed in CaCo-2 cells, these cells were tested for their utility in a cytopathogenic plaque assay.

3.3 Comparison of different plaque assay overlays

Three overlay techniques, commonly used for plaque assays, were tested for their suitability (Matrosovich et al. 2006). CaCo-2 cells were infected in six-well plates with HCoV-NL63 LLC-MK2 NP. After one hour, supernatants were removed, cells washed with PBS, and overlaid in parallel with CMC, agarose and Avicel as described in 2.2.3.3. The plaque assays were fixed and stained as described in 2.2.3.4. As shown in Figure 11, plaques were visible with all three overlays, but staining was clearest with Avicel.

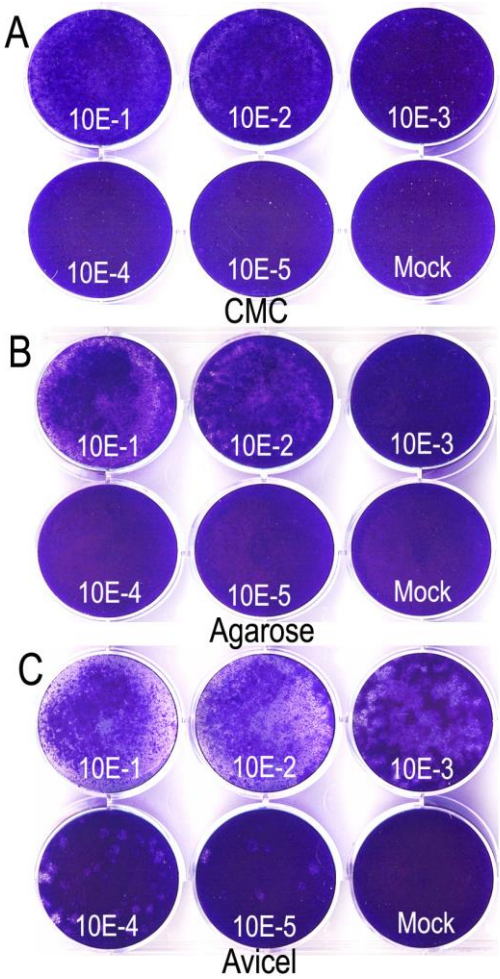

Figure 11: Plaque assay for HCoV-NL63 on CaCo-2 cells using different overlays.
HCoV-NL63 was serially diluted on CaCo-2 cells (10^{-1} until 10^{-5}). After 1 h of virus adsorption different overlays were added. After 5 days cells were fixed with 4% formaldehyde and stained with 0.2% crystal violet solution. A) carboxymethyl-cellulose; B) agarose; C) Avicel.

3.4 Optimization of incubation times

HCoV-NL63 culture with LLC-MK2 cells takes more than 7 days until first signs of weak CPE become visible (Fouchier et al. 2004). In order to test whether incubation times could be reduced with CaCo-2 cells, five plaque assays on virus dilution series were done with Avicel overlays and terminated by fixation after 1, 2, 3, 4, and 5 days, respectively. On days 1 and 2, no plaques were visible (not shown). Termination at day 3 yielded plaques only at high virus concentration (Figure 12).

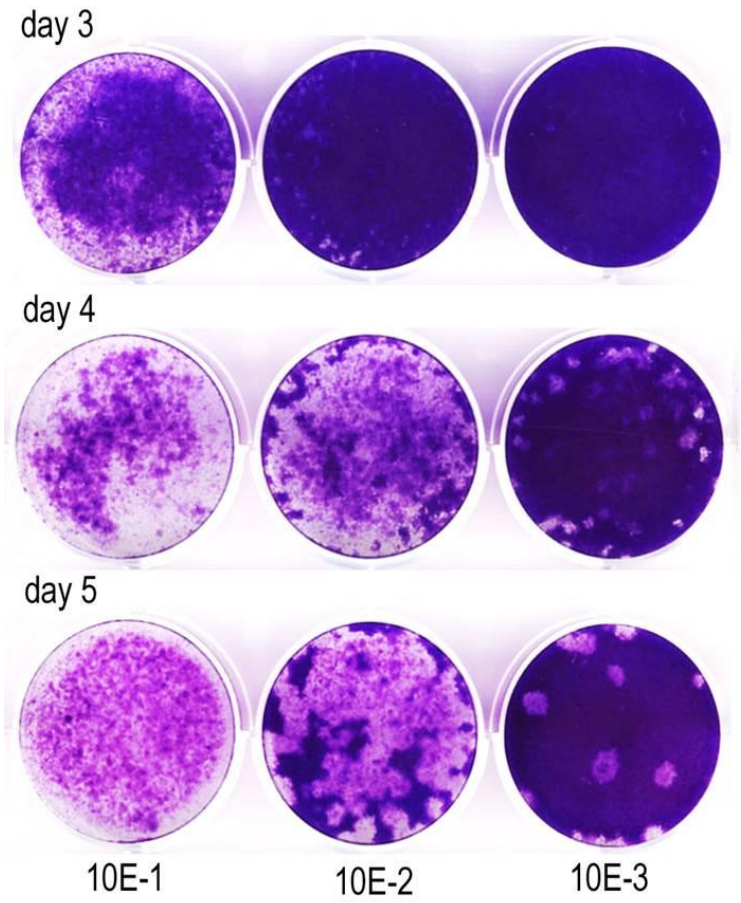

Figure 12: Plaque assays with different incubation times.

Plaque assays were performed with Avicel overlay and incubated for 3, 4, and 5 days, respectively. The dilution factor of LLC-MK2 NP virus stock used for infection is shown on the bottom.

From day 4 onward, plaques were visible in the lowest detectable virus concentration. Plaques on day 5 were larger, but did not increase in number. For all subsequent experiments fixation was done at 4 dpi.

3.5 Plaque preparation

In order to obtain virus stock solutions with higher infectivity, our standard virus stock LLC-MK2 NP (2.2.3.1) was plaque-purified using the agarose overlay. Because life staining of cells with neutral red solution was not successful on CaCo-2 cells (not shown), we used an alternative technique of plaque preparation.

Limiting dilution infections were done on six-well plates and were overlaid with agarose. After 5 days, cytopathic foci were identified by scanning through the wells with the naked eye. Plaques were visible as turbid foci in the cell monolayer through the clear agarose overlay. The positions were marked and checked for a CPE with an inverted microscope at low

magnification. Plaque purification was done as described in 2.2.3.5.

Three rounds of purification were done. After the last round, a virus stock was produced in a 25 cm^2 flask with a confluent CaCo-2 monolayer as described in 2.2.3.1. The purified virus was referred to as CaCo-2 PP (for plaque-purified).

To compare the infectivity of the plaque-purified virus with the parental LLC-MK2 virus stock (LLC-MK2 NP), viral titers were determined by Avicel plaque assay. Results are shown in Figure 13.

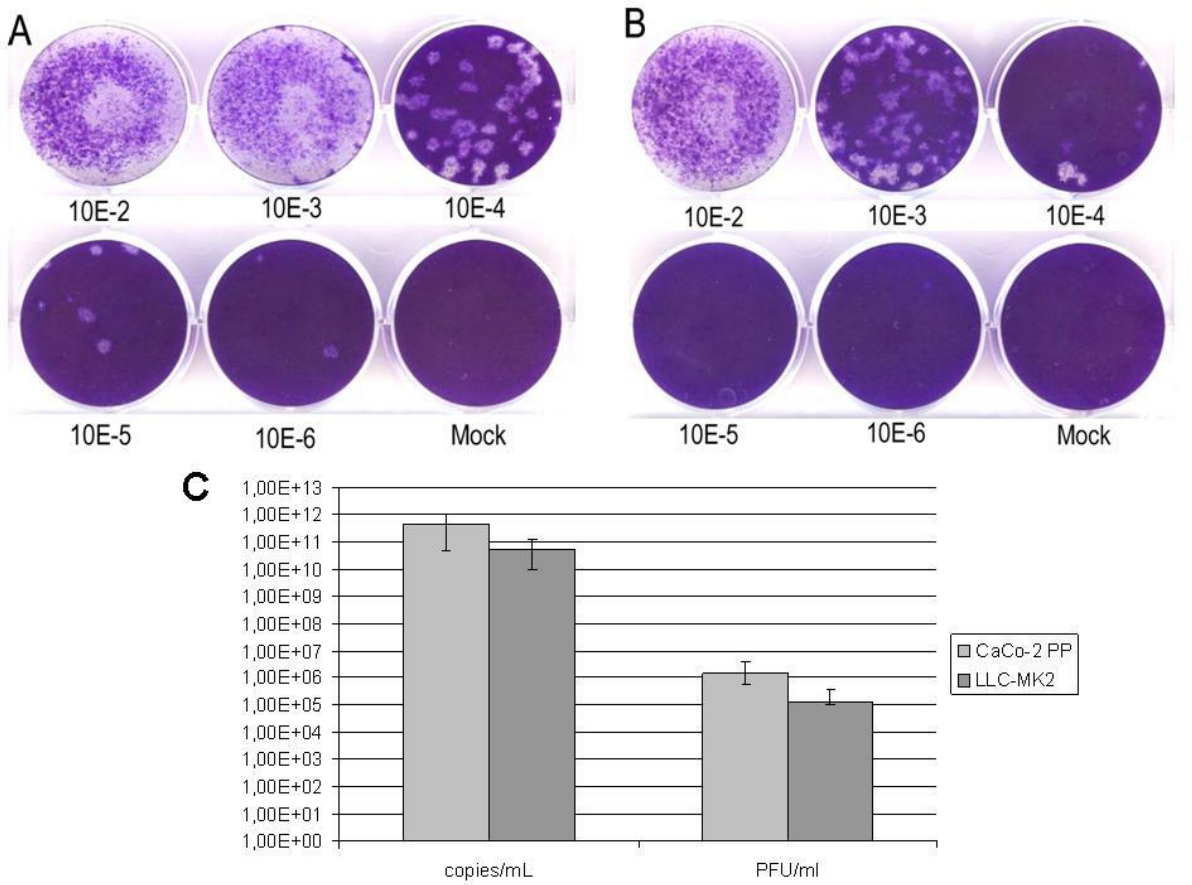

Figure 13: Effect of plaque purification.

A: plaque assay with Avicel overlay on purified virus stock CaCo-2 PP. B: plaque assay on non-purified virus stock LLC-MK2 NP. C, viral RNA copies per ml of supernatant (left) and plaque forming units per ml of supernatant (right) for CaCo-2 PP and LLC-MK2 NP virus stocks (log scale). Error bars show ranges of three independent experiments.

CaCo-2 PP was about 10-fold more infectious than LLC-MK2 NP. Plaque assays were repeated three times (not shown). Mean titers were determined to be 1.4 x 10^6 PFU/ml and 1.3 x 10^5 PFU/ml, respectively, for CaCo-2 PP and LLC-MK2 NP. Absolute quantification of virus RNA by real-time RT-PCR yielded 4.8 x 10^{11} RNA copies/ml for CaCo-2 PP and 5.3 x

10^{10} copies/ml for LLC-MK2 NP. The high discrepancy between PFU/ml and RNA copies/ml could result from generation of defective interfering particles.

3.6 Adaptation of HCoV-NL63 to CaCo-2 cells and full genome sequencing

The HCoV-NL63 stock CaCo-2 PP was further adapted to CaCo-2 cells by ten consecutive limiting dilution infection series (2.2.3.5), followed by the production of a new virus stock on CaCo-2 cells (2.2.3.1). This stock was designated HCoV-NL63 CaCo-2 LD (for limiting dilution).

A plaque assay was carried out on CaCo-2 six-well plates and repeated two times on 24-well plates. The mean titer was determined to be 3.1 x 10^6 PFU/ml for HCoV-NL63 CaCo-2 LD. Compared to HCoV-NL63 CaCo-2 PP the infectivity increased more than double. This new CaCo-2 adapted virus was fully sequenced and the genome was compared to the parental strain HCoV-NL63 LLC-MK2 NP and GeneBank accession number NC_005831 (Table 25).

Table 25: Sequence comparison between GenBank NC_005831, HCoV-NL63 CaCo-2 LD and LLC-MK2 NP. Position is based on the GenBank entry NC_005831. Yellow background: CaCo-2 LD matches LLC-MK2 NP but not NC_005831; green background: CaCo-2 LD matches NC_005831 but not LLC-MK2 NP, red background: CaCo-2 matches none. * double peaks, a smaller C-peak is also visible, nt = nucleotide; aa = amino acid.

		NC_005831		LLC-MK2 NP		CaCo-2 LD	
position	**gene**	**nt**	**aa**	**nt**	**aa**	**nt**	**aa**
327	nsp1	C	Serine	T*	Leucine	T	Leucine
2956	nsp2	T	Proline	A	Proline	A	Proline
2977	nsp2	T	Alanine	A	Alanine	A	Alanine
4740	nsp3	C	Alanine	C	Alanine	T	Valine
10565	nsp6	T	Serine	T	Serine	C	Proline
12442	nsp11/12	G	Alanine	G	Alanine	G/T *	Alanine/Serine
12477	nsp12	C	Cysteine	T	Cysteine	T	Cysteine
16875	nsp13	C	Threonine	T*	Isoleucine	C	Threonine
17621	nsp14	C	Phenylalanine	C	Phenylalanine	T	Serine
21162	ORF2 (spike)	C	Phenylalanine	C	Phenylalanine	T	Proline
21217	ORF2 (spike)	C	Serine	C	Serine	T	Phenylalanine
21390	ORF2 (spike)	T	Leucine	T	Leucine	G	Valine
22525	ORF2 (spike)	C	Alanine	T	Valine	C	Alanine
23466	ORF2 (spike)	C	Glutamine	A*	Lysine	C	Glutamine

The sequence of HCoV-NL63 CaCo-2 LD retained four mutations of its parental LLC-MK2 NP virus stock (yellow, Table 25). Three of those were silent mutations. All mutations were

located in the ORF 1a/b. Interestingly three of the mutations found in the LLC-MK2 NP virus stock were reverted to the original NC_005831 sequence in CaCo-2 LD (green, Table 25). However, two of those mutations in LLC-MK2 NP had underlying bases that corresponded to NC_005831.
Seven mutations of CaCo-2 LD were new, non-silent and corresponded to neither LLC-MK2 NP, nor NC_005831 (red, Table 25). Four of the mutations were located in the ORF 1a/b and three in the spike (ORF 2) region. The mutations at position 327, 12442, 17621 and 21217 were found exclusively in HCoV-NL63 CaCo-2 LD when compared to other laboratory strains (van der Hoek et al. 2004; Donaldson et al. 2008) and clinical isolates (Fouchier et al. 2004; Pyrc et al. 2006)

Sequencing 5' and 3' ends of HCoV-NL63For the sequence verification of the 5' and 3' end of the viral genome a RNA ligase-mediated rapid amplification of cDNA ends (RLM-RACE, see 2.2.1.19) was carried out. The sequence of the 3' end complied with the sequence data from the GenBank entry for HCoV-NL63 Amsterdam 1 (NC_005831). The sequencing results of the 5'RACE indicated an additional guanidine at the most proximal 5' end of the genome. This finding was concordant to the sequence data from another human coronavirus NL63 strain associated with pneumonia (GenBank accession number AY518894) that was isolated simultaneously in 2004 by R. Fouchier and coworkers (Fouchier et al. 2004). The additional guanidine was thus included into the primer design for the 5' end of the full-length HCoV-NL63 cDNA clone.

3.7 Cloning strategy

The cloning strategy for the full-length HCoV-NL63 cDNA clone was based on the gradually assembly of the full-length cDNA genome using a pBelo vector backbone. pBelo BACs have proven to allow for stable integration and modification of full-length coronavirus cDNA genomes (e.g. SARS CoV).
The full-length HCoV-NL63 genome was divided into seven subfragments by means of naturally occurring restriction sites. Unique restriction sites were preferred. These sites ideally had to be absent from the sequence of the vector backbone. Available restriction sites allowed the identification of fragments from two to seven kilobase pairs in size, as illustrated in Figure 14. However a few multiple occurring restriction sites had to be used and deleted on subclone level before further assembly of the full-length HCoV-NL63 cDNA clone. The division of the full-length HCoV-NL63 cDNA genome into subfragments also enabled other sequence modifications like introduction of mutations on the subclone level. The cloning strategy, including necessary sequence alterations, is summarized in Figure 14.

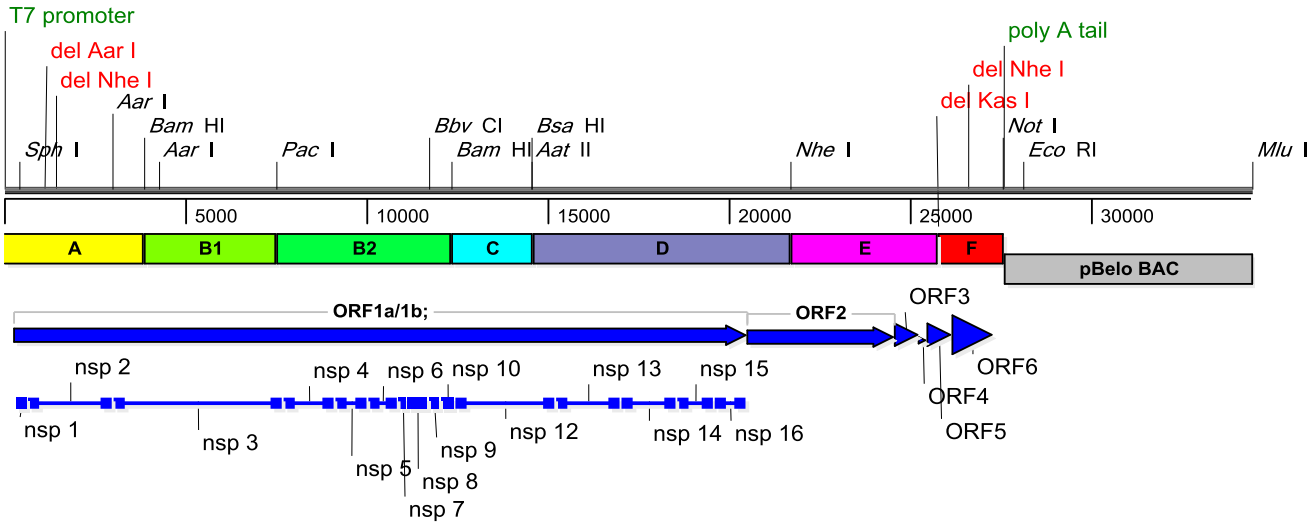

Figure 14: Schematic overview of the full-length recombinant HCoV-NL63 cloning strategy

Map of the full-length recombinant HCoV-NL63 clone (rNL63 wt). Drawn to scale using Lasergene SeqBuilder. Subclone fragments A to F illustrated in yellow (A), green (B1 and B2), light blue (C), dark blue (D), pink (E) and red (F). pBelo BAC backbone illustrated in grey. Restriction sites used for the assembly of subclones and the full-length-clone are shown in italic. Deleted restriction sites are presented in red. Additional sequences introduced by primers during the assembly of the clone are labeled green.

Generally the HCoV-NL63 genome fragments were amplified from cDNA with PCR using a proofreading DNA polymerase, digested with restriction enzymes and ligated with modified pBelo BAC vector fragments (named “left” and “right arm”).

A set of HCoV-NL63 genomic cDNAs served as templates for all subcloned PCR fragments. Primer for cDNA synthesis were chosen downstream of the subclones’ reverse primer. Usage of the same reverse primer for cDNA synthesis and PCR worked well for shorter fragments (< 2kb) in one-step RT PCR reactions, but frequently failed for longer fragments in a two-step RT PCR.

The pBelo BAC cloning strategy required the modification of the pBelo BAC vector according to the characteristics of the HCoV-NL63 cloning strategy. This modified vector backbone was derived from pBelo as described in 2.2.1.22. Additionally an HCoV-NL63 specific linker had to be introduced for the construction of subclones and the sequential assembly of the full-length clone. This procedure is described in detail below (3.7.1, 3.7.2, 3.7.3).

The resulting pBelo BAC vector contained a single *EcoRI* site located in the chloramphenicol resistance gene. As the screening of *E. coli* clones was always performed under antibiotic pressure, the assembly of the clones often included a digestion with *EcoRI* leading to a

disruption of the chloramphenicol resistance gene. This strategy assured low background of *E. coli* clones carrying i.e. plasmids with wrong orientation or consecution of the single fragments or missing plasmid parts. The risk of generating false-positive *E. coli* clones was additionally reduced by the dephosphorylation of plasmid parts. As at least one phosphorylated plasmid end is necessary for a successful ligation (2.2.1.20), a religation is circumvented by dephosphorylation. Generally the plasmid fragments with either the intact chloramphenicol resistance gene or the major part of the resistance gene were dephosphorylated prior to gel purification and ligation.
Ligation, transformation and screening of *E. coli* clones was always done as described in 2.2 Methods. Screening of *E. coli* clones always comprised the analysis of the pBelo BAC size by gel electrophoresis, a verification of size and pBelo BAC integrity using PCR and sequencing of PCR products. These procedures are not mentioned again for every construction step depicted below.

3.7.1 Construction of the HCoV-NL63-modified vector backbone

The restriction sites of *AatII*, *MluI*, *EcoRI* and *NotI* were essential for the assembly of all pBelo BAC based subclones and the full-length clone (see Figure 15). A *MluI* site was introduced with the most 5' end forward primer (NL63T7fwd +pspom Mlu), including also the T7 promoter sequence and a *PspOMI* restriction site. The *AatII* site and a *NotI* site were already present in the MCS of pBeloAd4, the *AatII* site was located a few bases upstream of the *NotI* site. pBelo dNco3 contained a single *NotI* site, the MCS was absent.
The first subclone was generated to achieve a modified vector backbone containing the restriction sites in the correct order (*MluI*, *AatII*, *NotI*) and to introduce the *MluI* site as well as the T7 promoter. This subclone served as a backbone for the assembly of all HCoV-NL63 subclones. It was built by assembling parts of pBelodNco3, pBeloAd4 and the first 500 base pairs of the HCoV-NL63 genome. The assembly is illustrated in Figure 15.
All three fragments were ligated in one single reaction, the resulting pBelo BAC was designated A0 (Figure 15).

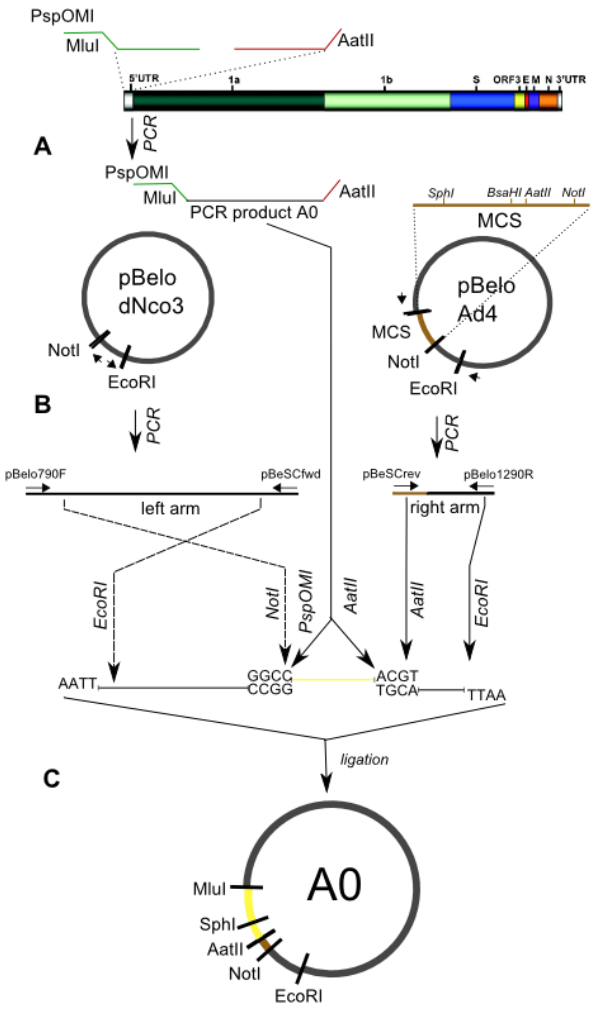

Figure 15: Construction of the modified pBelo BAC for cloning of the full-length HCoV-NL63 genome. **A:** Additional restriction sites were added to the PCR product using extended primer. Template: cDNA from full-length RNA of HCoV-NL63 stock LLC-MK2 NP. Forward primer (green) contains recognition sites for *PspOMI*, *MluI* and T7. Reverse primer (red) contains an *AatII* restriction site. The PCR product generated with these primers contains a *PspOMI*, *MluI* and T7 site at its 5'end and an *AatII* site at its 3'end. **B:** The "left arm" of the vector backbone was amplified from pBelodNco3 using pBelo790F as forward and pBeSCfwd as reverse primer. The resulting 6.8 kilobase pair PCR product enclosed the unique *NotI* and *EcoRI* restriction sites. The "right arm" of the vector backbone was amplified using pBeSCrev as forward, pBelo1290R as reverse primer and pBeloAd4 as template. The length of the resulting PCR product was approximately 900 base pairs; it contained the MCS with the unique *AatII* and an additional *NotI* recognition site and parts of the chloramphenicol resistance gene, containing the unique *EcoRI* site. **C:** The PCR products were digested with: *EcoRI* and *NotI* (left arm), *PspOMI* and *AatII* (HCoV-NL63 A0), *AatII* and *EcoRI* (right arm). *NotI* and *PspOMI* have different recognition sites but digestion leads to matching overhangs. Ligation of these matching overhangs leads to the deletion of both, the *NotI* and the *PspOMI* site. Therefore ligation of the two vector arms (left and right) and the HCoV-NL63 insert A0 led to a clone with deleted *NotI* and *PspOMI* sites at the left arm-HCoV-NL63-junction. *AatII* and *EcoRI* restriction sites were not modified. The resulting clone (A0) contained all required unique restriction sites in the correct consecution (*MluI – AatII – NotI – EcoRI*).

The following construction of the subclone A0F introduced the 3’ end of the HCoV-NL63 genome into the pBelo backbone and thus enabled the insertion of the remaining HCoV-NL63 genome in between the 3’ and the 5’ ends of the cDNA genome.
Based on the subclone A0, containing the 5’ end of the HCoV-NL63 genome, the *AatII* and *NotI* sites were used to introduce the F fragment containing the 3’ end of the genome into the plasmid. The right arm was amplified as described for subclone A0. Digestion was done with *EcoRI* and *NotI*. The left arm was amplified using pBeSCfw and pBelo790F for priming and subclone A0 as template, creating a PCR product containing the A0 fragment and the major part of the vector backbone. Digestion was done using *EcoRI* and *AatII*.
The insert was amplified from cDNA with primers NL 25644 F +Aat and NL27553R+20t+NotI; introducing a novel *NotI* site downstream of the poly(A)tail at the 3’ end as well as a novel *AatII* site for ligation with the A0 fragment. All three fragments were ligated in one single unidirectional ligation reaction of the compatible ends. The resulting BAC was designated A0F (see Figure 16).

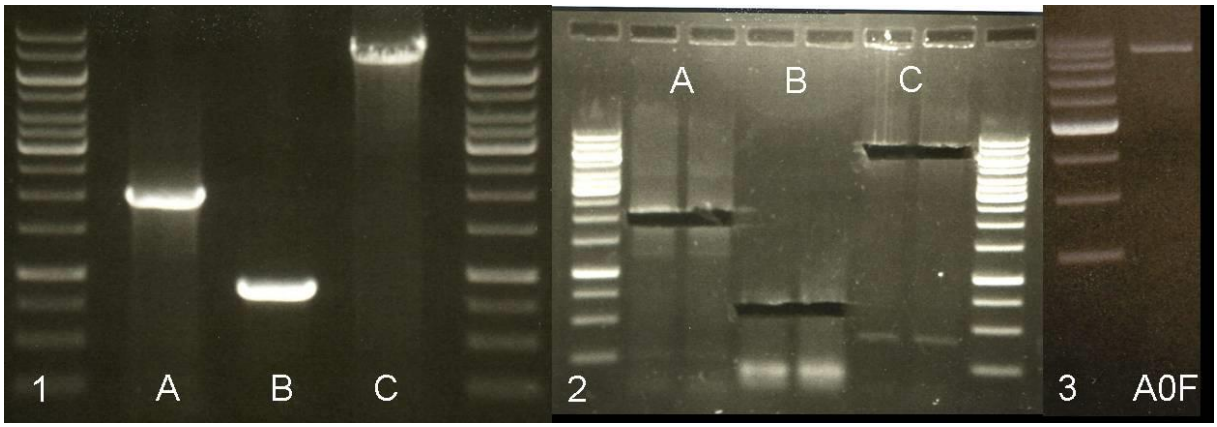

Figure 16: Construction of subclone A0F. 1: PCR products used for the assembly of subclone A0F. A: fragment F, B: right arm of pBelo, C: left arm of pBelo. These PCR products were purified using phenol/chloroform extraction as described in 2.2.1.5, digested and dephosphorylated (B: right arm) as described in 2.2.1.20, and purified again using alcohol precipitation as described in 2.2.1.5.. 2: Preparative agarose gel, stained post-run according to 2.2.1.6, photographed after excision of nucleic acid fragments corresponding to the correct size (A: fragment F with a size of 1.9 kb, B: right arm with a size of 0.6 kb and C: left arm with a size of 7.5 kb) for assembly of subclone A0F. 3: Positive subclone A0F with a size of 9.5 kb. Molecular weight markers: 1&2: GeneRuler 1 kb DNA Ladder, 3: Supercoiled DNA Ladder, see 2.1.11.

This subclone was later assembled to subclone AF, which was essential for the construction of the full-length clone by combination of the sequentially assembled HCoV-NL63 cDNA subclones.

3.7.2 Construction of the subclones A- E

The first subclones to be assembled were simultaneously subcloned into pBelo BAC and pSMART (2.2.1.22). For the subcloning using the pSMART vector backbone, a subset of phosphorylated primers was designed enclosing the chosen restriction sites for the future assembly of the subclones into a pBelo BAC-based full-length clone. The phosphorylated PCR products were then directly ligated to the dephosphorylated pSMART vector backbone, thus omitting the restriction and dephosphorylation steps needed for the pBelo BAC cloning strategy.

For the subcloning into pBelo BAC all fragments were amplified using a proofreading polymerase (see 2.2.1.11 and 0). The PCR products were purified by either phenol/chloroform extraction (2.2.1.5) or the bead-based Ampure system (2.2.1.3).

A set of genomic HCoV-NL63 cDNAs served as template for the amplification of insert DNA fragments, modified pBelo BAC plasmid DNA served as template for the amplification of the right and left vector arm.

All fragments were digested with appropriate restriction enzymes for unidirectional ligation and partially dephosphorylated (see 2.2.1.20), purified and ligated according to 2.2.1.21. Figure 17 shows amongst others an example of the pBelo BAC based cloning of subclone B2 with a two-step ligation strategy.

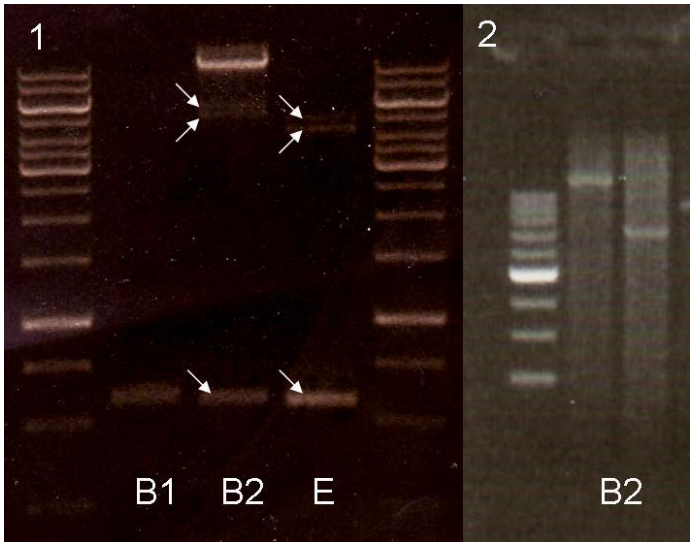

Figure 17: Ligation intermediates and subclones. 1: Ligation intermediates visualized using a preparative gel. Fragments for the two step assembly of the subclones B1, B2 and E. Ligation of the pBelo right arm with B1 (only the 0.6 kb fragment of the pBelo right arm is visible), B2 (upper arrow: ligation product with the correct size, middle arrow: fragment B2 sized 5 kb, lower arrow: pBelo right arm) and E (upper arrow: ligation product with the correct size, middle arrow: fragment E sized 4.2 kb, lower arrow: pBelo right arm). Molecular weight marker: GeneRuler 1 kb DNA Ladder (see 2.1.11) **2:** Isolated plasmid DNA from the construction of subclone B2. Screening for positive clones from a one-step ligation of all three fragments (B2, right arm, left arm), the first of the two plasmid DNAs has the correct size of 11.9 kb. Molecular weight marker: Supercoiled DNA Ladder, see 2.1.11.

Following this strategy the insert was first ligated to the right arm of pBelo, excised from the agarose gel, purified and then ligated to the left arm of pBelo. After this second ligation the ligation reaction was added to competent *E. coli* cells. Transformation was done either chemically or using electroporation as described in 2.2.1.22. However, the assembly of the different subclones a one-step ligation strategy with all three fragments in one ligation reaction usually resulted in more *E. coli* colonies with more positive clones, respectively. Compared to the pBelo BAC cloning, the ratio of empty vectors was higher using the pSMART cloning kit. Therefore further assembly of subclones was exclusively done using pBelo BAC.

3.7.2.1 Construction of subclone A

The fragment A was first cloned into pSMART and subsequently into pBelo A0F (3.7.1). Using the pSMART kit the fragment A was ligated to a pSMART low copy vector carrying a kanamycin resistance gene after being amplified by PCR using Phusion polymerase with the phosphorylated primers 350F and 4000R_Aat, covering the HCoV-NL63 genome from bases 350 to 4053 (position from GenBank entry NC_005831). Two of 16 clones were positive (Figure 18), showing a size of approximately 6 kb. This corresponded to the size of the vector (2 kb) plus an insert of approximately 4 kb.

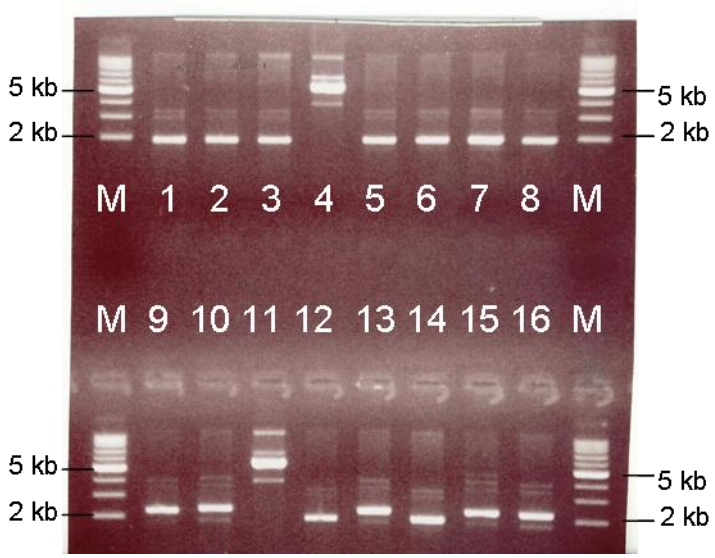

Figure 18: Fragment A in pSMART

Agarose gel electrophoresis (TAE, 0.8%) of plasmids prepared from single colonies numbered 1-16. M: Supercoiled DNA ladder 2-10 kb (Promega). Empty vectors had a size of approximately 2 kb. Plasmids from clones number 4 (upper lane) and number 11 (lower lane) migrated at the height of the 6 kb band. They were considered as putative positive because the size was corresponding to vector (2 kb) including an insert (4 kb).

Sequencing results of the positive clones showed a point mutation at position 327 (NC_005831), the correction of this mutation was done after ligation to A0F in the subclone

AF (see 3.7.3.1).

3.7.2.2 Construction of subclone B1

The first approach for the cloning of fragment B1 was done generating a PCR product with phosphorylated primers NL3716F and NL7520R+AatII and using the pSMART kit. 29 clones were screened and no positive clones were found. In parallel, directed cloning into a pBelo vector was tested. For this approach Fragment B1 was amplified by Phusion polymerase PCR from cDNA with the primers NL3716FplusMluI and NL7520R_2+AatII yielding a PCR product from base 3716 to 7543 (position from GenBank entry NC_005831) with introduced *MluI* and *AatII* restriction sites at the 5' and 3' end, respectively. The PCR product was digested with *MluI* and *AatII*. For the ligation the left arm was amplified from subclone A0 with pBeSCfw and pBelo790F, and the right arm was amplified from pBeloAD4 with pBeSCrev and pBelo1290R. Both arms were digested with *EcoRI*, the left arm additionally with *MluI* and the right arm with *AatII*. After gel purification the fragment B1 and the two arms were ligated to a plasmid sized 10.7 kb and further treated as described in 3.7.3. The cloned B1 fragment showed 100% identity with the reference sequence.

3.7.2.3 Construction of subclone B2

Fragment B2 was amplified by Phusion polymerase PCR from cDNA with the primers NL7430FplusMluI and NL 12460 R +Aat yielding a PCR product from base 7426 to 12473 (position from GenBank entry NC_005831) introducing the same restriction sites as described for subclone B1. PCR and digestion was done according to subclone B1. The insert of the 11.9 kb sized plasmid was identical with the reference sequence.

3.7.2.4 Construction of subclone C

The fragment C had a size of only 2.3 kb and was the first fragment to be subcloned. The PCR product was amplified using primers S12300plusMluI and NL 14629 R, the amplification product comprised the bases 12264 to 14629 of NC_05831. The *MluI* site was introduced by the forward primer, an *AatII* recognition site is located naturally in the HCoV-NL63 genome at position 14573-14578 (NC_005831). It was digested with *MluI* and *AatII* and ligated, as described for fragment B1 and B2, to the digested left and right arm of subclone A0 and pBeloAD4, respectively. The only positive clone had a size of 9.2 kb and showed a silent marker mutation at position 12477 and an insertion of one additional A at position 14117 (NC_005831). This insertion could not be found when performing and sequencing a one-step RT PCR from the original genomic RNA. Therefore it had to be PCR acquired and was corrected (see 3.7.2.7).

3.7.2.5 Construction of subclone D

Fragment D, sized 7.3 kb, was the largest fragment to subclone. Due to the lack of alternative restriction sites, this fragment had to be amplified from cDNA in one continuous sequence. Several sets of cDNA primers and cDNA reaction setups as well as subsequent PCR reactions were tested and optimized. Finally, a PCR using a proofreading polymerase (Herculase) with an increased input of cDNA yielded sufficient amounts of the desired fragment without any potentially interfering side products (see Figure 19 lanes five to eight).

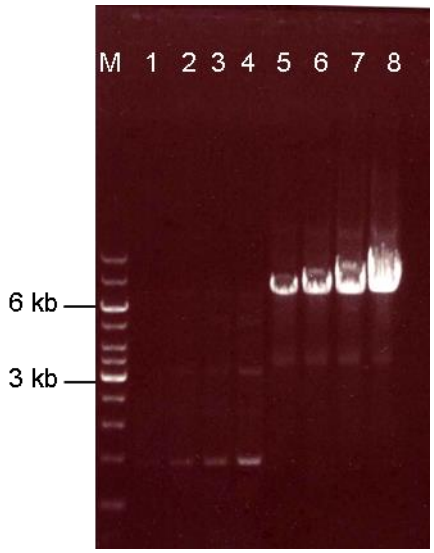

Figure 19: PCR product of fragment D – optimization of PCR reactions with cDNA templates.
PCR products of fragment D amplified with a proofreading polymerase (Herculase) according to 0. Different cDNAs and increasing volume of cDNA template were used for the optimization of the PCR reaction. M: GeneRuler 1 kb DNA Ladder. Lane 1-4 PCR products using cDNA generated with primer 25873R_2 and following input volumes of cDNA: lane 1: 4 µl, lane 2: 6 µl, lane 3: 8 µl, lane 4: 10 µl. Lane 4-8 PCR products using cDNA generated with primer 22251R and following volumes of cDNA template: lane 5: 4 µl, lane 6: 6 µl, lane 7: 8 µl, lane 8: 10 µl.

For the generation of the 7.3 kb PCR product the primers NL 14507 F and NL 21824 R plusNotI were used. The PCR product was concordant to position 14507 to 21824 of the reference sequence NC_05831. The PCR product was digested with *AatII*, naturally located at position 14573-14578 (NC_005831) of the HCoV-NL63 genome and *NotI*, which site was introduced by the reverse primer during PCR.
The construction of the pBelo arms differed from the strategy of subclones B1, B2 and C regarding the restriction enzymes used. All the subclones containing sequences located downstream of the HCoV-NL63 genomes' *AatII* site used a left arm amplified from A0 with the primers pBeSCfw and pBelo790F digested with *EcoRI* and *AatII*. The right arm was

amplified from A0 or pBeloAD4 using the primers pBeSCrev and pBelo1290R. It was digested with *NotI* and *EcoRI*.
For fragment D a two-step ligation was necessary, because the strategy of simultaneous ligation of three fragments failed.
For a two-step ligation, the fragment D was first ligated to the left arm, gel purified and afterwards ligated to the right arm, yielding a plasmid sized 14.6 kb. Positive clones had a non-silent point mutation at position 16875 (NC_005831, see Table 23) changing Threonine to Isoleucine. This point mutation was corrected (see 3.7.2.7).

3.7.2.6 Construction of subclone E

Fragment E was amplified from cDNA by Phusion polymerase PCR using primers S 21637+Aat and NL 25873 RplusNotI. The PCR product was processed as described for fragment D.
The 11.6 kb sized positive clones had two non-silent point mutations at position 22525 and 23466 (NC_005831, see Table 23), both mutations were corrected (3.7.2.7).

3.7.2.7 Correction of the subclones

Corrections were done using the Phusion (2.2.1.16) and QuickChange II (2.2.1.17) site directed mutagenesis kits. Primers were designed according to the manufacturers' recommendations and re-designed when the generation of PCR products or clones failed.
Correction of subclone C
The insertion in subclone C was corrected using the phosphorylated primers NL63-pB-C-mut2002F and NL63-pB-C-mut2002R2 and the QuickChange mutagenesis kit. Single colonies were analyzed for the correct sequence at position 14117 (NC_005831).
Correction of subclone D
The point mutation at position 16875 (NC_005831) in subclone D was corrected using the Phusion site-directed mutagenesis kit with phosphorylated primers D2936corFw and D2936corRev. The annealing temperature had to be lowered to 58°C for the generation of a PCR amplicon. The PCR product was successfully ligated, transformed and yielded positive clones with a correct sequence.
Correction of subclone E
For the correction of subclone E both point mutations were changed in parallel using the Phusion site-directed mutagenesis kit. In one reaction, the point mutation at position 22525 (NC_005831) was corrected with primers pB_E_mut1562F_2 and pB_E_mut1562R_2, in a second reaction the mutation at position 23466 (NC_005831) was corrected with primers pB_E_mut2503F_2 and pB_E_mut2503R_2. The mutagenesis PCRs were ligated transformed and resulting colonies were screened for positive clones with the correct

sequence.
Clones with the correct sequence, one corrected at position 22525 and the other at position 23466, were digested with *BsrGI*. This enzyme had a recognition site at position 23272 to 23277 from HCoV-NL63 (NC_005831) and in the *repE* gene of the pBelo backbone. Ligation of the fragment parts containing the corrected point mutations resulted in clones with a sequence according to GenBank Accession Number NC_005831 at position 22525 as well as 23466.

3.7.3 Assembly of the subclones

For the generation of the full-length cDNA clone the subclones were gradually assembled to bigger subclones as described below, finally resulting into two subclones containing the 5' and the 3' half of the HCoV-NL63 cDNA genome (subclone ABC and ADEF, see Figure 20). These two subclones were joined and resulted into the full-length HCoV-NL63 clone.

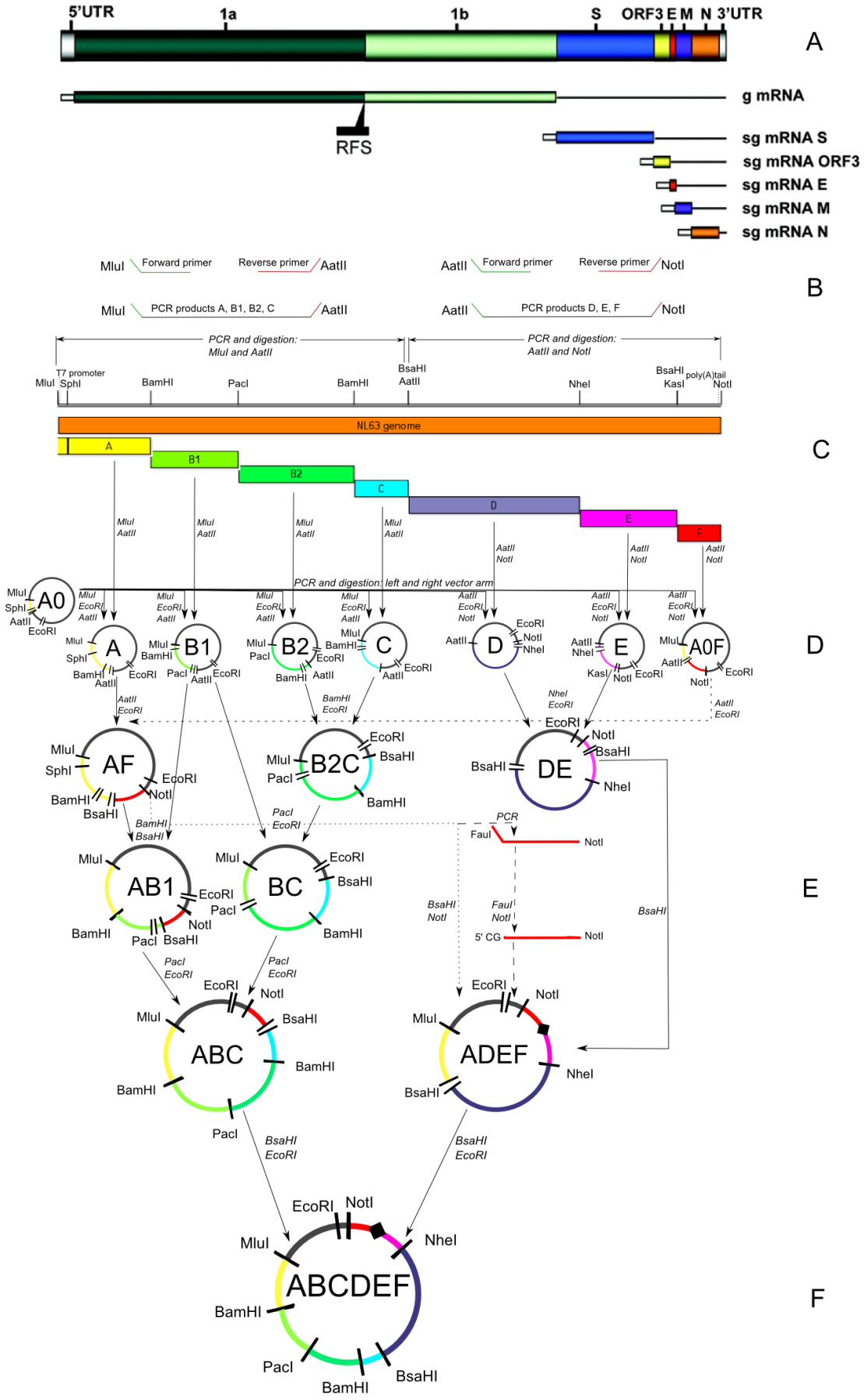
5'UTR
1a
1b
S
ORF3
E
M
N
3'UTR
A
g mRNA
RFS
sg mRNA S
sg mRNA ORF3
sg mRNA E
sg mRNA M
sg mRNA N
MluI
Forward primer
Reverse primer
AatII
B
PCR products A, B1, B2, C
PCR products D, E, F
NotI
PCR and digestion:
MluI and AatII
AatII and NotI
T7 promoter
SphI
BamHI
PacI
NheI
BsaHI
KasI
poly(A)tail
NL63 genome
C
A
B1
B2
C
D
E
F
PCR and digestion: left and right vector arm
A0
EcoRI
AatII
NotI
NheI
A0F
AF
B2C
DE
AB1
BC
ABC
ADEF
ABCDEF
PCR
FauI
5' CG
D
E
F

Figure 20: Assembly of subclones and full-length HCoV-NL63 clone.

From A to F: HCoV-NL63 genome, the resulting cloning strategy and the effective assembly of the full-length clone. **A:** Illustration of HCoV-NL63 genome and the subgenomic mRNAs (Pyrc et al. 2007). **B:** PCR products generated from a set of cDNAs from full-length RNA of HCoV-NL63 stock LLC-MK2 NP. PCR products for fragments A, B1, B2 and C were generated using forward primers with an additional *MluI* site and reverse primers with an additional *AatII* site. PCR products for fragments D, E and F were generated using forward primers carrying an additional *AatII* site and reverse primers with an additional *NotI* site. **C:** Cloning strategy in scale of the HCoV-NL63 genome (see schematic overview in A). Existing unique (except of *BamHI*) restriction sites for the assembly are highlighted. PCR products containing the genome fragments are illustrated in different colors (yellow: A0 and A, light green: B1, dark green: B2, blue: C, violet: D, pink: E, red: F). Construction of the modified pBelo BAC A0 is depicted in Figure 15**. D:** Construction of the subclones, using the modified pBelo BAC A0 as vector backbone (Exception: subclone A was initially cloned into pSMART). PCR products and BAC inserts are illustrated in their corresponding colors. Restriction enzymes used for the digestion of the PCR products and the PCR generated vector arms are depicted in italics, restriction sites used for the further assembly are highlighted. **E:** Assembly of subclones containing a single fragment up to half-length clones (ABC and ADEF). For the assembly plasmids were digested and ligated; restriction enzymes employed are shown in italics. Fragments for the assembly of subclone ADEF were generated using PCR and digestion, the ligation of *FauI* and *KasI* restricted fragments led to the deletion of the *KasI*/*BsaHI* site (black diamond) connecting fragments E and F. **F:** Assembly of the full-length HCoV-NL63 clone using *BsaHI* and *EcoRI* restricted subclones ABC and ADEF.

3.7.3.1 Assembly of subclone AF

For the construction of the subclone AF, fragment A was amplified from the pSMART clone (3.7.2.1) using vector primers SL1 and SR2 and Phusion DNA polymerase (2.2.1.11). This PCR product was digested with *SphI* and *AatII*.

The receiving vector backbone including the A0 and the F fragment was prepared in two ways: The first method comprised preparation of plasmid DNA (Midi scale) from subclone A0F (3.7.1), followed by an *EcoRI* digestion. The reaction was precipitated and washed, resuspended, split and a second digestion with either *SphI* or *AatII* followed, leaving a left arm sized 6.6 kb containing the 5' end (A0) and a right arm sized 2.5 kb containing the F fragment.

The second method used a PCR with the primer pairs pBeSCfw-pBelo790F for the left arm and pBeSCrev-pBelo1290R for the right arm. The PCR products were digested with *SphI* and *EcoRI* for preparation of the left arm; the right arm was digested with *AatII* and *EcoRI*. Sizes of the digested fragments were 6.6 and 2.5 kb, respectively.

The digested plasmids and PCR products were gel-purified and ligated in two separate reactions, either the plasmid-based left and right vector arms together with the A insert in a two-step ligation reaction, or the PCR-based arms together with the A insert in a one-step ligation reaction. The ligation reactions were transformed into chemically competent *E. coli* cells (stbl3); single colonies were isolated and screened using PCR as well as performing

plasmid preparations and agarose gel electrophoresis.
Interestingly the ligation of PCR products in a one-step ligation reaction proved to be much more effective than the ligation with vector arms originally prepared and digested from plasmids and ligated in two steps (Figure 21).

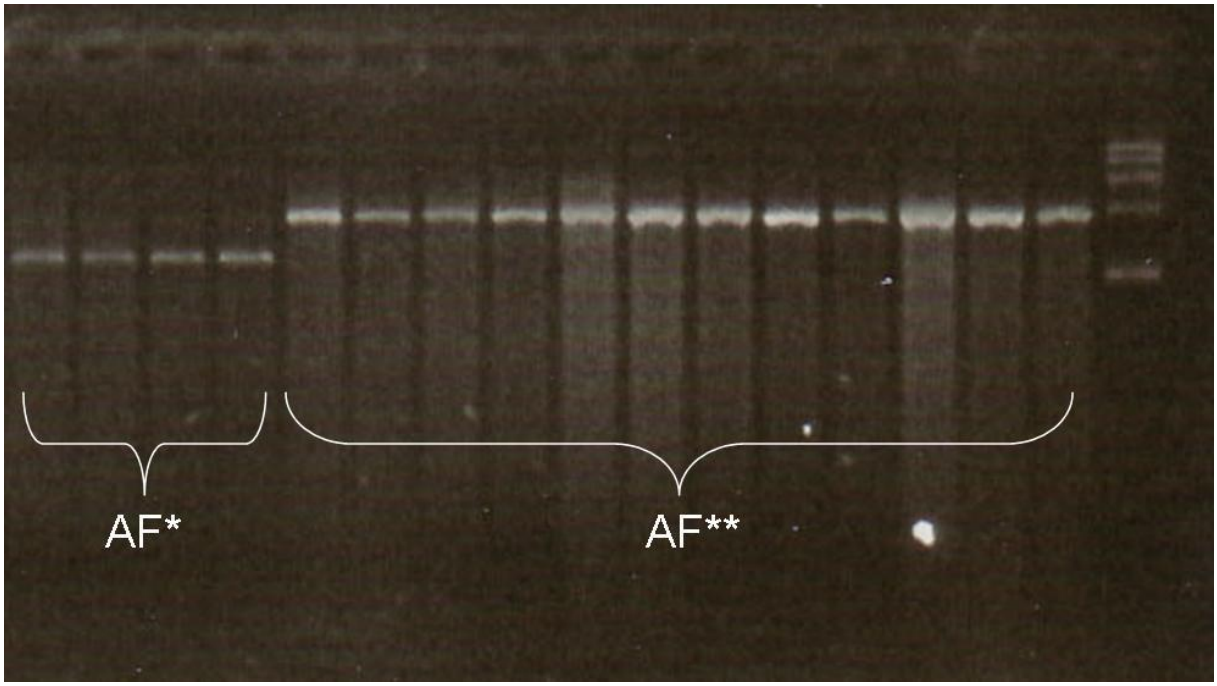

Figure 21: Screening of AF subclones. Screening of isolated plasmid DNA for positive clones from different ligation strategies: AF*: ligation of fragment A and pBelo right arm first, then addition of pBelo left arm containing fragment F, all clones are negative and have a size of 9.5 kb, corresponding to the size of subclone A0F. AF**: one step ligation of three digested fragments (fragment A, pBelo right arm, pBelo left arm containing fragment F). All fragments were initially obtained by using PCR. All clones have a size of 13 kb, corresponding to the calculated size of subclone AF. Molecular weight marker: Supercoiled DNA Marker Set, see 2.1.11.

In Figure 21 the correct size of the screened plasmid DNA from clones of the one step ligation (AF**) indicates a high efficacy of this method compared to the two step ligation (AF*) with no clones containing plasmid DNA of the correct size.

Correction of subclone AF

Three mutations were noticed in comparison to the reference sequence NC_005831, two of them silent. The non-silent mutation at position 327 (NC_005831) was corrected using the Phusion site-directed mutagenesis kit (2.2.1.16) with the primers NL63-pB-NLA3-mut494F and NL63-pB-NLA3-mut494R2.

Deletion of *AarI*, *NheI*

Three restriction sites of subclone AF were deleted to enable the cloning strategy depicted in Figure 20. The *NheI* digestion for the connection of fragment D and E required the deletion of

NheI sites in the fragments A and F (see Figure 14).
Two Phusion site-directed mutagenesis kit reactions were carried out using subclone AF as template, one deleting the *NheI* site in fragment A, using primers ORF1a1b_delNhe_fw and ORF1a1b_delNhe_rev; one deleting the *NheI* site in fragment F using primers ORF6delNhe_fw and ORF6delNhe_rev. Plasmids were digested with *EcoRI* and *BamHI* and the parts of the subclones containing the deleted restriction sites were ligated. A subclone with deleted *NheI* sites in fragments A and F was chosen and used as template for other Phusion site-directed mutagenesis kit reactions, deleting the *AarI* site. Primers ORF1_delAar_fw2 and ORF1_delAar_rev2 were used for the PCR reaction. One of the positive clones was chosen and the insert (fragment A plus F) was sequenced in total. It showed to be concordant with the GenBank sequence NC_05831 except of the tolerated silent mutations (see HCoV-NL63 LLC-MK2 NP in Table 23) and the introduced mutations leading to the deletion of *NheI* and *AarI* restriction sites.

Deletion of *KasI*

The whole HCoV-NL63 cloning strategy depended on a final digestion with *AatII* and a ligation of the compatible ends thereof. As already described for subclone AF, the digestion and ligation of PCR products worked well using *AatII*, whereas the digestion and ligation of plasmid preparations was less effective (see 3.7.3.1). For the assembly of bigger subclones, the cloning strategy was changed in favor of *BsaHI*. This enzyme recognizes the *AatII* as well as the *KasI* site. Therefore the *KasI* site of fragment F had to be deleted.
The modification was done in parallel to both subclones AF (described here) and ADEF (described below 3.7.3.6).
A preparation of subclone AF plasmid was digested with *NotI* and *BsaHI* (see 3.7.3.6). This resulted in an 11 kb fragment containing the vector backbone and the fragment A, and two smaller fragments (1.8 and 0.15 kb). The two smaller fragments represented the digestion products of fragment F after cutting the *AatII* and the *KasI* site with *BsaHI*. The 11 kb fragment, also used for the construction of ADEF with deleted *KasI*, was ligated to the 1.8 kb fragment, joining the *AatII* and the *KasI* restriction sites. This slightly smaller subclone AF lacked a short stretch of the F fragment and joined the *AatII* and *KasI* site to a *BsaHI* site. Clones were first sequenced for the absence of the *AatII* and *KasI* sites and the presence of the *BsaHI* site and then in total. The plasmid was designated subclone AF “del”.

3.7.3.2 Assembly of subclone AB1

For the construction of AB1 preparations of the plasmids AFdel (3.7.3.1) and B1 (3.7.2.2) were used. The plasmids were digested with *BamHI* and *BsaHI*, yielding two fragments of 12.6 and 0.2 kb for AF del and two fragments of 7.0 and 3.7 kb for B1. The 12.6 kb fragment

contained the sequence of fragment A, a part of fragment F and the vector backbone. The 3.7 fragment contained fragment B1. They were ligated to a 16.3 kb pBelo BAC designated AB1.

3.7.3.3 Assembly of subclone B2C

For the assembly of subclone B2C plasmid preparations of subclone B2 (3.7.2.3) and C (3.7.2.4) were digested with *EcoRI* and *BamHI*. After complete digestion subclone B2 was separated in an 11.2 kb and a 0.7 kb fragment and subclone C in a 6.4 and 2.8 kb fragment. The 11.2 kb fragment contained fragment B2 and the left arm of the vector backbone and was ligated to the right arm of the vector backbone containing fragment C, resulting in a 14 kb subclone B2C.

3.7.3.4 Assembly of subclone DE

The assembly of subclone DE was done using plasmid preparations of the subclones D and E. Both plasmids were digested with *NheI* and *EcoRI*. Fragment D was digested in two fragments sized 13.9 and 0.7 kb, for fragment E the sizes were 6.9 and 4.7 kb, respectively. The 13.9 kb part containing fragment D and the left arm of the vector backbone as well as the 4.7 kb part containing fragment E and the right arm of the vector backbone were ligated to the subclone DE sized 18.6 kb.

3.7.3.5 Assembly of subclone BC

For the assembly of subclone BC plasmid preparations of subclone B1 and subclone B2C were digested with *PacI* and *EcoRI*, yielding a 10.1 and a 0.6 kb fragment for B1 and a 7.7 and a 6.4 kb fragment for B2C. The B1 and major vector backbone containing 10.1 kb fragment and the B2C containing 7.7 kb fragment were ligated to the resulting 17.8 subclone BC.

3.7.3.6 Assembly of subclone ADEF

As already described in 3.7.3.1, the digestion of plasmids with *AatII* was crucial for the cloning of the full-length HCoV-NL63 clone. Despite several changes in the reaction setup, no complete digestion of plasmids could be achieved. The changes comprised variation of enzyme units, proteinase K incubation before restriction, prolonged incubation times, digestion after linearization of the plasmid, different enzyme providers and a switch of the *E. coli* host. This finding was concordant to the observation made during the assembly of subclone AF, indicating an efficient digestion and ligation of PCR products in contrast to a poor digestion and ligation of plasmids (3.7.3.1).

The only efficient solution was a change of the cloning strategy in favor of *BsaHI*. *BsaHI* (GR'CGYC) recognized the central *AatII* restriction site (GACGT'C) as well as the fragment E

to F linking *KasI* restriction site (G'GCGCC). Given that *AatII* and *KasI* were part of the original cloning strategy, with *AatII* being more essential, this switch necessitated the deletion of the *KasI* site.

Deletion of *KasI* and the assembly of ADEF from the subclone AF and DE were done simultaneously. Three fragments were generated for the deletion of the *KasI* site:

The first fragment comprised the F fragment and was amplified from subclone AF using the forward primer *KasI*_del_lang, introducing a G for a C in the *KasI* recognition site (GGCG**C**C → GGCG**G**C) and containing a 5' proximal *FauI* restriction site. Primer pBelo1290R was used as reverse primer. The PCR product was digested with *NotI* and *FauI*, leaving a 1.8 kb fragment with compatible overhangs for the ligation with *NotI* and *BsaHI* digested DNA (see Figure 20).

For the generation of the second fragment the DE subclone was digested with *BsaHI*, cutting at the *AatII* and the *KasI* site. The digestion resulted in two fragments, one containing mainly the vector backbone (7.5 kb) and the other containing the fragments D and E (11.2 kb).

The third fragment was generated by the digestion of subclone AF with *NotI* and *BsaHI*, leading to a 11 kb fragment containing the vector backbone and the fragment A, and two smaller fragments (1.8 and 0.15 kb).

All three fragments (1.8kb fragment F, 11.2 kb fragments DE and 11 kb pBelo BAC including fragment A) were ligated to subclone ADEF with a deleted *KasI* site in the F fragment (see Figure 14 and Figure 20).

3.7.3.7 Assembly of subclone ABC

For the construction of subclone ABC plasmid preparations of subclones AB1 and BC were used. The plasmids were digested using *PacI* and *EcoRI*, resulting in two 13.5 and 2.5 kb fragments regarding AB1. The bigger fragment comprised the major part of the vector and fragments A and B1.

The BC plasmid was cut in a 7.7 and a 10.1 kb sized fragment. The former comprised fragments B2, C and the right arm of the vector; the latter contained fragment B1 and the bigger, left arm of the vector. The 7.7 kb fragment was ligated to the 13.5 kb fragment, and resulted in subclone ABC.

3.7.3.8 Assembly of the NL full-length cDNA clone

For the assembly of the full-length cDNA clone (Figure 14 and Figure 20) plasmid preparations of the subclones ADEF and ABC were digested with *BsaHI* and *EcoRI*. This resulted in a 13.6 and a 10.4 kb sized fragment for ADEF and a 20.9 and 0.6 kb sized fragment for ABC. The 13.6 kb fragment containing DEF and the right arm of the vector was ligated to the 20.9 kb fragment containing ABC and the left arm of the vector. In total 12

different ligation reactions with various fragments from different digestions were set up and over 200 clones were screened until one positive clone was found. Sequencing was concordant to GenBank entry NC_005831, except for the naturally occurring marker mutations (position 2956, 2977, 12477, see Table 23) and introduced restriction sites (position 1087, 1405, 25753, 26582, see Figure 14). The full-length recombinant HCoV-NL63 clone was designated rNL63 wt (for wild type), see Figure 22 B.

3.8 *In vitro* transcription (IVT) of full-length rNL63 and N gene

The recombinant full-length clone was equipped with the previously introduced single cutting *NotI* recognition site behind the poly (A) tail, which allowed the linearization of the plasmid. The linearized DNA was purified and served as template for *in vitro* synthesis of capped RNA using the introduced T7 promoter and a T7-based transcription kit. For the initial transcriptions the mMESSAGE mMACHINE kit (Ambion) was used. Complying with the guidelines for optimization of yield for long transcripts, the GTP to Cap analog ratio was altered to approximately 1:1.

According to Enjuanes et al. (Almazan et al. 2004; Schelle et al. 2005) the efficiency of initial replication in coronavirus reverse genetic systems is increased by cotransfection of nucleocapsid mRNA. Therefore the N gene was amplified from the full-length rNL63 wt plasmid using primers NL_N+SP6fw and NL_27553R+20trev. An SP6 promoter sequence was introduced within the forward primer sequence. The PCR product was purified and *in vitro* transcribed using a SP6-based transcription kit.

After *in vitro* transcription, the capped RNAs were purified using phenol/chloroform and precipitated with isopropyl alcohol. The yield of RNA was increased notably when incubating the RNA/isopropyl alcohol mixture over night at -20°C. The RNA pellets were resuspended in 15-30 µl nuclease-free water and quantified using photometry. RNA concentrations of 2 to 5 µg/µl were obtained.

Some of the transcripts were analyzed using conventional agarose gel electrophoresis with DEPC treated buffers and solutions (Figure 22). The HCoV-NL63 transcripts were compared to a SARS CoV transcript that has already been successfully transfected into BHK cells previously. All full-length transcripts presented a smear from high to low molecular weight, starting with a faint but unambiguous high molecular band, except for the overloaded lane 3 (Figure 22).

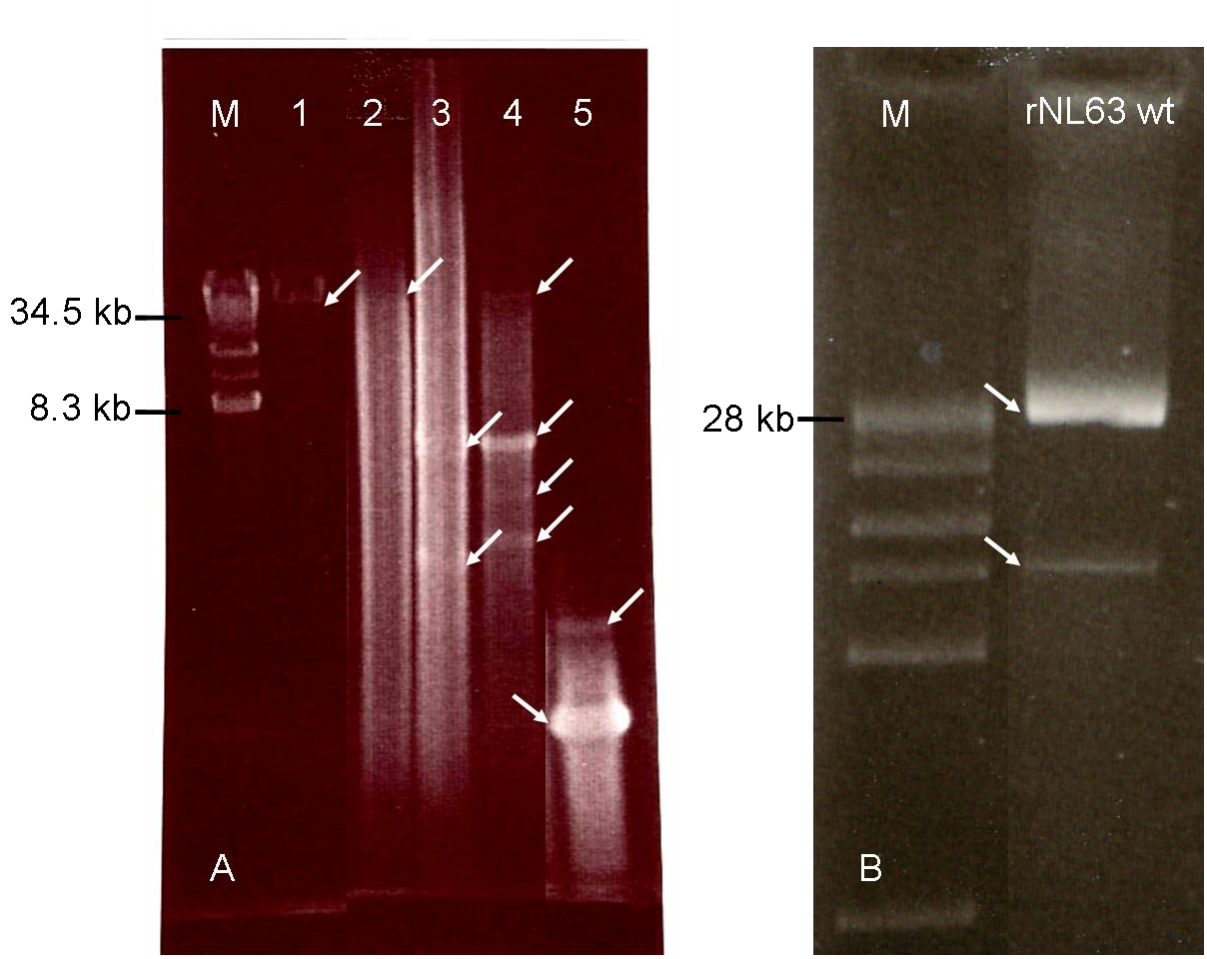

Figure 22: *In vitro* transcripts of Coronavirus full genome and N. Plasmid preparation of rNL63 wt.
A: *In vitro* transcripts (selection). M: High molecular weight DNA marker; lane 1: linearized HCoV-NL63 full-length plasmid rNL63 wt (arrow, 34.481 kb). Lane 2: *in vitro* transcribed and capped, functional SARS CoV RNA, arrow indicates the putative full-length RNA transcript. Lane 3-4: *in vitro* transcribed and capped HCoV-NL63 RNA; upper arrow indicates a putative full-length RNA transcript, lower arrows indicate distinct bands originating from either smaller or coiled RNA transcripts. Lane 5: 1:10 diluted capped HCoV-NL63 N RNA transcript, arrows indicating bands with higher and lower molecular weight or with different secondary structures (coiled, relaxed).
B: Plasmid preparation of rNL63 wt. M: Supercoiled DNA Marker Set. rNL63 wt: upper band represents the supercoiled plasmid of rNL63 wt (approximately 35 kb), lower band represents linearized plasmid.

The major difference between the transcripts of SARS CoV and HCoV-NL63 were distinct bands within the smear, clearly visible in the HCoV-NL63 transcripts (lane 3 and 4, Figure 22). The N transcripts of HCoV-NL63 showed a faint additional band and smear of higher molecular weight (Figure 22, lane 5, upper arrow).

3.9 Transfection into mammalian cells

For the transfection into mammalian cells, usually 10 µg *in vitro* transcribed and capped full-length virus RNA was transfected together with 2 µg *in vitro* transcribed and capped N gene RNA. A successful transfection was achieved using a comparatively low concentrated full-length HCoV-NL63 transcript of 1 µg/µl. 7.5 µg of full-length RNA were co-transfected with 3.5 µg N gene RNA into LLC-MK2 as well as CaCo-2 cells. Transfection of N gene RNA alone served as negative control. The cells were mixed with the RNA, pulsed and seeded in cell culture flasks as described in (2.2.2.5). Flasks were sampled at days 0, 4, 7 and 9.

3.10 Rescue of rNL63 wt

The transfected cells were monitored by real-time RT PCR, detecting viral nucleic acids, and cytopathic effects (CPE) were monitored macro- and microscopically. Since only a fraction of the added RNA was internalized by the cells, the real-time RT PCR results (Figure 23) showed high values for HCoV-NL63 RNA on day 0.

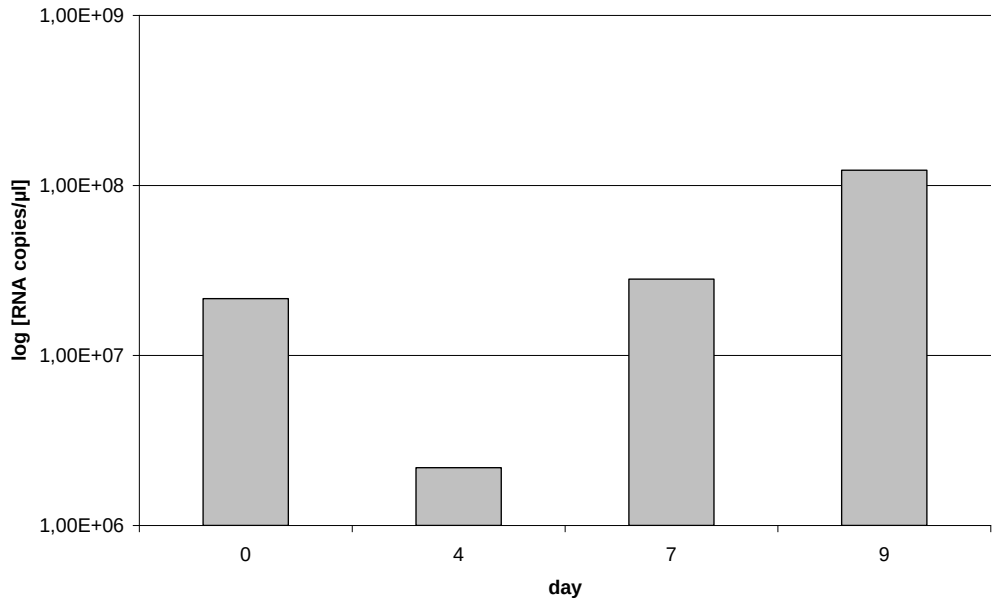

Figure 23: Quantification of viral RNA from rNL63 wt in cell supernatant post transfection.
Results of Light Cycler analysis from LLC-MK2 cell culture supernatant after transfection with rNL63 wt *in vitro* transcribed (IVT) RNA. Samples were taken on day 0, 4, 7 and 9 post transfection. Sampling on day 0 was done immediately after seeding the electroporated LLC-MK2 cells into a cell culture flask. RNA copies decreased between day 0 and day 4 due to degradation of excess IVT RNA in the cell culture supernatant. Concentration of virus RNA increased again at day 4, 7 and 9 to a maximum on day 9. Increase of RNA copies in cell culture supernatant samples represented an increase of recombinant virus particles.

The RNA in the supernatant was degraded slowly; this effect is visualized by the decreased RNA value on day 4. Between day 4 and day 7 the recombinant virus replication increased

notably, the viral RNA concentration in the samples rose and equaled the value of day 0. Virus replication continued and exceeded the initial value at day 9. Virus replication was only detected in LLC-MK2 cells. The negative controls with exclusive transfection of N gene RNA remained negative; also the CaCo-2 cells transfected with full-length genome and N gene RNA did not show any measurable signs of virus replication.
The RNA that was extracted from the samples was also used for the verification of the origin of rescued virus. This was done by analyzing the genetic properties like marker mutations, introduced for the deletion of restriction sites (see below).
Cell culture supernatant containing the novel, recombinant virus was prepared as described for virus stocks (2.2.3.1) and stored at -70°C. A plaque purification assay was done using CaCo-2 cells (see 3.10.3).

3.10.1 Proof of marker mutations

The introduced marker mutations were verified in two different ways. First, the *NheI* site that was deleted in the A fragment (see 3.7.3.1) was evidenced by amplification and digestion of the PCR products originating from the virus HCoV-NL63 LLC-MK2 NP and the recombinant virus rNL63 wt. For this purpose the RNA from the rescued recombinant virus as well as some RNA from HCoV-NL63 LLC-MK2 NP were amplified in a one-step RT PCR with primers 1688R and 880F, sequenced, purified and digested with *NheI*. Figure 24 A and B show the electropherogram of the *NheI* site being functional for HCoV-NL63 LLC-MK2 NP (A) and deleted for rNL63 wt (B). In Figure 24 C, the first two lanes show the approximately 800 bp product amplified from HCoV-NL63 LLC-MK2 NP without (lane 1) and with (lane 2) *NheI* restriction. The cleavage into two fragments sized 250 and 550 bp indicated clearly the presence of the *NheI* site. Lanes 3 and 4 show the 800 bp PCR product amplified from rNL63 wt without (lane 3) and with (lane 4) *NheI* digestion, proving the absence of the *NheI* site and therefore the recombinant origin of the virus.

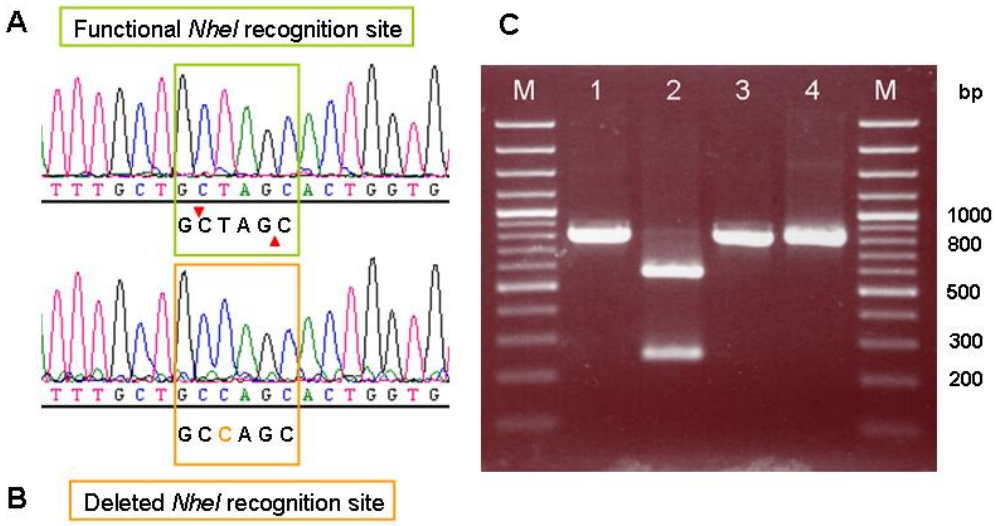

Figure 24: Verification of recombinant HCoV-NL63 (rNL63 wt) by sequencing and *NheI* digestion.
One-step RT-PCR of RNA preparations from transfected (rNL63 wt IVT) and infected (wild type virus) LLC-MK2 cell cultures was performed. PCR products were sequenced (see A and B). The deletion of the *NheI* restriction site was verified by restriction of the purified PCR product and succeeding gel electrophoresis (see C).
A: Electropherogram of the wild type virus (HCoV-NL63 LLC-MK2 NP) sequence. PCR product was sequenced using primer 1154F. The sequence covers the functional *NheI* restriction site at base pair position 1403-1408 (Reference sequence: Amsterdam 1, Accession No. NC_005831) boxed in green. **B:** Electropherogram of the recombinant virus (rNL 63 wt) sequence. PCR product and sequencing was done according to A. The deleted *NheI* restriction site is boxed in orange. **C:** *NheI* restriction of PCR products. M: GeneRuler 100 bp Plus DNA Ladder. Lane 1: 800 bp one-step RT PCR product of wild type virus (HCoV-NL63 LLC-MK2 NP). Lane 2: 800 bp one-step RT PCR product of wild type virus (HCoV-NL63 LLC-MK2 NP, see lane 1) after digestion with *NheI*, producing two 550 and 250 bp fragments. Lane 3: 800 bp one-step RT-PCR product of recombinant HCoV-NL63 (rNL63 wt). Lane 4: 800 bp one-step RT PCR product of recombinant HCoV-NL63 (rNL63 wt, see lane 3) after incubation with *NheI*, the one-step RT PCR product remains 800 bp in size, the recognition site for *NheI* is deleted.

The second evidence was given by sequencing the deleted *AarI* site in fragment A. For this purpose the RNAs from rNL63 wt as well as from HCoV-NL63 LLC-MK2 NP were amplified in a one-step RT PCR with primers 1471R and 398F, purified and sequenced in forward direction with primer 771F and in reverse direction with primer 1471R. Figure 25 shows the sequencing results for *AarI*. The sequence variation is boxed, showing an intact *AarI* recognition site for HCoV-NL63 LLC-MK2 NP. Concordant with the sequence of the full-length clone, the results from sequencing the rNL63 wt virus showed clearly a “G” in the electropherogram, confirming it to be a recombinant virus with deleted *AarI* recognition site.

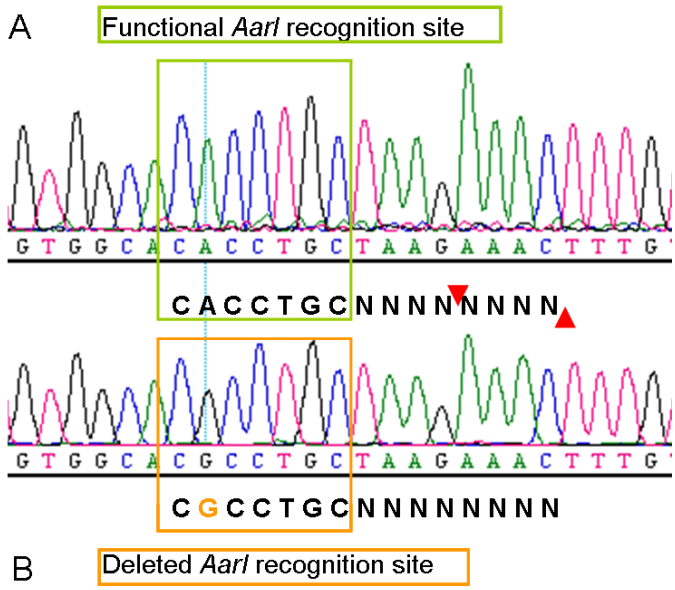

Figure 25: Verification of the *AarI* restriction site deletion in the recombinant HCoV-NL63 (rNL63 wt). One-step RT-PCR products from RNA preparations of transfected (rNL63 wt) and infected (wild type virus) cell cultures were sequenced using primer 771F. The sequence covers the functional and mutated *AarI* restriction site at base pair position 1086-1092 (Reference sequence: Amsterdam 1, Accession No. NC_005831). **A:** Electropherogram of wild type virus (HCoV-NL63 LLC-MK2 NP) with functional *AarI* restriction site boxed in green. **B:** Electropherogram of recombinant HCoV-NL63 (rNL63 wt) with deleted *AarI* restriction site boxed in orange.

With these findings further tests were done to confirm the presence of viable recombinant virus.

3.10.2 Immunofluorescence Assay (IFA) of rNL63 wt

Virus replication of rNL63 wt was analyzed by detecting the expression of viral proteins in infected CaCo2 cell cultures using an immunofluorescence assay (2.2.4.2). The nucleocapsid and the matrix protein were successfully detected using Anti-N antibodies and Anti-M antibodies, as shown in Figure 26.

The nucleocapsid protein was mainly detected in the cytoplasm of the infected CaCo-2 cells (Figure 26 A). The matrix protein was located around the nucleus, indicating a position in or close to the rough ER (Figure 26 B) and ERGIC as previously described (Muller et al. 2010). Therefore the presence of viable, recombinant rNL63 wt virus could be assumed.

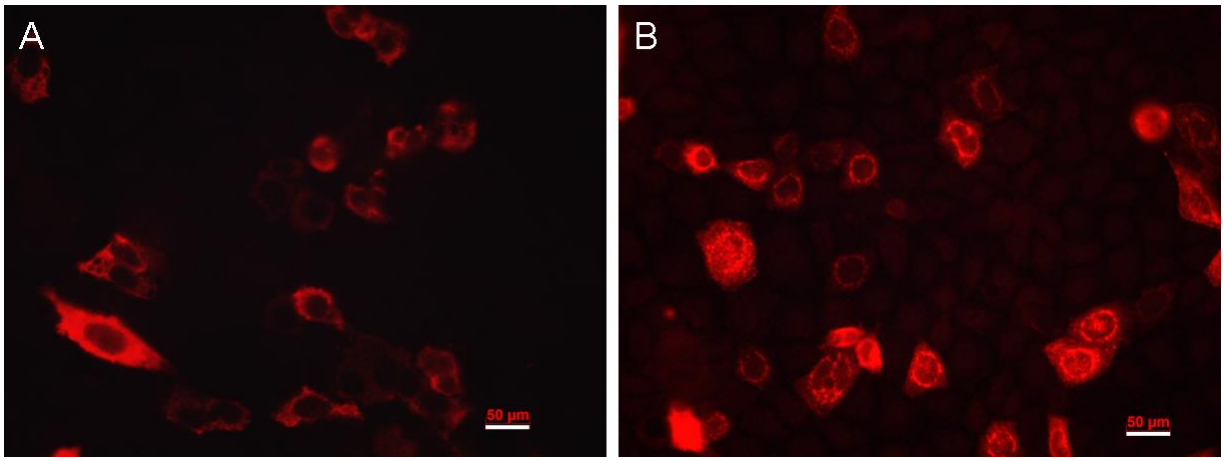

Figure 26: Immunofluorescence Assay of recombinant HCoV-NL63 (rNL63 wt).
Caco-2 cells were seeded on a 24-well plate and infected with recombinant HCoV-NL63 (rNL63 wt). Four days after infection cells were fixed with PFA (4%) for 15 min and permeabilized with 100% acetone for 10 min. Afterwards the cells were washed with PBS and then incubated with the primary antibody, diluted 1:100 in sample buffer at 37°C for 1 h. For the detection of the different viral proteins (M, N) peptide generated rabbit antisera (Muller 2007) were applied. Secondary detection was done with a rhodamine-conjugated goat-anti-mouse antibody at 37°C in a wet chamber for 30 min. Slides were mounted with DakoCytomation Fluorescent Mounting Medium and analyzed by fluorescent microscopy at a magnification of 400-fold. White bar represents 50 µm. **A:** CaCo-2 cells infected with rNL63 wt, primary antibody Rabbit Anti N serum 1:100, secondary antibody Anti-Rabbit Cy3. **B:** CaCo-2 cells infected with rNL63 wt, primary antibody Rabbit Anti M serum 1:100, secondary antibody Anti-Rabbit Cy3.

3.10.3 Plaque purification

As soon as viral replication could be detected and confirmed in the transfected cells, plaque purification was done, in order to minimize defective interfering particles and to gain a recombinant virus of high viability.

Interestingly the recombinant virus showed extremely small plaques (Figure 27 B) compared to HCoV-NL63 LLC-MK2 NP (Figure 27 A). The plaques of the recombinant virus became visible after 7-10 days using agarose overlay. They were very hard to see either macroscopically or microscopically and plaque picking was difficult due to the small size. In the third round of plaque purification, the plaque morphology changed to bigger, visible plaques with HCoV-NL63 LLC-MK2 NP-like appearance (Figure 27 C).

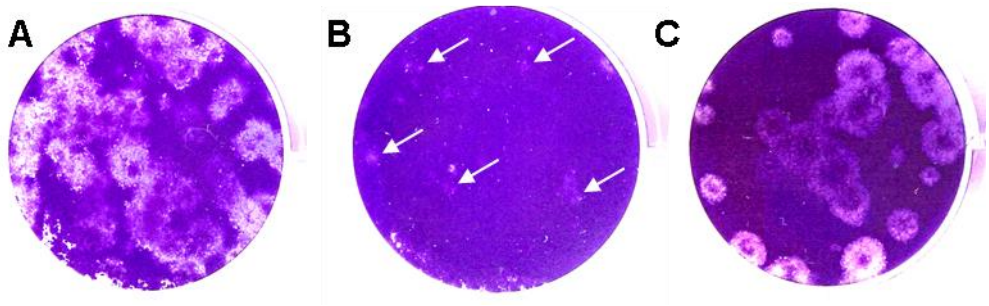

Figure 27: Comparative plaque assay of wild type and recombinant HCoV-NL63.
CaCo-2 cells were seeded on six-well plates and infected with wild type (HCoV-NL63 LLC-MK2 NP) and recombinant (rNL63 wt) virus. Infected cells were overlaid with 1.6% Avicel in DMEM and incubated at 37°C and 5% CO2. On day 5 Avicel overlay was removed, cells were fixed with PFA (4%) for 15 min and stained with crystal violet solution for 15 minutes. **A:** Large and clearly visible plaques of wild type virus (HCoV-NL63 LLC-MK2 NP). **B:** Very small and hardly visible plaques of recombinant virus rNL63 wt. White arrows indicate the location of the plaques. **C:** Large and clearly visible plaques of plaque purified rNL63 wt.

After the third round of plaque purification using CaCo-2 cells, a virus stock was generated as described in (2.2.3.1); marker mutations were verified by sequencing a one-step RT PCR product from the virus stock as described in 3.10.1.
A comparison of growth kinetic from plaque purified rNL wt and HCoV-NL63 CaCo-2 PP virus stocks showed a similar amount of viral RNA after 168 hours in cell culture supernatant of infected CaCo-2 cell cultures (Figure 28 A).

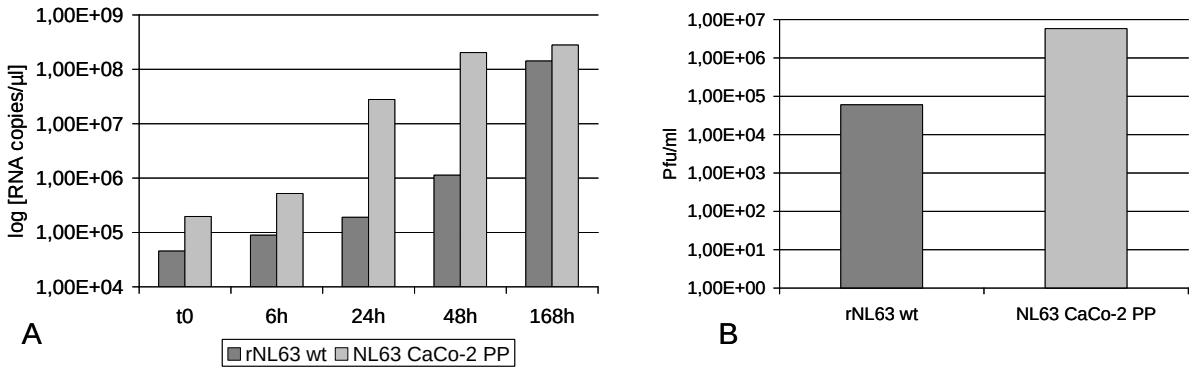

Figure 28: Quantification of viral RNA and plaque forming units (Pfu) from plaque purified rNL63 wt and HCoV-NL63 CaCo-2 PP in CaCo-2 cell culture supernatant. A: Results of Light Cycler analysis from CaCo-2 cell culture supernatant after infection with rNL63 wt and HCoV-NL63 CaCo-2 PP virus stocks. Samples were taken after 6, 24, 48 and 168 hours. **B:** Comparative plaque assay of plaque purified rNL63 wt and HCoV-NL63 CaCo-2 PP virus stocks. CaCo-2 cell cultures were seeded on six-well plates, infected with the respective virus stock and overlaid with Avicel as described above. Plaques were counted on day five.

The slower growth of rNL 63 wt within the first 48 hours presumably resulted from the hundredfold difference in plaque forming units (Figure 28 B) of the virus stocks rNL wt and NL63 CaCo-2 PP used for the infection of the CaCo-2 cell cultures. Further plaque

purification of rNL63 wt could be performed to recover a virus stock with a similar titer compared to HCoV-NL63 CaCo-2 PP, resulting in similar growth kinetics.

4 Discussion

4.1 Susceptibility studies with HCoV-NL63 and development of a plaque assay

HCoV-NL63 is causative for up to 10% of common colds, especially in winter time, and can lead to hospitalization of predominantly young children and elderly persons. A major obstacle when working with HCoV-NL63 is that it replicates slowly and at relatively low titers in all current cell cultures, such as LLC-MK2 and Vero-B4 cells (Fouchier et al. 2004; van der Hoek et al. 2004). Because the virus contributes to a very weak and diffuse CPE in these cells, there is no cytopathic-based plaque assay available for HCoV-NL63.

By conducting a broad-range susceptibility study using 12 cell lines, CaCo-2 cells were found to support HCoV-NL63 replication significantly better than hitherto used culture cells, especially when compared to the standard cultivation cell line LLC-MK2. A pronounced cytopathogenic effect was observed and was the foundation for the development of a plaque assay. Plaque assays make use of viscous overlays to cover cells immediately after infection, thus limiting virus spread and restricting virus growth to foci of cells at the sites of initial infection. If a virus does not cause CPE in cells, these foci may be visualized by immunostaining (Battegay et al. 1991; Matrosovich et al. 2006).

If viruses induce strong cytopathogenic effects, cells are lyzed and the generated plaques can be visualized by staining of the residual intact cells. Cytopathogenic plaque assays are compatible with high-throughput drug screenings (Leyssen et al. 2003; Leyssen et al. 2008) and allow virus plaque purification and subcloning of virus. This in turn is helpful in obtaining virus stocks with optimized infectivity, e.g., by decreasing the amount of defective interfering (di) particles that accumulate during serial passaging of CoV (Makino et al. 1984).

It was interesting to note that the virus stocks obtained from LLC-MK2 as well as from CaCo-2 cells had rather high RNA concentrations as opposed to their infectivities. PFU / RNA ratios were 2.92×10^{-6} for CaCo-2 PP and 2.45×10^{-6} for LLC-MK2 NP. This high excess of RNA over infectious units might be attributable to the virus harvesting procedure, possibly releasing nonpackaged RNA along with virus particles during freeze-thawing. Because PFU / RNA ratios were very similar for both stocks, it appeared unlikely that elimination of defective interfering particles had contributed to the gain of infectivity.

After the additional purification of CaCo-2 adapted virus stock by ten consecutive limiting dilution series, several mutations of the HCoV-NL63 genome could be observed. Three of these mutations were identified in the spike region, which might represent an adaptation to

the CaCo-2 ACE2 receptor molecule and could contribute to the higher infectivity ($3.1x10^6$ versus $1.3x10^5$ PFU/ml) of the resulting virus stock HCoV-NL63 CaCo-2 LD.

A recent publication describes the genomic changes of FIPV associated with viral adaptation at different tissue passage levels (Phillips et al. 2013). The complete genome of FIPV strain WSU 79-1146 was sequenced at passage 1, 8 and 50. An overall low mutation rate was calculated from the resulting amino acid differences. Nevertheless twenty-one amino acid differences were observed in the polyprotein 1a/ab between the different passages, nine in the structural proteins (spike, 3a, 3c, small membrane, nucleocapsid and 7a), respectively. Only one residue change was observed in the spike glycoprotein, which reverted back on subsequent passages and might help to explain the lack of differences in growth kinetic between the passages. In contrast to the observation made during the FIPV adaptation, in this work consecutive passages using CaCo-2 cell cultures led to an increase of infectivity, paralleled by three amino acid changes in the spike protein.

Although the positions of the mutations in the spike gene (21162, 21217, 21390 in GenBank NC_05831) are located outside of the three described HCoV-NL63 ACE2 receptor binding domains (RBD) (Wu et al. 2009), two of them (21162 and 21390 in GenBank NC_05831) seem to be common loci for mutations, as they are also found in the strains Amsterdam 57 and Amsterdam 496. The mutation at position 21217 (in GenBank NC_05831) exclusively occurs in strain HCoV-NL63 CaCo-2 LD. This finding could indicate a correlation between the change of the spike protein sequence and increased infectivity during adaptation to CaCo-2 cell cultures.

Further mutations were observed in the nsp 3, 6, 11/12 and 14 genes. Two of them (nsp 11/12 and 14) being unique for the CaCo-2 adapted strain, the other two mutations could also be observed in other circulating HCoV-NL63 strains. These mutations could either represent an adaptation to CaCo-2 cells or they occurred randomly. Interestingly Angelini et al recently published that transfection of SARS-CoV nsp 3, 4 and 6 induce double membrane vesicles (DMV) in HEK293T cell cultures (Angelini et al. 2013). The observed mutations in nsp 3 and 6 of the CaCo-2 adapted HCoV-NL63 CaCo-2 LD strain might influence the DMV formation and virus proliferation in CaCo-2 cell lines and therefore explain the higher infectivity compared to HCoV-NL63 LLC-MK2 NP. Another effect described by Eckerle et al. could contribute to the mutation rate of the CaCo-2 adapted HCoV-NL63. The nsp 14 exonuclease activity is required for replication fidelity of MHV and SARS-CoV, the genetic inactivation of ExoN results in a 15-fold decrease of replication fidelity in MHV and a 21-fold increase in mutation frequency during replication of SARS-CoV in culture (Eckerle et al. 2010). Although the SARS-CoV nsp 14-ExoN mutant viruses demonstrate stable growth defects, hitherto unknown effects of the mutation in the HCoV-NL63 CaCo-2 LD nsp 14 gene

might contribute to a higher mutation rate and faster adaptation to CaCo-2 cell cultures, including the higher infectivity described above.
A stepwise introduction of the observed mutations into the full-length HCoV-NL63 cDNA clone and the analysis of their effects, i.e. using the novel plaque assay, could help to understand their function in the context of the complete viral genome.

4.2 Establishment of a reverse genetics system for HCoV-NL63

Reverse genetics systems are essential for the analysis and the understanding of viral gene functions. Additionally, reverse genetics systems based on relatively harmless common cold viruses like HCoV-NL63 could be used for gene delivery and chimeric vaccine development (Zust et al. 2007; Cervantes-Barragan et al. 2010; Ribes et al. 2010). Major advantages of coronavirus-based systems are that coronaviruses replicate exclusively in the cytoplasm, not involving mutagenic integrations into host genomes, and that they do not induce major immunological responses (replication in DMVs, expression of IFN antagonists) (Knoops et al. 2008; Perlman et al. 2009; Knoops et al. 2010; McBride et al. 2012). Reverse genetics systems were described for SARS-CoV (Yount et al. 2003; Almazan et al. 2006; Pfefferle et al. 2009), MHV (Yount et al. 2002; Coley et al. 2005), TGEV (Almazan et al. 2000; Yount et al. 2000; Gonzalez et al. 2002), IBV (Casais et al. 2001), HCoV-OC43 (St-Jean et al. 2006), HCoV-229E (Thiel et al. 2001; Thiel et al. 2005), FCoV (Tekes et al. 2008) and recently also for HCoV-NL63 (Donaldson et al. 2008). The major challenge for all approaches was the cloning of the large coronavirus RNA genome.
A reverse genetics system that is based on a BAC backbone, combined with a phage promoter-driven *in vitro* RNA synthesis from a cDNA full-length clone, and an efficient transfection of infectious RNA into the cytosol of susceptible mammalian cells is already well established in our workgroup for SARS-CoV (Pfefferle et al. 2009; Voss et al. 2009; Muth et al. 2010). The presented work describes the development of a similar reverse genetics system for HCoV-NL63. Several obstacles were encountered during this process paralleling the observations made by another group that published a reverse genetic system for HCoV-NL63 in 2008 (Donaldson et al. 2008).
Compared to other coronaviruses, the HCoV-NL63 genome shows an extremely low GC content of 34% (Pyrc et al. 2004) whereas U is highly represented (39%).
Reasonable primer design for the construction of the subclones was complicated by the very low GC content of the HCoV-NL63 genome. In addition, some of the subclones had to be constructed from large RT PCR products, requiring excellent RNA and cDNA quality. Nevertheless, after optimization of the reverse transcription reaction, fragments as large as 8 kb could easily be amplified from cDNA and subcloned into pBelo BAC.

The high U content of the HCoV-NL63 genome and of the nascent RNA during RNA synthesis from a cDNA template however, could hamper the *in vitro* transcription using T7 polymerases. A stretch of the last three Us (position 20636-20643, Accession Nr. NC_005831) could possibly lead to a pause in transcription, as shown for T7 and T3 polymerases (Lyakhov et al. 1998). After electrophoresis and staining of the in vitro transcribed full length RNA, multiple bands could be visualized (see Figure 22). This might indicate the formation of secondary structures, the premature termination of transcription, leading to a reduced yield of full-length RNA, or both.

Another challenge was introduced with the unexpectedly low performance of *AatII* restriction using pBelo BAC as a template. Complete or nearly complete digestion could only be observed when using PCR products as template. Several approaches of troubleshooting experiments could neither improve nor explain the poor restriction efficiency of *AatII* using pBelo BACs as templates. Due to this circumstance, the whole cloning strategy had to be changed to a *BsaHI* dependent restriction and assembly strategy. With this change of the cloning strategy, more silent mutations had to be introduced into naturally occurring restriction sites for the successful assembly of a full-length clone.

Despite of these drawbacks the full-length HCoV-NL63 genome could be assembled into six subclones and finally to a full-length cDNA clone. The subclones as well as the full-length clone provided a valuable stock for collaborating workgroups, because it superseded the laborious RNA extraction and cDNA synthesis steps and allowed easy amplification and modification of any genomic HCoV-NL63 sequence.

As already mentioned above, HCoV-NL63 replicates at lower titers with minor growth rates when compared to SARS-CoV. The identification of CaCo-2 cells supporting HCoV-NL63 replication was a first step and a basis to generate a reverse genetics system. However, CaCo-2 cells were difficult to electroporate and further optimization would be necessary to use those cells for the production of recombinant HCoV-NL63 virus. Therefore LLC-MK2 cells were used for transfection of full length RNA despite of some difficulties in rescuing viable recombinant virus.

It is remarkable, that the successfully rescued recombinant virus described in this work initially showed very small plaques (see Figure 27) indicating a weak cytopathic effect and replication. Only after several passages the original phenotype was displayed by rNL63 wt in the novel plaque assay. This supports the observation of another group that published a reverse genetics system for HCoV-NL63 (Donaldson et al. 2008). In their work three passages of the transfected LLC-MK2 host cells and cell supernatants were necessary until virus replication could be demonstrated. Considering both findings one could assume that, after transfection, LLC-MK2 may not support replication of recombinant virus sufficiently.

An interesting new approach could be found in the novel cell culture techniques of primary human respiratory epithelial cells used for the cultivation of some formerly unculturable respiratory viruses like HKU1 (Pyrc et al. 2010; Dominguez et al. 2013). Moreover human airway epithelium (HAE) cell cultures represent robust universal culture system that supports isolation, replication and comparison of all contemporary HCoV strains (Dijkman et al. 2013), including the novel Middle East respiratory syndrome (MERS) coronavirus (Kindler et al. 2013). Rescue of recombinant virus might be improved by involving air-liquid interface cell cultures.

The virus stock used as genetic background for the reverse genetics system described in this work showed seven mutations compared to NC_05831.2 (see Table 25); three of them had clearly an underlying HCoV-NL63 Amsterdam 1 sequence. All four non silent mutations were corrected according to the GenBank sequence. The sequence of HCoV-NL63 Amsterdam 1 deposited at GenBank represents the sequence of a patients' isolate (original Accession Nr. AY567487 (van der Hoek et al. 2004)) from the respiratory tract that was not yet adapted to growth in cell culture. This might explain the lag in replication of the recombinant virus after transfection seen in this work, as well as the need for several passages of the transfected host cells and their supernatant described by Donaldson et al (Donaldson et al. 2008). Using a viral genetic background adapted to transfectable cell lines like LLC-MK2 could strongly improve transfection efficiency and reduce the time to rescue of a recombinant virus.

Another explanation for the difficulties in rescuing a viable recombinant virus could be found in silent or untranslated regions of the HCoV-NL63 genome, i.e. in the so called "codon pair bias" described by Coleman et al. (Coleman et al. 2008) or "long range RNA-RNA interactions" described by Guan et al. (Guan et al. 2012). With the introduction of silent mutations to enable the full-length cloning strategy, codons were possibly changed to naturally less frequently used codons, or the sequence inter-stem-loop domains were altered, leading to reduced rates of translation and therefore to a reduced probability of virus rescue. In addition to the naturally poor replication of HCoV-NL63 and all the other potentially interfering factors like premature termination of the transcription, inefficient linearization of the transcription template or insufficient transfection efficiency, the modification of the genome sequence in domains that were hitherto thought to be silent or uncritical, could be part of the explanation of the difficult virus rescue of recombinant HCoV-NL63.

The importance of having coronavirus infectious cDNA clones at hand either for basic research or vaccine development has been stressed recently by the occurrence of novel Middle East respiratory syndrome (MERS) coronavirus (Danielsson et al. 2012; Zaki et al. 2012; de Groot et al. 2013). Both SARS-CoV and MERS-CoV have shown how vulnerable we are to emerging coronaviruses (Braden et al. 2013; MMWR 2013). The high diversity of

coronaviruses in small mammals like bats and rodents (Gloza-Rausch et al. 2008; Drexler et al. 2010; Lau et al. 2010; Lau et al. 2012) as well as in birds (Woo et al. 2009; Woo et al. 2012) together with the destruction of habitats make zoonotic introductions into the human population more likely (Patz et al. 2004; Jones et al. 2008; Field 2009; Jones et al. 2013). Creating attenuated coronaviruses by reverse genetics and using them as a tool for the delivery of antigens was already proven to be feasible for e.g. the development of attenuated IBV vaccine (Britton et al. 2012), for the immunization of mice against rotavirus using TGEV based vectors (Ribes et al. 2010) and the delivery of antigens and immunostimulatory cytokines to dendritic cells using MHV and HCoV-229E vaccine vectors (Cervantes-Barragan et al. 2010). Only one year after the emergence of MERS-CoV a recombinant MERS-CoV vaccine candidate was engineered using reverse genetics based on a cDNA clone (Almazan et al. 2013), in parallel an additional MERS-CoV reverse genetics system was published (Scobey et al. 2013). Both of them will allow for testing of therapeutical components, studying gene function and additional design of vaccine candidates. This rapid response to the threat of suddenly emerging viruses like SARS-CoV and MERS-CoV underlines the importance and usefulness of reverse genetics systems, including infectious cDNA clones for by now relatively harmless common cold viruses like HCoV-NL63.

5 Summary

In 2004 a novel human coronavirus designated HCoV-NL63 was isolated in the Netherlands. The fact that it uses the same entry receptor as SARS-CoV could make HCoV-NL63 an important model for the identification of antiviral agents and the study of the pathogenesis of coronaviruses. The aim of this thesis was the construction and characterization of a novel reverse genetics system for HCoV-NL63. Initially the genome of the parental HCoV-NL63 stain Amsterdam 1 was sequenced and different cell cultures were tested for susceptibility to identify suitable cell lines for propagation of HCoV-NL63. Based on the discovery of a highly susceptible cell line, CaCo-2, a novel plaque assay for HCoV-NL63 was established. This plaque assay was optimized with regards to medium and incubation times. Repeated limiting dilution culture yielded a CaCo-2 adapted virus stock with increased replication and more pronounced plaque morphology as compared to the parental strain Amsterdam 1. The optimization of virus culture was essential for the construction and rescue of recombinant HCoV-NL63. Following a strategy of sequential assembly of pBelo BAC subclones, a stable, full-length infectious HCoV-NL63 cDNA clone was created. The cDNA clone served as template for phage promoter-driven *in vitro* synthesis of infectious RNA which is transfected into the cytosol of susceptible mammalian cells. Introduction of sequence alterations was enabled on subclone level. The straightforward subsequent construction of novel full-length cDNA clones enables future manipulations that help improving the understanding of viral gene functions. The novel reverse genetics system offers translational perspectives such as chimeric vaccine development and gene delivery. It will also be a valuable tool for future *in vivo* investigation of the pathogenesis conferred by HCoV-NL63.

6 Zusammenfassung (Summary in German)

Im Jahr 2004 wurde in den Niederlanden ein neues humanes Coronavirus, HCoV-NL63, isoliert. Aufgrund der der Nutzung desselben zellulären Rezeptors wie SARS-CoV könnte HCoV-NL63 als Modellorganismus für die Identifikation antiviraler Substanzen sowie zur Untersuchung der Pathogenität von Coronaviren herangezogen werden. Ein infektiöser cDNA Klon ist für die Untersuchung der Rolle und Funktion viraler Gene und Proteine im Viruskontext essentiell. Daher wurde in der hier vorgestellten Arbeit die Konstruktion eines neuen reversen Genetiksystems für das humane Coronavirus NL63 angestrebt. Hierzu wurde zunächst das Genom des für die Konstruktion verwendeten Ausgangsstammes HCoV-NL63 Amsterdam 1 sequenziert. Zusätzlich wurden verschiedenen Zelllinien auf ihre Suszeptibilität für HCoV-NL63 untersucht. Mit der Zelllinie CaCo-2 konnte eine höchst suszeptible Zelllinie identifiziert werden, die für die Etablierung eines neuartigen Plaque Assays für HCoV-NL63 herangezogen werden konnte. Dieser Plaque Assay wurde hinsichtlich der Overlay-Medien und Inkubationszeiten optimiert. Außerdem wurde durch wiederholte Endpunkttitration des Ausgangsstammes HCoV-NL63 Amsterdam 1 ein auf CaCo-2 adaptierter Virusstamm erzeugt, der eine verstärkte Replikation und eine deutlichere Plaquemorphologie aufweist. Die erzielten Verbesserungen in der Viruskultur waren Voraussetzung für die Konstruktion eines neuartigen reversen Genetiksystems für HCoV-NL63. Ein stabiler, die volle Länge des HCoV-NL63 Genoms beinhaltender cDNA Klon konnte erfolgreich konstruiert werden, indem pBelo BAC Subklone sequenziell zusammengefügt wurden. Dieser Klon diente als Matrize für phagenpromotoren-getriebene *in vitro* Synthese infektiöser RNA, die in das Cytosol suszeptibler Säugerzellen transfiziert wurde. Auf Ebene der Subklone können Sequenzänderungen eingeführt werden. Der folgende, vergleichsweise einfache Zusammenbau eines neuen, durchgehenden cDNA Klons ermöglicht eine vereinfachte Mutagenese des HCoV-NL63 Genoms. Das im Rahmen dieser Arbeit konstruierte reverse Genetiksystem für HCoV-NL63 wird ein wertvolles Hilfsmittel für die Entwicklung rekombinanter Vakzinen oder Transduktionstechniken darstellen, sowie die Untersuchung der Pathogenese der HCoV-63 Infektion erleichtern.

7 References

Abdul-Rasool, S. and B. C. Fielding (2010). "Understanding Human Coronavirus HCoV-NL63." Open Virol J **4**: 76-84.

Acheson, N., H. (2007). Coronaviruses. Fundamentals of Molecular Virology. W. Sons, Wiley & Sons. **1:** 201-213.

Almazan, F., M. L. Dediego, et al. (2006). "Construction of a severe acute respiratory syndrome coronavirus infectious cDNA clone and a replicon to study coronavirus RNA synthesis." J Virol **80**(21): 10900-6.

Almazan, F., M. L. Dediego, et al. (2013). "Engineering a replication-competent, propagation-defective middle East respiratory syndrome coronavirus as a vaccine candidate." MBio **4**(5).

Almazan, F., C. Galan, et al. (2004). "The nucleoprotein is required for efficient coronavirus genome replication." J Virol **78**(22): 12683-8.

Almazan, F., J. M. Gonzalez, et al. (2000). "Engineering the largest RNA virus genome as an infectious bacterial artificial chromosome." Proc Natl Acad Sci U S A **97**(10): 5516-21.

Angelini, M. M., M. Akhlaghpour, et al. (2013). "Severe acute respiratory syndrome coronavirus nonstructural proteins 3, 4, and 6 induce double-membrane vesicles." MBio **4**(4).

Arden, K. E., M. D. Nissen, et al. (2005). "New human coronavirus, HCoV-NL63, associated with severe lower respiratory tract disease in Australia." J Med Virol **75**(3): 455-62.

Bastien, N., K. Anderson, et al. (2005). "Human coronavirus NL63 infection in Canada." J Infect Dis **191**(4): 503-6.

Bastien, N., J. L. Robinson, et al. (2005). "Human coronavirus NL-63 infections in children: a 1-year study." J Clin Microbiol **43**(9): 4567-73.

Battegay, M., S. Cooper, et al. (1991). "Quantification of lymphocytic choriomeningitis virus with an immunological focus assay in 24- or 96-well plates." J Virol Methods **33**(1-2): 191-8.

Bohl, E. H., R. K. Gupta, et al. (1972). "Immunology of transmissible gastroenteritis." J Am Vet Med Assoc **160**(4): 543-9.

Bohl, E. H., R. K. Gupta, et al. (1972). "Antibody responses in serum, colostrum, and milk of swine after infection or vaccination with transmissible gastroenteritis virus." Infect Immun **6**(3): 289-301.

Bradburne, A. F., M. L. Bynoe, et al. (1967). "Effects of a "new" human respiratory virus in volunteers." Br Med J **3**(5568): 767-9.

Braden, C. R., S. F. Dowell, et al. (2013). "Progress in global surveillance and response capacity 10 years after severe acute respiratory syndrome." Emerg Infect Dis **19**(6): 864-9.

Britton, P., M. Armesto, et al. (2012). "Modification of the avian coronavirus infectious bronchitis virus for vaccine development." Bioeng Bugs **3**(2): 114-9.

Buonavoglia, C., N. Decaro, et al. (2006). "Canine coronavirus highly pathogenic for dogs." Emerg Infect Dis **12**(3): 492-4.

Casais, R., V. Thiel, et al. (2001). "Reverse genetics system for the avian coronavirus infectious bronchitis virus." J Virol **75**(24): 12359-69.

Cervantes-Barragan, L., R. Zust, et al. (2010). "Dendritic cell-specific antigen delivery by coronavirus vaccine vectors induces long-lasting protective antiviral and antitumor immunity." MBio **1**(4).

Chasey, D. and S. F. Cartwright (1978). "Virus-like particles associated with porcine epidemic diarrhoea." Res Vet Sci **25**(2): 255-6.

Chiu, S. S., K. H. Chan, et al. (2005). "Human coronavirus NL63 infection and other

coronavirus infections in children hospitalized with acute respiratory disease in Hong Kong, China." Clin Infect Dis **40**(12): 1721-9.
Chu, D. K., J. S. Peiris, et al. (2008). "Genomic characterizations of bat coronaviruses (1A, 1B and HKU8) and evidence for co-infections in Miniopterus bats." J Gen Virol **89**(Pt 5): 1282-7.
Chu, D. K., L. L. Poon, et al. (2006). "Coronaviruses in bent-winged bats (Miniopterus spp.)." J Gen Virol **87**(Pt 9): 2461-6.
Coleman, J. R., D. Papamichail, et al. (2008). "Virus attenuation by genome-scale changes in codon pair bias." Science **320**(5884): 1784-7.
Coley, S. E., E. Lavi, et al. (2005). "Recombinant mouse hepatitis virus strain A59 from cloned, full-length cDNA replicates to high titers in vitro and is fully pathogenic in vivo." J Virol **79**(5): 3097-106.
Cunningham, C. H. (1970). "Avian infectious bronchitis." Adv Vet Sci Comp Med **14**: 105-48.
Danielsson, N. and M. Catchpole (2012). "Novel coronavirus associated with severe respiratory disease: case definition and public health measures." Euro Surveill **17**(39).
de Groot, R. J., S. C. Baker, et al. (2013). "Middle East respiratory syndrome coronavirus (MERS-CoV): announcement of the Coronavirus Study Group." J Virol **87**(14): 7790-2.
Dijkman, R., M. F. Jebbink, et al. (2008). "Human coronavirus NL63 and 229E seroconversion in children." J Clin Microbiol **46**(7): 2368-73.
Dijkman, R., M. F. Jebbink, et al. (2013). "Isolation and characterization of current human coronavirus strains in primary human epithelial cell cultures reveal differences in target cell tropism." J Virol **87**(11): 6081-90.
Dominguez, S. R., T. J. O'Shea, et al. (2007). "Detection of group 1 coronaviruses in bats in North America." Emerg Infect Dis **13**(9): 1295-300.
Dominguez, S. R., E. A. Travanty, et al. (2013). "Human Coronavirus HKU1 Infection of Primary Human Type II Alveolar Epithelial Cells: Cytopathic Effects and Innate Immune Response." PLoS One **8**(7): e70129.
Donaldson, E. F., B. Yount, et al. (2008). "Systematic assembly of a full-length infectious clone of human coronavirus NL63." J Virol **82**(23): 11948-57.
Drexler, J. F., F. Gloza-Rausch, et al. (2010). "Genomic characterization of severe acute respiratory syndrome-related coronavirus in European bats and classification of coronaviruses based on partial RNA-dependent RNA polymerase gene sequences." J Virol **84**(21): 11336-49.
Drosten, C., S. Gunther, et al. (2003). "Identification of a novel coronavirus in patients with severe acute respiratory syndrome." N Engl J Med **348**(20): 1967-76.
Ebihara, T., R. Endo, et al. (2005). "Detection of human coronavirus NL63 in young children with bronchiolitis." J Med Virol **75**(3): 463-5.
Eckerle, L. D., M. M. Becker, et al. (2010). "Infidelity of SARS-CoV Nsp14-exonuclease mutant virus replication is revealed by complete genome sequencing." PLoS Pathog **6**(5): e1000896.
Enjuanes, L., C. Sanchez, et al. (1995). "Tropism and immunoprotection in transmissible gastroenteritis coronaviruses." Dev Biol Stand **84**: 145-52.
Erles, K., C. Toomey, et al. (2003). "Detection of a group 2 coronavirus in dogs with canine infectious respiratory disease." Virology **310**(2): 216-23.
Etchevers, H. (2007). DNA sequencing and quick clean-up. Nature protocols.
Field, H. E. (2009). "Bats and emerging zoonoses: henipaviruses and SARS." Zoonoses Public Health **56**(6-7): 278-84.
Fouchier, R. A., N. G. Hartwig, et al. (2004). "A previously undescribed coronavirus associated with respiratory disease in humans." Proc Natl Acad Sci U S A **101**(16): 6212-6.
Garwes, D. J. (1988). "Transmissible gastroenteritis." Vet Rec **122**(19): 462-3.
Glowacka, I., S. Bertram, et al. (2011). "Evidence that TMPRSS2 activates the severe acute respiratory syndrome coronavirus spike protein for membrane fusion and reduces

viral control by the humoral immune response." J Virol **85**(9): 4122-34.
Gloza-Rausch, F., A. Ipsen, et al. (2008). "Detection and prevalence patterns of group I coronaviruses in bats, northern Germany." Emerg Infect Dis **14**(4): 626-31.
Gomaa, M. H., J. R. Barta, et al. (2008). "Complete genomic sequence of turkey coronavirus." Virus Res **135**(2): 237-46.
Gonzalez, J. M., P. Gomez-Puertas, et al. (2003). "A comparative sequence analysis to revise the current taxonomy of the family Coronaviridae." Arch Virol **148**(11): 2207-35.
Gonzalez, J. M., Z. Penzes, et al. (2002). "Stabilization of a full-length infectious cDNA clone of transmissible gastroenteritis coronavirus by insertion of an intron." J Virol **76**(9): 4655-61.
Gough, R. E., W. J. Cox, et al. (1996). "Isolation and identification of infectious bronchitis virus from pheasants." Vet Rec **138**(9): 208-9.
Guan, B. J., Y. P. Su, et al. (2012). "Genetic evidence of a long-range RNA-RNA interaction between the genomic 5' untranslated region and the nonstructural protein 1 coding region in murine and bovine coronaviruses." J Virol **86**(8): 4631-43.
Guan, Y., B. J. Zheng, et al. (2003). "Isolation and characterization of viruses related to the SARS coronavirus from animals in southern China." Science **302**(5643): 276-8.
Hagemeijer, M. C., M. H. Verheije, et al. (2010). "Dynamics of coronavirus replication-transcription complexes." J Virol **84**(4): 2134-49.
Hamre, D. and J. J. Procknow (1966). "A new virus isolated from the human respiratory tract." Proc Soc Exp Biol Med **121**(1): 190-3.
Hattermann, K., M. A. Muller, et al. (2005). "Susceptibility of different eukaryotic cell lines to SARS-coronavirus." Arch Virol **150**(5): 1023-31.
Heald-Sargent, T. and T. Gallagher (2012). "Ready, set, fuse! The coronavirus spike protein and acquisition of fusion competence." Viruses **4**(4): 557-80.
Hofmann, H., K. Pyrc, et al. (2005). "Human coronavirus NL63 employs the severe acute respiratory syndrome coronavirus receptor for cellular entry." Proc Natl Acad Sci U S A **102**(22): 7988-93.
Hofmann, M. and R. Wyler (1988). "Propagation of the virus of porcine epidemic diarrhea in cell culture." J Clin Microbiol **26**(11): 2235-9.
Holmes, K. V. and L. Enjuanes (2003). "Virology. The SARS coronavirus: a postgenomic era." Science **300**(5624): 1377-8.
Huang, I. C., B. J. Bosch, et al. (2006). "SARS coronavirus, but not human coronavirus NL63, utilizes cathepsin L to infect ACE2-expressing cells." J Biol Chem **281**(6): 3198-203.
Huang, J. C., S. L. Wright, et al. (1983). "Isolation of coronavirus-like agent from horses suffering from acute equine diarrhoea syndrome." Vet Rec **113**(12): 262-3.
Jonassen, C. M., T. Kofstad, et al. (2005). "Molecular identification and characterization of novel coronaviruses infecting graylag geese (Anser anser), feral pigeons (Columbia livia) and mallards (Anas platyrhynchos)." J Gen Virol **86**(Pt 6): 1597-607.
Jones, B. A., D. Grace, et al. (2013). "Zoonosis emergence linked to agricultural intensification and environmental change." Proc Natl Acad Sci U S A **110**(21): 8399-404.
Jones, K. E., N. G. Patel, et al. (2008). "Global trends in emerging infectious diseases." Nature **451**(7181): 990-3.
Kaiser, L., N. Regamey, et al. (2005). "Human coronavirus NL63 associated with lower respiratory tract symptoms in early life." Pediatr Infect Dis J **24**(11): 1015-7.
Kim, L., J. Hayes, et al. (2000). "Molecular characterization and pathogenesis of transmissible gastroenteritis coronavirus (TGEV) and porcine respiratory coronavirus (PRCV) field isolates co-circulating in a swine herd." Arch Virol **145**(6): 1133-47.
Kindler, E., H. R. Jonsdottir, et al. (2013). "Efficient Replication of the Novel Human Betacoronavirus EMC on Primary Human Epithelium Highlights Its Zoonotic Potential." MBio **4**(1).

Knoops, K., M. Kikkert, et al. (2008). "SARS-coronavirus replication is supported by a reticulovesicular network of modified endoplasmic reticulum." PLoS Biol **6**(9): e226.
Knoops, K., C. Swett-Tapia, et al. (2010). "Integrity of the early secretory pathway promotes, but is not required for, severe acute respiratory syndrome coronavirus RNA synthesis and virus-induced remodeling of endoplasmic reticulum membranes." J Virol **84**(2): 833-46.
Kusanagi, K., H. Kuwahara, et al. (1992). "Isolation and serial propagation of porcine epidemic diarrhea virus in cell cultures and partial characterization of the isolate." J Vet Med Sci **54**(2): 313-8.
Lambert, S. B., K. M. Allen, et al. (2007). "Community epidemiology of human metapneumovirus, human coronavirus NL63, and other respiratory viruses in healthy preschool-aged children using parent-collected specimens." Pediatrics **120**(4): e929-37.
Lau, S. K., R. W. Poon, et al. (2010). "Coexistence of different genotypes in the same bat and serological characterization of Rousettus bat coronavirus HKU9 belonging to a novel Betacoronavirus subgroup." J Virol **84**(21): 11385-94.
Lau, S. K., P. C. Woo, et al. (2005). "Severe acute respiratory syndrome coronavirus-like virus in Chinese horseshoe bats." Proc Natl Acad Sci U S A **102**(39): 14040-5.
Lau, S. K., P. C. Woo, et al. (2007). "Complete genome sequence of bat coronavirus HKU2 from Chinese horseshoe bats revealed a much smaller spike gene with a different evolutionary lineage from the rest of the genome." Virology **367**(2): 428-39.
Lau, S. K., P. C. Woo, et al. (2012). "Isolation and characterization of a novel Betacoronavirus subgroup A coronavirus, rabbit coronavirus HKU14, from domestic rabbits." J Virol **86**(10): 5481-96.
Lau, S. K., P. C. Woo, et al. (2006). "Coronavirus HKU1 and other coronavirus infections in Hong Kong." J Clin Microbiol **44**(6): 2063-71.
Le Poder, S. (2011). "Feline and canine coronaviruses: common genetic and pathobiological features." Adv Virol **2011**: 609465.
Leyssen, P., N. Charlier, et al. (2003). "Prospects for antiviral therapy." Adv Virus Res **61**: 511-53.
Leyssen, P., E. De Clercq, et al. (2008). "Molecular strategies to inhibit the replication of RNA viruses." Antiviral Res **78**(1): 9-25.
Li, W., Z. Shi, et al. (2005). "Bats are natural reservoirs of SARS-like coronaviruses." Science **310**(5748): 676-9.
Lissenberg, A., M. M. Vrolijk, et al. (2005). "Luxury at a cost? Recombinant mouse hepatitis viruses expressing the accessory hemagglutinin esterase protein display reduced fitness in vitro." J Virol **79**(24): 15054-63.
Liu, S., J. Chen, et al. (2005). "Isolation of avian infectious bronchitis coronavirus from domestic peafowl (Pavo cristatus) and teal (Anas)." J Gen Virol **86**(Pt 3): 719-25.
Lyakhov, D. L., B. He, et al. (1998). "Pausing and termination by bacteriophage T7 RNA polymerase." J Mol Biol **280**(2): 201-13.
Makino, S., F. Taguchi, et al. (1984). "Analysis of genomic and intracellular viral RNAs of small plaque mutants of mouse hepatitis virus, JHM strain." Virology **139**(1): 138-51.
Masters, P. S. (2006). "The molecular biology of coronaviruses." Adv Virus Res **66**: 193-292.
Matrosovich, M., T. Matrosovich, et al. (2006). "New low-viscosity overlay medium for viral plaque assays." Virol J **3**: 63.
Matsuyama, S., N. Nagata, et al. (2010). "Efficient activation of the severe acute respiratory syndrome coronavirus spike protein by the transmembrane protease TMPRSS2." J Virol **84**(24): 12658-64.
McBride, R. and B. C. Fielding (2012). "The role of severe acute respiratory syndrome (SARS)-coronavirus accessory proteins in virus pathogenesis." Viruses **4**(11): 2902-23.
McIntosh, K., W. B. Becker, et al. (1967). "Growth in suckling-mouse brain of "IBV-like" viruses from patients with upper respiratory tract disease." Proc Natl Acad Sci U S A

58(6): 2268-73.
Mengeling, W. L., A. D. Boothe, et al. (1972). "Characteristics of a coronavirus (strain 67N) of pigs." Am J Vet Res **33**(2): 297-308.
Mihindukulasuriya, K. A., G. Wu, et al. (2008). "Identification of a novel coronavirus from a beluga whale by using a panviral microarray." J Virol **82**(10): 5084-8.
MMWR (2013). "Updated Information on the Epidemiology of Middle East Respiratory Syndrome Coronavirus (MERS-CoV) Infection and Guidance for the Public, Clinicians, and Public Health Authorities, 2012-2013." MMWR Morb Mortal Wkly Rep **62**(38): 793-6.
Moes, E., L. Vijgen, et al. (2005). "A novel pancoronavirus RT-PCR assay: frequent detection of human coronavirus NL63 in children hospitalized with respiratory tract infections in Belgium." BMC Infect Dis **5**(1): 6.
Muller, M. A. (2007). Studies on human pathogenic coronaviruses - survey for coronaviruses in African bat species and characterization of the novel human coronavirus NL63 (HCoV-NL63) open reading frame 3 (ORF3). Department of Biology, Chemistry and Pharmacy. Berlin, Freie Universität Berlin.
Muller, M. A. (2007). Studies on human pathogenic coronaviruses – survey for coronaviruses in African bat species and characterization of the novel human coronavirus NL63 (HCoV-NL63) open reading frame 3 (ORF3). Biology, Chemistry and Pharmacy of Freie Universität Berlin. Berlin, Freie Universität Berlin.
Muller, M. A., L. van der Hoek, et al. (2010). "Human coronavirus NL63 open reading frame 3 encodes a virion-incorporated N-glycosylated membrane protein." Virol J **7**: 6.
Muth, D., M. A. Müller, et al. (2010). Influence of SARS-related bat-Coronavirus ORF6 on virus replication in primate and bat cell culture. Nationales Symposium für Zoonosenforschung 2010. Berlin.
Na, Y. R., S. H. Seok, et al. (2010). "Microbiological quality assessment of laboratory mice in Korea and recommendations for quality improvement." Exp Anim **59**(1): 25-33.
Nelson, J. B. (1957). "The enhancing effect of murine hepatitis virus on the cerebral activity of pleuropneumonia-like organisms in mice." J Exp Med **106**(2): 179-90.
Pasternak, A. O., W. J. Spaan, et al. (2006). "Nidovirus transcription: how to make sense...?" J Gen Virol **87**(Pt 6): 1403-21.
Patz, J. A., P. Daszak, et al. (2004). "Unhealthy landscapes: Policy recommendations on land use change and infectious disease emergence." Environ Health Perspect **112**(10): 1092-8.
Peiris, J. S., S. T. Lai, et al. (2003). "Coronavirus as a possible cause of severe acute respiratory syndrome." Lancet **361**(9366): 1319-25.
Pensaert, M. B. and P. de Bouck (1978). "A new coronavirus-like particle associated with diarrhea in swine." Arch Virol **58**(3): 243-7.
Perlman, S. and J. Netland (2009). "Coronaviruses post-SARS: update on replication and pathogenesis." Nat Rev Microbiol **7**(6): 439-50.
Perlman, S., R. Schelper, et al. (1987). "Late onset, symptomatic, demyelinating encephalomyelitis in mice infected with MHV-JHM in the presence of maternal antibody." Microb Pathog **2**(3): 185-94.
Pfefferle, S., V. Krahling, et al. (2009). "Reverse genetic characterization of the natural genomic deletion in SARS-Coronavirus strain Frankfurt-1 open reading frame 7b reveals an attenuating function of the 7b protein in-vitro and in-vivo." Virol J **6**: 131.
Pfefferle, S., S. Oppong, et al. (2009). "Distant relatives of severe acute respiratory syndrome coronavirus and close relatives of human coronavirus 229E in bats, Ghana." Emerg Infect Dis **15**(9): 1377-84.
Phillips, J. E., D. A. Hilt, et al. (2013). "Comparative sequence analysis of full-length genome of FIPV at different tissue passage levels." Virus Genes.
Poon, L. L., D. K. Chu, et al. (2005). "Identification of a novel coronavirus in bats." J Virol **79**(4): 2001-9.
Principi, N., S. Bosis, et al. (2010). "Effects of coronavirus infections in children." Emerg

Infect Dis **16**(2): 183-8.
Pyrc, K., B. Berkhout, et al. (2007). "The novel human coronaviruses NL63 and HKU1." J Virol **81**(7): 3051-7.
Pyrc, K., R. Dijkman, et al. (2006). "Mosaic structure of human coronavirus NL63, one thousand years of evolution." J Mol Biol **364**(5): 964-73.
Pyrc, K., M. F. Jebbink, et al. (2004). "Genome structure and transcriptional regulation of human coronavirus NL63." Virol J **1**: 7.
Pyrc, K., A. C. Sims, et al. (2010). "Culturing the unculturable: human coronavirus HKU1 infects, replicates, and produces progeny virions in human ciliated airway epithelial cell cultures." J Virol **84**(21): 11255-63.
Reusken, C. B., P. H. Lina, et al. (2010). "Circulation of group 2 coronaviruses in a bat species common to urban areas in Western Europe." Vector Borne Zoonotic Dis **10**(8): 785-91.
Ribes, J. M., J. Ortego, et al. (2010). "Transmissible gastroenteritis virus (TGEV)-based vectors with engineered murine tropism express the rotavirus VP7 protein and immunize mice against rotavirus." Virology.
Rice, C. M., R. Levis, et al. (1987). "Production of infectious RNA transcripts from Sindbis virus cDNA clones: mapping of lethal mutations, rescue of a temperature-sensitive marker, and in vitro mutagenesis to generate defined mutants." J Virol **61**(12): 3809-19.
Roberts, J. D., B. D. Preston, et al. (1989). "Fidelity of two retroviral reverse transcriptases during DNA-dependent DNA synthesis in vitro." Mol Cell Biol **9**(2): 469-76.
Rota, P. A., M. S. Oberste, et al. (2003). "Characterization of a novel coronavirus associated with severe acute respiratory syndrome." Science **300**(5624): 1394-9.
Saif, L. J., E. H. Bohl, et al. (1972). "Isolation of porcine immunoglobulins and determination of the immunoglobulin classes of transmissible gastroenteritis viral antibodies." Infect Immun **6**(4): 600-9.
Sambrook, J. and D. W. Russell (2001). Molecular cloning : a laboratory manual, Cold Spring Harbor Laboratory Press.
Sanger, F., S. Nicklen, et al. (1977). "DNA sequencing with chain-terminating inhibitors." Proc Natl Acad Sci U S A **74**(12): 5463-7.
Sawicki, S. G., D. L. Sawicki, et al. (2007). "A contemporary view of coronavirus transcription." J Virol **81**(1): 20-9.
Schelle, B., N. Karl, et al. (2005). "Selective replication of coronavirus genomes that express nucleocapsid protein." J Virol **79**(11): 6620-30.
Scobey, T., B. L. Yount, et al. (2013). "Reverse genetics with a full-length infectious cDNA of the Middle East respiratory syndrome coronavirus." Proc Natl Acad Sci U S A **110**(40): 16157-16162.
Semler, B. L., A. J. Dorner, et al. (1984). "Production of infectious poliovirus from cloned cDNA is dramatically increased by SV40 transcription and replication signals." Nucleic Acids Res **12**(12): 5123-41.
Shibata, I., T. Tsuda, et al. (2000). "Isolation of porcine epidemic diarrhea virus in porcine cell cultures and experimental infection of pigs of different ages." Vet Microbiol **72**(3-4): 173-82.
Snijder, E. J., P. J. Bredenbeek, et al. (2003). "Unique and conserved features of genome and proteome of SARS-coronavirus, an early split-off from the coronavirus group 2 lineage." J Mol Biol **331**(5): 991-1004.
St-Jean, J. R., M. Desforges, et al. (2006). "Recovery of a neurovirulent human coronavirus OC43 from an infectious cDNA clone." J Virol **80**(7): 3670-4.
Stadler, K., V. Masignani, et al. (2003). "SARS--beginning to understand a new virus." Nat Rev Microbiol **1**(3): 209-18.
Stair, E. L., M. B. Rhodes, et al. (1972). "Neonatal calf diarrhea: purification and electron microscopy of a coronavirus-like agent." Am J Vet Res **33**(6): 1147-56.
Talbot, H. K., B. E. Shepherd, et al. (2009). "The pediatric burden of human coronaviruses

evaluated for twenty years." Pediatr Infect Dis J **28**(8): 682-7.
Tang, X. C., J. X. Zhang, et al. (2006). "Prevalence and genetic diversity of coronaviruses in bats from China." J Virol **80**(15): 7481-90.
Tekes, G., R. Hofmann-Lehmann, et al. (2008). "Genome organization and reverse genetic analysis of a type I feline coronavirus." J Virol **82**(4): 1851-9.
Thiel, V., J. Herold, et al. (2001). "Infectious RNA transcribed in vitro from a cDNA copy of the human coronavirus genome cloned in vaccinia virus." J Gen Virol **82**(Pt 6): 1273-81.
Thiel, V. and S. G. Siddell (2005). "Reverse genetics of coronaviruses using vaccinia virus vectors." Curr Top Microbiol Immunol **287**: 199-227.
Tischer, B. K. and B. B. Kaufer (2012). "Viral bacterial artificial chromosomes: generation, mutagenesis, and removal of mini-F sequences." J Biomed Biotechnol **2012**: 472537.
Torrecilhas, A. C., E. Faquim-Mauro, et al. (1999). "Interference of natural mouse hepatitis virus infection with cytokine production and susceptibility to Trypanosoma cruzi." Immunology **96**(3): 381-8.
Tyrrell, D. A. and M. L. Bynoe (1965). "Cultivation of a Novel Type of Common-Cold Virus in Organ Cultures." Br Med J **1**(5448): 1467-70.
Vabret, A., J. Dina, et al. (2006). "Detection of the new human coronavirus HKU1: a report of 6 cases." Clin Infect Dis **42**(5): 634-9.
Vabret, A., T. Mourez, et al. (2005). "Human coronavirus NL63, France." Emerg Infect Dis **11**(8): 1225-9.
van der Hoek, L., G. Ihorst, et al. (2010). "Burden of disease due to human coronavirus NL63 infections and periodicity of infection." J Clin Virol **48**(2): 104-8.
van der Hoek, L., K. Pyrc, et al. (2006). "Human coronavirus NL63, a new respiratory virus." FEMS Microbiol Rev **30**(5): 760-73.
van der Hoek, L., K. Pyrc, et al. (2004). "Identification of a new human coronavirus." Nat Med **10**(4): 368-73.
van der Hoek, L., K. Sure, et al. (2005). "Croup is associated with the novel coronavirus NL63." PLoS Med **2**(8): e240.
van der Werf, S., J. Bradley, et al. (1986). "Synthesis of infectious poliovirus RNA by purified T7 RNA polymerase." Proc Natl Acad Sci U S A **83**(8): 2330-4.
Vennema, H., A. Poland, et al. (1998). "Feline infectious peritonitis viruses arise by mutation from endemic feline enteric coronaviruses." Virology **243**(1): 150-7.
Voss, D., S. Pfefferle, et al. (2009). "Studies on membrane topology, N-glycosylation and functionality of SARS-CoV membrane protein." Virol J **6**: 79.
Wang, M., M. Yan, et al. (2005). "SARS-CoV infection in a restaurant from palm civet." Emerg Infect Dis **11**(12): 1860-5.
Watanabe, S., J. S. Masangkay, et al. (2010). "Bat coronaviruses and experimental infection of bats, the Philippines." Emerg Infect Dis **16**(8): 1217-23.
Weingartl, H. M., J. Copps, et al. (2004). "Susceptibility of pigs and chickens to SARS coronavirus." Emerg Infect Dis **10**(2): 179-84.
Woo, P. C., S. K. Lau, et al. (2005). "Characterization and complete genome sequence of a novel coronavirus, coronavirus HKU1, from patients with pneumonia." J Virol **79**(2): 884-95.
Woo, P. C., S. K. Lau, et al. (2009). "Coronavirus diversity, phylogeny and interspecies jumping." Exp Biol Med (Maywood) **234**(10): 1117-27.
Woo, P. C., S. K. Lau, et al. (2009). "Comparative analysis of complete genome sequences of three avian coronaviruses reveals a novel group 3c coronavirus." J Virol **83**(2): 908-17.
Woo, P. C., S. K. Lau, et al. (2012). "Discovery of seven novel Mammalian and avian coronaviruses in the genus deltacoronavirus supports bat coronaviruses as the gene source of alphacoronavirus and betacoronavirus and avian coronaviruses as the gene source of gammacoronavirus and deltacoronavirus." J Virol **86**(7): 3995-4008.
Woo, P. C., S. K. Lau, et al. (2006). "Molecular diversity of coronaviruses in bats." Virology

351(1): 180-7.
Woo, P. C., M. Wang, et al. (2007). "Comparative analysis of twelve genomes of three novel group 2c and group 2d coronaviruses reveals unique group and subgroup features." J Virol **81**(4): 1574-85.
Wood, E. N. (1977). "An apparently new syndrome of porcine epidemic diarrhoea." Vet Rec **100**(12): 243-4.
Wu, K., W. Li, et al. (2009). "Crystal structure of NL63 respiratory coronavirus receptor-binding domain complexed with its human receptor." Proc Natl Acad Sci U S A **106**(47): 19970-4.
Wu, P. S., L. Y. Chang, et al. (2008). "Clinical manifestations of human coronavirus NL63 infection in children in Taiwan." Eur J Pediatr **167**(1): 75-80.
Yamashita, M., M. Yamate, et al. (2005). "Susceptibility of human and rat neural cell lines to infection by SARS-coronavirus." Biochem Biophys Res Commun **334**(1): 79-85.
Yount, B., K. M. Curtis, et al. (2000). "Strategy for systematic assembly of large RNA and DNA genomes: transmissible gastroenteritis virus model." J Virol **74**(22): 10600-11.
Yount, B., K. M. Curtis, et al. (2003). "Reverse genetics with a full-length infectious cDNA of severe acute respiratory syndrome coronavirus." Proc Natl Acad Sci U S A **100**(22): 12995-3000.
Yount, B., M. R. Denison, et al. (2002). "Systematic assembly of a full-length infectious cDNA of mouse hepatitis virus strain A59." J Virol **76**(21): 11065-78.
Yuan, J., C. C. Hon, et al. (2010). "Intraspecies diversity of SARS-like coronaviruses in Rhinolophus sinicus and its implications for the origin of SARS coronaviruses in humans." J Gen Virol **91**(Pt 4): 1058-62.
Zaki, A. M., S. van Boheemen, et al. (2012). "Isolation of a novel coronavirus from a man with pneumonia in Saudi Arabia." N Engl J Med **367**(19): 1814-20.
Zeng, Q., M. A. Langereis, et al. (2008). "Structure of coronavirus hemagglutinin-esterase offers insight into corona and influenza virus evolution." Proc Natl Acad Sci U S A **105**(26): 9065-9.
Ziebuhr, J., E. J. Snijder, et al. (2000). "Virus-encoded proteinases and proteolytic processing in the Nidovirales." J Gen Virol **81**(Pt 4): 853-79.
Zust, R., L. Cervantes-Barragan, et al. (2007). "Coronavirus non-structural protein 1 is a major pathogenicity factor: implications for the rational design of coronavirus vaccines." PLoS Pathog **3**(8): e109.

8 Appendix

8.1 Abbreviations

8.1.1 Viruses

BCoV	Bovine coronavirus
BtCoV	Bat coronavirus
CMV	Cytomegalovirus
FIPV	Feline Infectious Peritonitis Virus
HCoV-HKU1	Human coronavirus HKU1
HCoV-NL63	Human coronavirus NL63
HCoV-229E	Human coronavirus 229E
HCoV-OC43	Human coronavirus OC43
IBV	Infectious Bronchitis Virus
MHV	Murine Hepatitis Virus
PEDV	Porcine Epidemic Diarrhea Virus
SARS-CoV	SARS coronavirus
TGEV	Transmissible Gastroenteritis Virus

8.1.2 Others

A	Adenine
aa	Amino acid
ACE2	Angiotensin converting enzyme 2
Anti M	Antiserum against M protein
Anti N	Antiserum against N protein
ATCC	American Type Culture Collection
ATP	Adenosine Triphosphate
BAC	Bacterial artificial chromosome
BNI	Bernhard-Nocht-Institute
bp	Base pair
BSA	Bovine Serum Albumin
C	Cytosine
cDNA	Complementary DNA

CIP	Calf intestine alkaline phosphatase
CMC	Carboxymethyl-cellulose sodium salt
CoV	Coronavirus
CPE	Cytopathogenic effect
Ct	Threshold cycle
CTP	Cytosine Triphosphate
C-terminus	Carboxyl-terminus
Cy5	Cyanine-5
°C	Degree Celsius
d	Day
dATP	Deoxyadenosine Triphosphate
dCTP	Deoxycytosine Triphosphate
dGTP	Deoxyguanosine Triphosphate
ddNTP	Dideoxynucleoside Triphosphate
dNTP	Deoxynucleoside Triphosphate
dTTP	Deoxythymidine Triphosphate
DEPC	Diethyl Pyrocarbonate
DMEM	Dulbecco's Modified Eagles Medium
DMSO	Dimethylsulfoxide
DNA	Deoxyribonucleic Acid
dpi	Days post infection
E. coli	*Escherichia coli*
e.g.	'exempli gratia' (for example)
EDTA	Ethylenediaminetetraacetic Acid
ER	Endoplasmic Reticulum
ERGIC	Endoplasmic Reticulum-Golgi Intermediate Compartment
Fc	Conserved part of an antibody
FCS	Fetal calf serum
Fig.	Figure
FITC	Fluorescein Isothiocyanate
g	Gram
G	Guanine
GTP	Guanosine Triphosphate
g_n	Gravitational force (9.81 m/s²)
ge	Genome equivalent
GFP	Green fluorescent protein

h	Hour
HCoV	Human coronavirus
HRP	Horseradish peroxidase
ID	Identification Data
IFA	Immunofluorescence Assay
IPTG	Isopropyl-Beta-d-Thiogalactopyranoside
kb	Kilobase
kbp	Kilobase pairs
kDa	Kilodalton
L	Liter
LB medium	Luria Bertani medium
M	Molar
M protein	Membrane protein
MCS	Multiple cloning site
ME	Beta-mercaptoethanol
min	Minute
ml	Milliliter
mM	Millimolar
MOI	Multiplicity of Infection
MOPS	3-(n-Morpholino)Propanesulfonic Acid
mRNA	Messenger RNA
µg	Microgram
µl	Microliter
n	Non specified number
NA	Nucleic acid
N protein	Nucleocapsid protein
n.d.	Not determined
Nm	Nanometer
NSP	Non-structural protein
nt	Nucleotide
N-terminus	Amino-terminus
OD	Optical Density
ORF	Open reading frame
PBS	Phosphate buffered saline
PCR	Polymerase chain reaction
PFA	Paraformaldehyde

PFU	Plaque forming units
pH	*"Potentia Hydrogenii "* Potential of Hydrogen - negative 10-base log (power) of the positive hydrogen ion concentration; measure of acidity
pi	Post infection
RNA	Ribonucleic acid
rNTP	Ribonucleotide triphosphate
rpm	Revolutions Per Minute
RT	Reverse Transcriptase
rxn	reaction
s	Second
S protein	Spike protein
SARS	Severe Acute Respiratory Syndrome
sg mRNA	Subgenomic mRNA
S.O.C.	Super optimal broth with Catabolite repression
SS	Superscript (RT Enzyme)
T	Thymine
TAE Buffer	Tris acetate EDTA buffer
TE buffer	Tris EDTA buffer
Tm	Melting temperature
Tris	Tris(Hydroxymethyl)aminomethane
TRS	Transcription regulating sequence
U	Uracil
UTP	Uridine Triphosphate
UTR	Untranslated region
v/v	Volume per volume
V	Volts
VLP	Virus like particles
w/v	Weight per volume
WHO	World Health Organization

8.2 Publications

Herzog P, Drosten C, Müller MA.
Plaque assay for human coronavirus NL63 using human colon carcinoma cells.
Virol J. 2008 Nov 12;5:138.

Glowacka I, Bertram S, **Herzog P**, Pfefferle S, Steffen I, Muench MO, Simmons G, Hofmann H, Kuri T, Weber F, Eichler J, Drosten C, Pöhlmann S.
Differential downregulation of ACE2 by the spike proteins of severe acute respiratory syndrome coronavirus and human coronavirus NL63.
J Virol. 2010 Jan;84(2):1198-205.

Pfefferle S, Schöpf J, Kögl M, Friedel CC, Müller MA, Carbajo-Lozoya J, Stellberger T, von Dall'Armi E, **Herzog P**, Kallies S, Niemeyer D, Ditt V, Kuri T, Züst R, Pumpor K, Hilgenfeld R, Schwarz F, Zimmer R, Steffen I, Weber F, Thiel V, Herrler G, Thiel HJ, Schwegmann-Wessels C, Pöhlmann S, Haas J, Drosten C, von Brunn A.
The SARS-coronavirus-host interactome: identification of cyclophilins as target for pan-coronavirus inhibitors.
PLoS Pathog. 2011 Oct;7(10):e1002331.

Erklärung zur Dissertation

Ich erklare, dass ich

- die Dissertation personlich, selbststandig und ohne unerlaubte fremde Hilfe angefertigt habe,
- keine anderen, als die von mir angegebenen Quellen und Hilfsmittel benutzt habe,
- diese oder eine ahnliche Arbeit an keiner anderen Universitat zur Erlangung eines Titels eingereicht habe,
- noch keinen Promotionsversuch unternommen habe.

Bonn, den

_____

Petra Herzog

Acknowledgments

I would like to express my very great appreciation to Prof. Christian Drosten for offering the chance to work on this exciting thesis and helping me to get deep insights into reverse genetics and coronavirology.
I also would like to offer my special thanks to Prof. Bernhard Misof for reviewing this work and to Prof. Sahl and Prof. Dahl for taking part in the graduation commission.

I am particularly grateful for the discussions with and the assistance given by my lab colleagues Doreen Muth, Marcel Müller, Brit Häcker and Susanne Pfefferle, not only concerning lab-related topics. I would also like to thank some co-workers from the Bernhard Nocht Institute and the Institute of Virology, University of Bonn, Ingrid Müller, Stephan Ölschläger and Jan-Felix Drexler, for useful advice and interesting talks.

Special thanks have to be given to the former artus GmbH and especially to the members and co-founders Thomas Laue, Rainer Söller and Thomas Grewing for creating an interesting working environment and giving me the opportunity to graduate while being employed by the company, and to all the dear colleagues who kept motivating and supporting me like Karin Rottengatter and Markus Hess.

Finally I would like to thank my family and friends for constant support, special thank goes to Christian Stehning for keeping his good temper all the time.